

**LECTURE NOTES
ON
ANALYSIS OF AIRCRAFT STRUCTURES**

Sangram Samal, Professor

Department of Aeronautical Engineering

UNIT-1

INTRODUCTION TO AIRCRAFT STRUCTURAL COMPONENTS AND ENERGY METHODS

AIRCRAFT STRUCTURAL COMPONENTS

Aircraft are generally built up from the basic components of

- Wings
- Fuselages
- Tail units
- Control surfaces

There are variations in particular aircraft; for example, a delta wing aircraft would not necessarily possess a horizontal tail, although this is present in a canard configuration such as that of the Eurofighter(Typhoon).

Each component has one or more specific functions and must be designed to ensure that it can carry out these functions safely.

Loads on Structural Components

The structure of an aircraft is required to support two distinct classes of load:

the first, termed **ground loads**- includes all loads encountered by the aircraft during movement or transportation on the ground such as taxiing and landing loads, towing, and hoisting loads, and the second, **air loads**- comprises loads imposed on the structure during flight by maneuvers and gusts.

The two classes of loads may be further divided into **surface forces**- which act upon the surface of the structure, such as aerodynamic and hydrostatic pressure, and **body forces**- which act over the volume of the structure and are produced by gravitational and inertial effects.

Basically, all air loads are the results of the pressure distribution over the surfaces of the skin produced by steady flight, maneuver, or gust conditions. Generally, these results cause

- **direct loads**
- **bending**
- **shear and**
- **torsion**

in all parts of the structure in addition to local, normal pressure loads imposed on the skin.

Conventional aircraft usually consist of fuselage, wings, and tailplane. The **fuselage** contains crew and payload, the latter being passengers, cargo, weapons, plus fuel, depending on the type of aircraft and its function; the wings provide the lift, and the tailplane is the main contributor to directional control. In addition, ailerons, elevators, and the rudder enable the pilot to maneuver the aircraft and maintain its stability in flight, while wing flaps provide the necessary increase of

lift for takeoff and landing. Figure 1.2 shows typical aerodynamic force resultants experienced by an aircraft in steady flight.

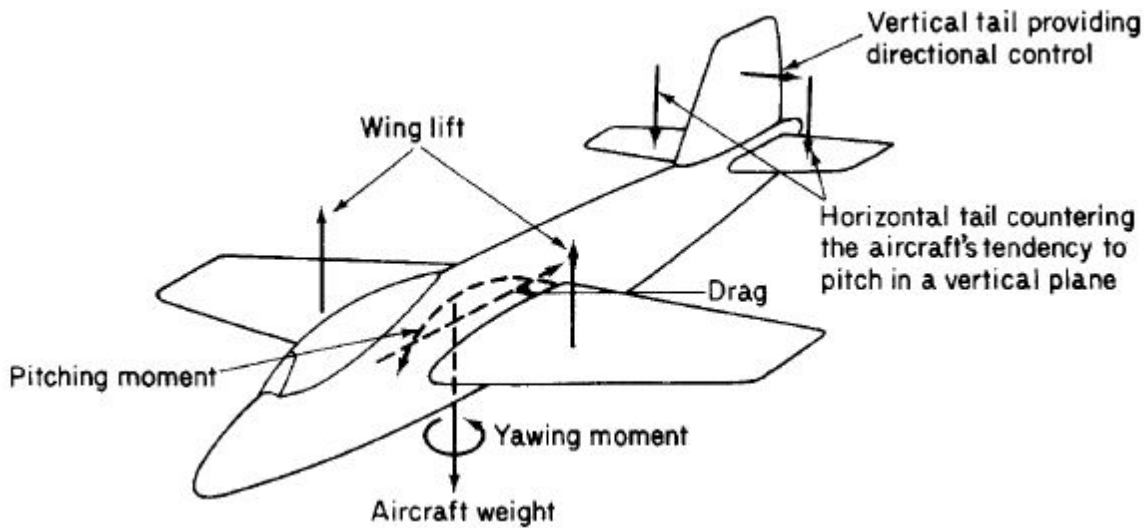


Figure 1.1 Structural components of aircraft and various loads acting on them

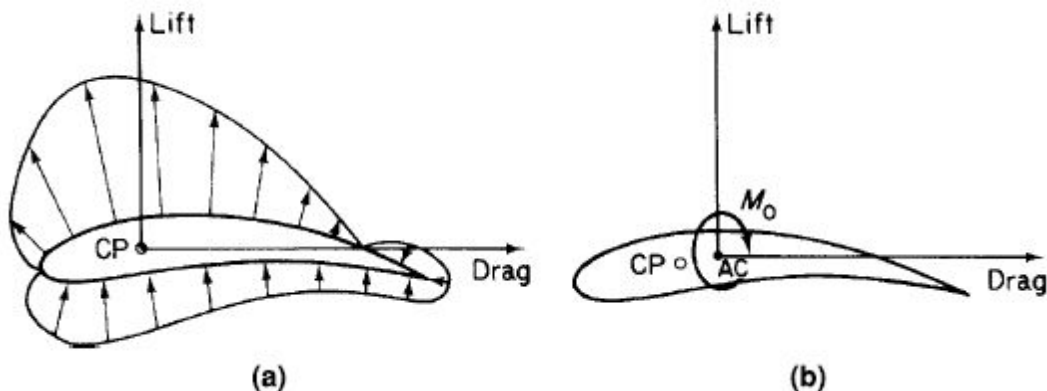


Figure 1.1 Principal aerodynamic forces on an aircraft during flight. (a) Pressure distribution around an aerofoil; (b) transference of lift and drag loads to the A/C.

The force on an aerodynamic surface (wing, vertical or horizontal tail) results from a differential pressure distribution caused by incidence, camber, or a combination of both. Such a pressure distribution, shown in Fig. 1.2(a), has vertical (lift) and horizontal (drag) resultants acting at a center of pressure (CP). (In practice, lift and drag are measured perpendicular and parallel to the flight path, respectively.) Clearly, the position of the CP changes as the pressure distribution varies with speed or wing incidence.

However, there is, conveniently, a point in the aerofoil section about which the moment due to the lift and drag forces remains constant. We therefore replace the lift and drag forces acting at

the CP by lift and drag forces acting at the aerodynamic center (AC) plus a constant moment M_0 , as shown in Fig. 1.2(b). (Actually, at high Mach numbers the position of the AC changes due to compressibility effects.)

While the chordwise pressure distribution fixes the position of the resultant aerodynamic load in the wing cross section, the spanwise distribution locates its position in relation, say, to the wing root. A typical distribution for a wing/fuselage combination is shown in Fig. 1.3. Similar distributions occur on horizontal and vertical tail surfaces.

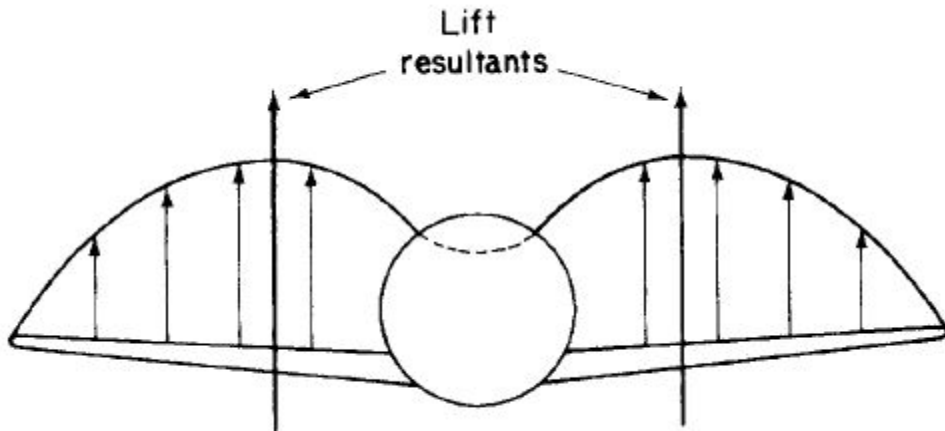


Figure 1.3 Typical lift distribution for a wing/fuselage combination.

Therefore, we see that wings, tailplane, and the fuselage are each subjected to direct, bending, shear, and torsional loads and must be designed to withstand critical combinations of these. Note that maneuvers and gusts do not introduce different loads but result only in changes of magnitude and position of the type of existing loads shown in Fig. 11.1.

Over and above these basic **in-flight loads**, fuselages may be pressurized and thereby support hoop stresses, wings may carry weapons and/or extra fuel tanks with resulting additional aerodynamic and body forces contributing to the existing bending, shear, and torsion, while the thrust and weight of engines may affect either fuselage or wings depending on their relative positions.

Ground loads encountered in landing and taxiing subject the aircraft to concentrated shock loads through the undercarriage system and the shock landing load produces a given shear, minimum bending plus torsion.

Other loads include engine **thrust on the wings** or fuselage which acts in the plane of symmetry but may, in the case of engine failure, cause severe fuselage **bending moments**, as shown in Fig.

1.4; concentrated shock loads during a catapult launch; and hydrodynamic pressure on the fuselages or floats of seaplanes.

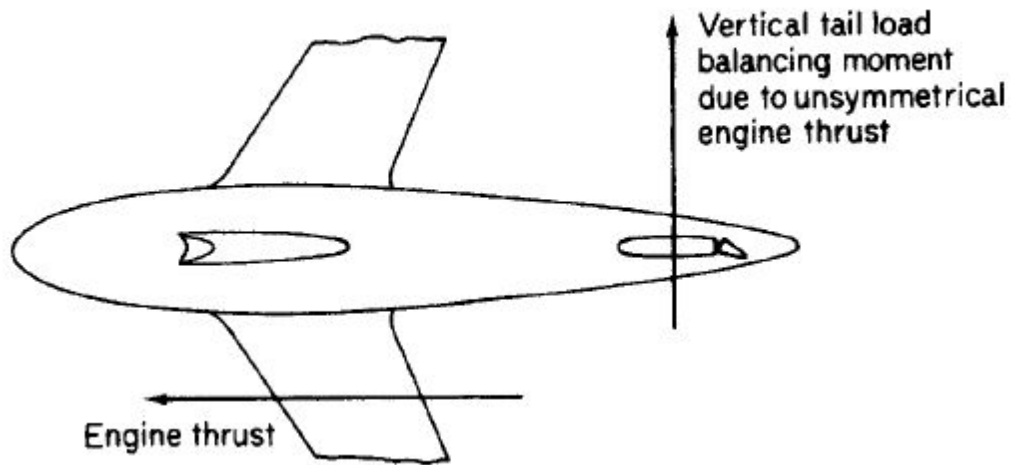


Figure 1.4 Fuselage and wing bending caused by an unsymmetrical engine load.

FUNCTION OF STRUCTURAL COMPONENTS

The basic functions of an aircraft's structure are to transmit and resist the applied loads, to provide an aerodynamic shape, and to protect passengers, payload, systems, and so forth from the environmental conditions encountered in flight. These requirements, in most aircraft, result in thin shell structures where the outer surface or skin of the shell is usually supported by longitudinal stiffening members and transverse frames to enable it to resist bending, compressive, and torsional loads without buckling. Such structures are known as **semi-monocoque**, while thin shells which rely entirely on their skins for their capacity to resist loads are referred to as **monocoque**.

First, we shall consider wing sections which, while performing the same function, can differ widely in their structural complexity, the wing of the small, light passenger aircraft, the De Havilland Canada Twin Otter, comprises a relatively simple arrangement of two spars, ribs, stringers, and skin, while the wing of the Harrier consists of numerous spars, ribs, and skin. However, no matter how complex the internal structural arrangement, the different components perform the same kind of function. The shape of the cross section is governed by aerodynamic considerations and clearly must be maintained for all combinations of load; this is one of the **functions of the ribs**. They also act with the skin in resisting the distributed aerodynamic pressure loads; they distribute concentrated loads (e.g., undercarriage and additional wing store loads) into the structure and redistribute stress around discontinuities, such as undercarriage wells, inspection panels, and fuel tanks, in the wing surface. Ribs increase the column buckling

stress of the longitudinal stiffeners by providing end restraint and establishing their column length; in a similar manner, they increase the plate buckling stress of the skin panels.

Types of structural joints

The fabrication of aircraft components, generally, involves the joining of one part of the component to another. For example, fuselage skins are connected to stringers and frames, whereas wing skins are connected to stringers and wing ribs unless, as in some military aircraft with high wing loadings, the stringers are machined integrally with the wing skin. With the advent of all metal—aluminum alloy—construction, **riveted joints** became the main form of connection with some **welding**, although aluminum alloys are difficult to weld, and, in the modern era, some **glued joints** which use epoxy resin.

In this section, we shall concentrate on the still predominant method of connection: riveting. In general, riveted joints are stressed in complex ways, and an accurate analysis is very often difficult to achieve because of the discontinuities in the region of the joint. Fairly crude assumptions as to joint behavior are made, but, when combined with experience, safe designs are produced.

Simple Lap Joint

Figure 1.5 shows two plates of thickness t connected together by a single line of rivets; this type of joint is termed a lap joint and is one of the simplest used in construction.

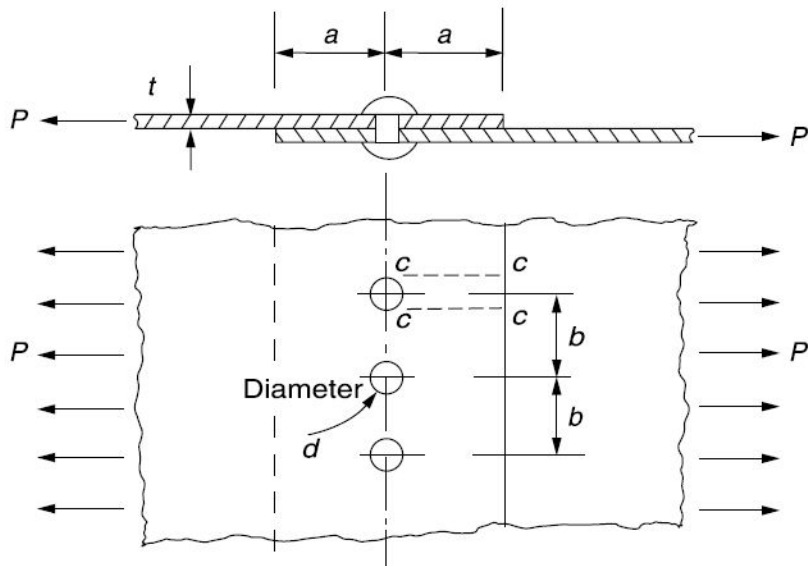


Figure 1.5 Simple riveted lap joint.

Suppose that the plates carry edge loads of $P/\text{unit width}$ that the rivets are of diameter d and are spaced at a distance b apart and that the distance from the line of rivets to the edge of each plate is a . There are four possible modes of failure which must be considered as follows.

Rivet Shear

The rivets may fail by shear across their diameter at the interface of the plates. Then, if the maximum shear stress the rivets will withstand is τ_1 , failure will occur when

$$Pb = \tau_1 \left(\frac{\pi d^2}{4} \right)$$

which gives

$$P = \frac{\pi d^2 \tau_1}{4b}$$

Bearing Pressure

Either the rivet or plate may fail due to bearing pressure. Suppose that Pb is this pressure then failure will occur when

$$\frac{Pb}{td} = p_b$$

so that

$$P = \frac{p_b t d}{b}$$

Plate Failure in Tension

The area of plate in tension along the line of rivets is reduced due to the presence of rivet holes. Therefore, if the ultimate tensile stress in the plate is ζ_{ult} , failure will occur when

$$\frac{Pb}{t(b-d)} = \sigma_{\text{ult}}$$

from which

$$P = \frac{\sigma_{\text{ult}} t(b - d)}{b}$$

Shear Failure in a Plate

Shearing of the plates may occur on the planes cc resulting in the rivets being dragged out of the plate. If the maximum shear stress at failure of the material of the plates is η_2 , then a failure of this type will occur when

$$Pb = 2at\tau_2$$

which gives

$$P = \frac{2at\tau_2}{b}$$

Joint Efficiency

The efficiency of a joint or connection is measured by comparing the actual failure load with that which would apply if there were no rivet holes in the plate. Then, for the joint shown in Fig. 11.5, the joint efficiency ϵ is given by

$$\eta = \frac{\sigma_{\text{ult}} t(b - d)/b}{\sigma_{\text{ult}} t} = \frac{b - d}{b}$$

Group-Riveted Joints

Rivets may be grouped on each side of a joint such that the efficiency of the joint is a maximum. Suppose that two plates are connected as shown in Fig. 1.6 and that six rivets are required on each side. If it is assumed that each rivet is equally loaded, then the single rivet on the line a will take one-sixth of the total load. The two rivets on the line bb will then share two-sixths of the load, while the three rivets on the line cc will share three-sixths of the load. On the line bb, the area of cross section of the plate is reduced by two rivet holes and that on the line cc by three rivet holes so that, relatively, the joint is as strong at these sections as at a. Therefore, a more efficient joint is obtained than if the rivets were arranged in, say, two parallel rows of three.

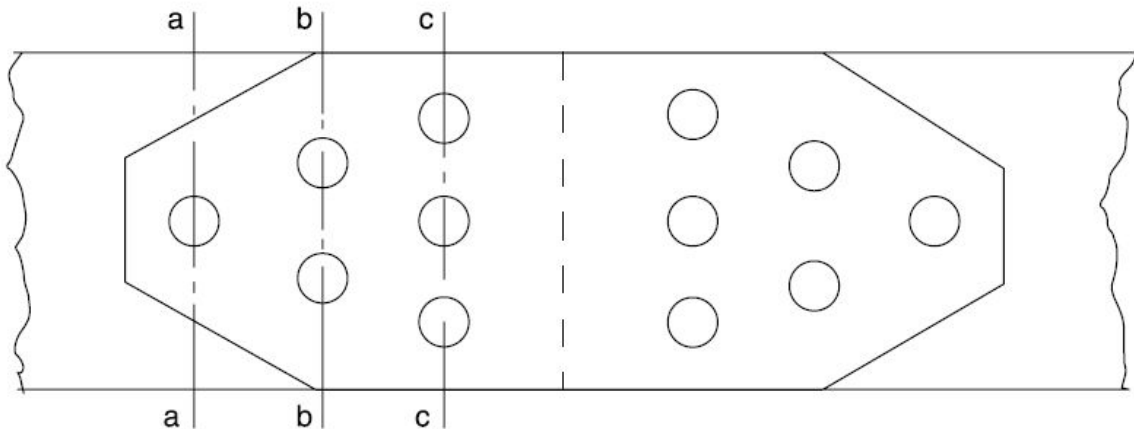


Figure 1.6 A group-riveted joint.

Eccentrically Loaded Riveted Joints

The bracketed connection shown in Fig. 1.7 carries a load P offset from the centroid of the rivet group. The rivet group is then subjected to a shear load P through its centroid and a moment or torque Pe about its centroid. It is assumed that the shear load P is distributed equally among the rivets, causing a shear force in each rivet parallel to the line of action of P . The moment Pe is assumed to produce a shear force S in each rivet, where S acts in a direction perpendicular to the line joining a particular rivet to the centroid of the rivet group. Furthermore, the value of S is assumed to be proportional to the distance of the rivet from the centroid of the rivet group. Then

$$Pe = \sum S r$$

If $S=kr$, where k is a constant for all rivets, then

$$Pe = k \sum r^2$$

from which

$$k = Pe / \sum r^2$$

and

$$S = \frac{Pe}{\sum r^2} r$$

The resultant force on a rivet is then the vector sum of the forces due to P and Pe .

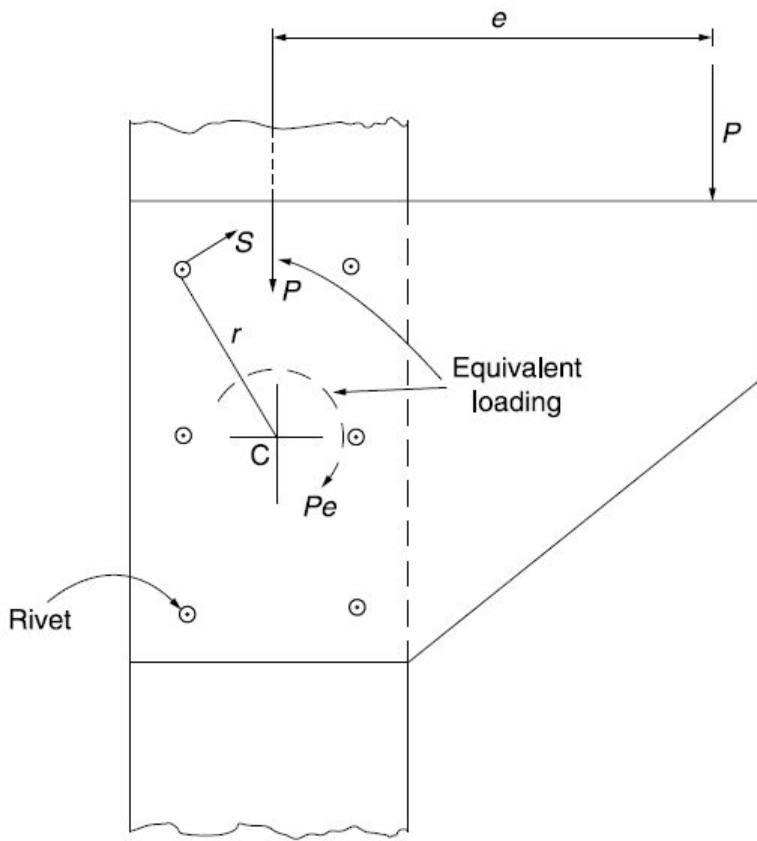


Figure 1.7 Eccentrically loaded joint.

Use of Adhesives

In addition to riveted connections, adhesives have been used and are still being used in aircraft construction, although, generally, they are employed in areas of low stress since their application is still a matter of research. Of these adhesives, epoxy resins are the most frequently used since they have the advantages over, say, polyester resins, of good adhesive properties, low shrinkage during cure so that residual stresses are reduced, good mechanical properties, and thermal stability. The modulus and ultimate strength of epoxy resin are, typically, 5000 and 100N/mm^2 . Epoxy resins are now found extensively as the matrix component in fibrous composites.

AIRFRAME LOADS

Aircraft Inertia Loads

The maximum loads on the components of an aircraft's structure generally occur when the aircraft is undergoing some form of acceleration or deceleration, such as in landings, take-offs, and maneuvers within the flight and gust envelopes. Thus, before a structural component can be designed, the inertia loads corresponding to these accelerations and decelerations must be calculated. For these purposes, we shall suppose that an aircraft is a rigid body and represent it by a rigid mass, m , as shown in Fig. 1.8. We shall also, at this stage, consider motion in the plane of the mass which would correspond to pitching of the aircraft without roll or yaw. We shall also suppose that the center of gravity (CG) of the mass has coordinates x, y referred to x and y axes having an arbitrary origin O ; the mass is rotating about an axis through O perpendicular to the xy plane with a constant angular velocity ω .

The acceleration of any point, a distance r from O , is $\omega^2 r$ and is directed toward O . Thus, the inertia force acting on the element, δm , is $\omega^2 r \delta m$ in a direction opposite to the acceleration, as shown in Fig. 1.8. The components of this inertia force, parallel to the x and y axes, are $\omega^2 r \delta m \cos \theta$ and $\omega^2 r \delta m \sin \theta$, respectively, or, in terms of x and y , $\omega^2 x \delta m$ and $\omega^2 y \delta m$. The resultant inertia forces, F_x and F_y , are then given by

$$F_x = \int \omega^2 x dm = \omega^2 \int x dm$$

$$F_y = \int \omega^2 y dm = \omega^2 \int y dm$$

in which we note that the angular velocity ω is constant and may therefore be taken outside the integral sign. In the above expressions, $\int x dm$ and $\int y dm$ are the moments of the mass, m , about the y and x axes, respectively, so that

$$F_x = \omega^2 \bar{x} m$$

and

$$F_y = \omega^2 \bar{y} m$$

If the CG lies on the x axis, $\bar{y} = 0$ and $F_y = 0$. Similarly, if the CG lies on the y axis, $\bar{x} = 0$. Clearly, if O coincides with the CG, $\bar{x} = \bar{y} = 0$ and $F_x = F_y = 0$.

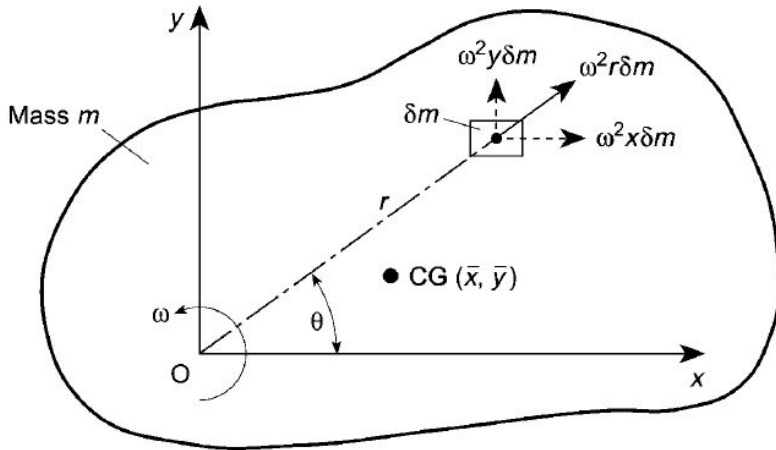


Figure 1.8 Inertia forces on a rigid mass having a constant angular velocity.

Suppose now that the rigid body is subjected to an angular acceleration (*or deceleration*) α in addition to the constant angular velocity, ω , as shown in Fig. 1.9. An additional inertia force, $\alpha r\delta m$, acts on the element δm in a direction perpendicular to r and in the opposite sense to the angular acceleration.

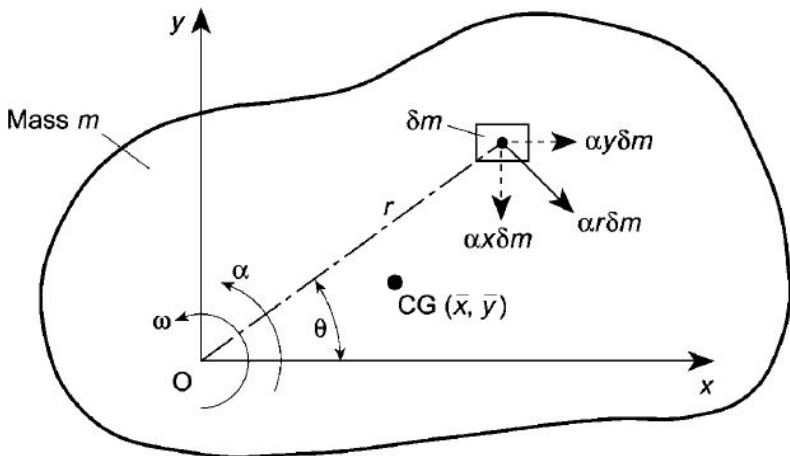


Figure 1.9 Inertia forces on a rigid mass subjected to an angular acceleration.

This inertia force has components $\alpha r\delta m \cos \theta$ and $\alpha r\delta m \sin \theta$, i.e. $\alpha x\delta m$ and $\alpha y\delta m$, in the y and x directions, respectively. Thus, the resultant inertia forces, F_x and F_y , are given by

$$F_x = \int \alpha y \, dm = \alpha \int y \, dm$$

and

$$F_y = - \int \alpha x \, dm = -\alpha \int x \, dm$$

for α in the direction shown. Then, as before

$$F_x = \alpha \bar{y} m$$

and

$$F_y = \alpha \bar{x} m$$

Also, if the CG lies on the x axis, $\bar{y} = 0$ and $F_x = 0$. Similarly, if the CG lies on the y axis, $\bar{x} = 0$ and $F_y = 0$.

The torque about the axis of rotation produced by the inertia force corresponding to the angular acceleration on the element δm is given by

$$\delta T_O = \alpha r^2 \delta m$$

Thus, for the complete mass

$$T_O = \int \alpha r^2 \, dm = \alpha \int r^2 \, dm$$

The integral term in this expression is the moment of inertia, I_O , of the mass about the axis of rotation. Thus,

$$T_O = \alpha I_O \quad (1)$$

Equation (1) may be rewritten in terms of I_{CG} , the moment of inertia of the mass about an axis perpendicular to the plane of the mass through the CG. Hence, using the parallel axes theorem

$$I_O = m(\bar{r})^2 + I_{CG}$$

where \bar{r} is the distance between O and the CG. Then

$$I_O = m[(\bar{x})^2 + (\bar{y})^2] + I_{CG}$$

and

$$T_O = m[(\bar{x})^2 + (\bar{y})^2]\alpha + I_{CG}\alpha$$

FACTORS OF SAFETY-FLIGHT ENVELOPE

The control of weight in aircraft design is of extreme importance. Increases in weight require stronger structures to support them, which in turn lead to further increases in weight and so on. Excesses of structural weight mean lesser amounts of payload, thereby affecting the economic viability of the aircraft. The aircraft designer is therefore constantly seeking to pare his aircraft's weight to the minimum compatible with safety. However, to ensure general minimum standards of strength and safety, airworthiness regulations lay down several factors which the primary structure of the aircraft must satisfy. These are the limit load, which is the maximum load that the aircraft is expected to experience in normal operation; the proof load, which is the product of the limit load and the proof factor (1.0–1.25); and the ultimate load, which is the product of the limit load and the ultimate factor (usually 1.5). The aircraft's structure must withstand the proof load without detrimental distortion and should not fail until the ultimate load has been achieved. The proof and ultimate factors may be regarded as factors of safety and provide for various contingencies and uncertainties.

The basic strength and flight performance limits for a particular aircraft are selected by the airworthiness authorities and are contained in the *flight envelope* or *V-n* diagram shown in Fig. 1.10.

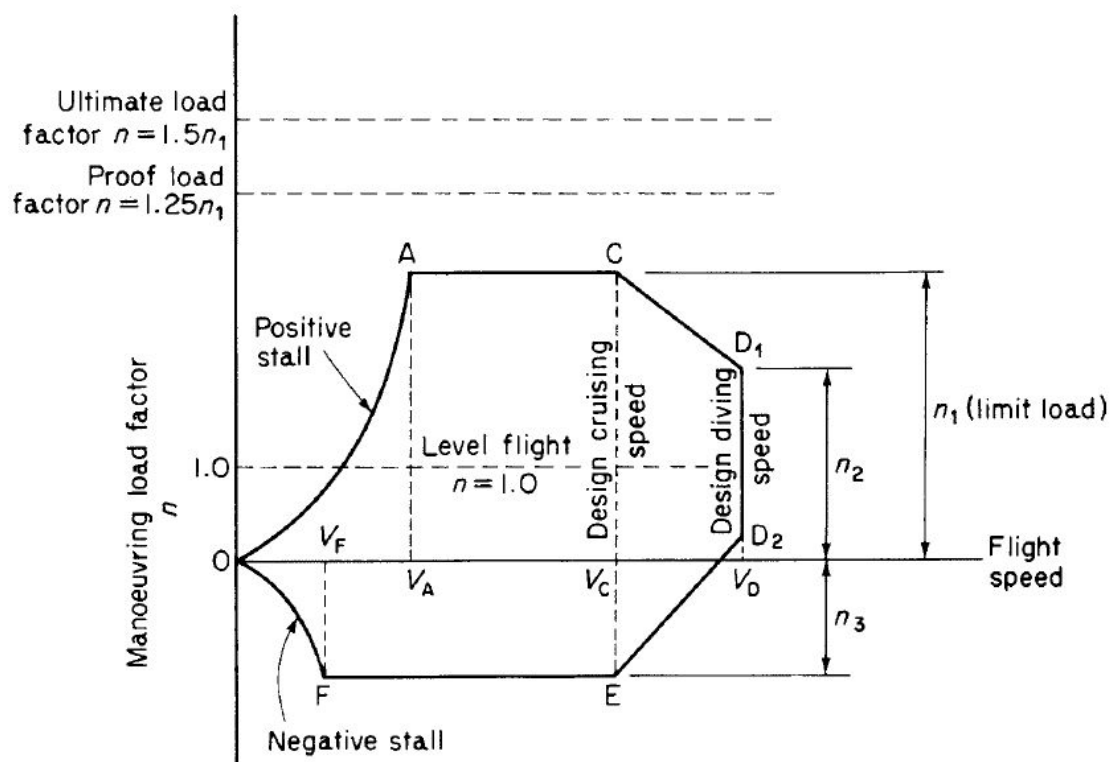


Figure 1.10 Flight envelope.

The curves OA and OF correspond to the stalled condition of the aircraft and are obtained from the well-known aerodynamic relationship

$$\text{Lift} = nW = \frac{1}{2}\rho V^2 S C_{L,\max}$$

Therefore, for speeds below V_A (positive wing incidence) and V_F (negative incidence), the maximum loads which can be applied to the aircraft are governed by $C_{L,\max}$. As the speed increases, it is possible to apply the positive and negative limit loads, corresponding to n_1 and n_3 , without stalling the aircraft so that AC and FE represent maximum operational load factors for the aircraft. Above the design cruising speed V_C , the cut-off lines CD_1 and D_2E relieve the design cases to be covered since it is not expected that the limit loads will be applied at maximum speed. Values of n_1 , n_2 , and n_3 are specified by the airworthiness authorities for particular aircraft;

A particular flight envelope is applicable to one altitude only because $C_{L,\max}$ is generally reduced with an increase of altitude, and the speed of sound decreases with altitude, thereby reducing the critical Mach number and hence the design diving speed V_D . Flight envelopes are therefore drawn for a range of altitudes from sea level to the operational ceiling of the aircraft.

SYMMETRIC MANEUVER LOADS

We shall now consider the calculation of aircraft loads corresponding to the flight conditions specified by flight envelopes. There are, in fact, an infinite number of flight conditions within the boundary of the flight envelope although, structurally, those represented by the boundary are the most severe. Furthermore, it is usually found that the corners A, C, D_1 , D_2 , E, and F (see Fig. 1.10) are more critical than points on the boundary between the corners so that, in practice, only the six conditions corresponding to these corner points need to be investigated for each flight envelope.

In symmetric maneuvers, we consider the motion of the aircraft initiated by movement of the control surfaces in the plane of symmetry. Examples of such maneuvers are loops, straight pull-outs, and bunts, and the calculations involve the determination of lift, drag, and tailplane loads at given flight speeds and altitudes.

Level Flight

Although steady level flight is not a maneuver in the strict sense of the word, it is a useful condition to investigate initially since it establishes points of load application and gives some idea of the equilibrium of an aircraft in the longitudinal plane. The loads acting on an aircraft in steady flight are shown in Fig. 1.11, with the following notation:

- L is the lift acting at the aerodynamic center of the wing.
- D is the aircraft drag.
- M_0 is the aerodynamic pitching moment of the aircraft less its horizontal tail.
- P is the horizontal tail load acting at the aerodynamic center of the tail, usually taken to be at approximately one-third of the tailplane chord.
- W is the aircraft weight acting at its CG.
- T is the engine thrust, assumed here to act parallel to the direction of flight in order to simplify calculation.

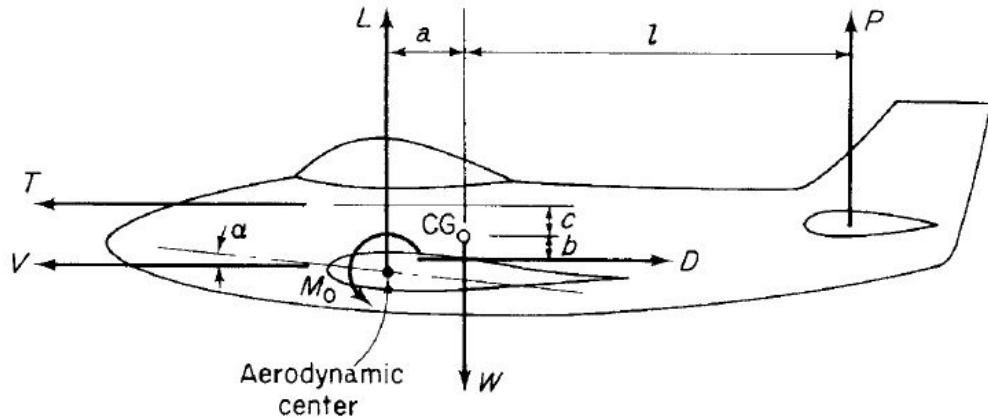


Figure 1.11 Aircraft loads in level flight.

The loads are in static equilibrium since the aircraft is in a steady, un-accelerated, level flight condition.

Thus, for vertical equilibrium

$$L + P - W = 0 \quad (2)$$

for horizontal equilibrium

$$T - D = 0 \quad (3)$$

and taking moments about the aircraft's CG in the plane of symmetry

$$La - Db - Tc - M_0 - Pl = 0 \quad (4)$$

For a given aircraft weight, speed, and altitude, Eqs. (2, 3 and 4) may be solved for the unknown lift, drag, and tail loads. However, other parameters in these equations, such as M_0 , depend upon the wing incidence α , which in turn is a function of the required wing lift so that, in practice, a method of successive approximation is found to be the most convenient means of solution.

As a first approximation, we assume that the tail load P is small compared with the wing lift L so that, from Eq. (2), $L \approx W$. From aerodynamic theory with the usual notation,

$$L = \frac{1}{2} \rho V^2 S C_L$$

Hence,

$$\frac{1}{2} \rho V^2 S C_L \approx W \quad (5)$$

Equation (5) gives the approximate lift coefficient C_L and thus (from $C_L - \alpha$ curves established by wind tunnel tests) the wing incidence α . The drag load D follows (knowing V and α) and hence we obtain the required engine thrust T from Eq. (3). Also, M_0 , a , b , c , and l may be calculated (again, since V and α are known) and Eq. (4) solved for P . As a second approximation, this value of P is substituted in Eq. (2) to obtain a more accurate value for L , and the procedure is repeated. Usually three approximations are sufficient to produce reasonably accurate values.

In most cases, P , D , and T are small compared with the lift and aircraft weight. Therefore, from Eq. (2) $L \approx W$, and substitution in Eq. (4) gives, neglecting D and T

$$P \approx W \frac{a}{l} - \frac{M_0}{l} \quad (6)$$

We see from Eq. (6) that if a is large, then P will most likely be positive. In other words, the tail load acts upward when the CG of the aircraft is far aft. When a is small or negative—in other words, a forward CG—then P will probably be negative and act downward.

General Case of a Symmetric Maneuver

In a rapid pull-out from a dive a downward load is applied to the tailplane, causing the aircraft to pitch nose upward. The downward load is achieved by a backward movement of the control column, thereby applying negative incidence to the elevators, or horizontal tail if the latter is all-moving. If the maneuver is carried out rapidly, the forward speed of the aircraft remains practically constant so that increases in lift and drag result from the increase in wing incidence only. Since the lift is now greater than that required to balance the aircraft weight, the aircraft

experiences an upward acceleration normal to its flight path. This normal acceleration combined with the aircraft's speed in the dive results in the curved flight path shown in Fig. 1.12. As the drag load builds up with an increase of incidence, the forward speed of the aircraft falls since the thrust is assumed to remain constant during the maneuver. It is usual, as we observed in the discussion of the flight envelope, to describe the maneuvers of an aircraft in terms of a maneuvering load factor n . For steady level flight $n = 1$, giving 1 g flight, although in fact the acceleration is zero. What is implied in this method of description is that the inertia force on the aircraft in the level flight condition is 1.0 times its weight. It follows that the vertical inertia force on an aircraft carrying out an ng maneuver is nW . We may, therefore, replace the dynamic conditions of the accelerated motion by an equivalent set of static conditions in which the applied loads are in equilibrium with the inertia forces. Thus, in Fig. 1.12, n is the maneuver load factor, while f is a similar factor giving the horizontal inertia force. Note that the actual normal acceleration in this particular case is $(n-1)g$.

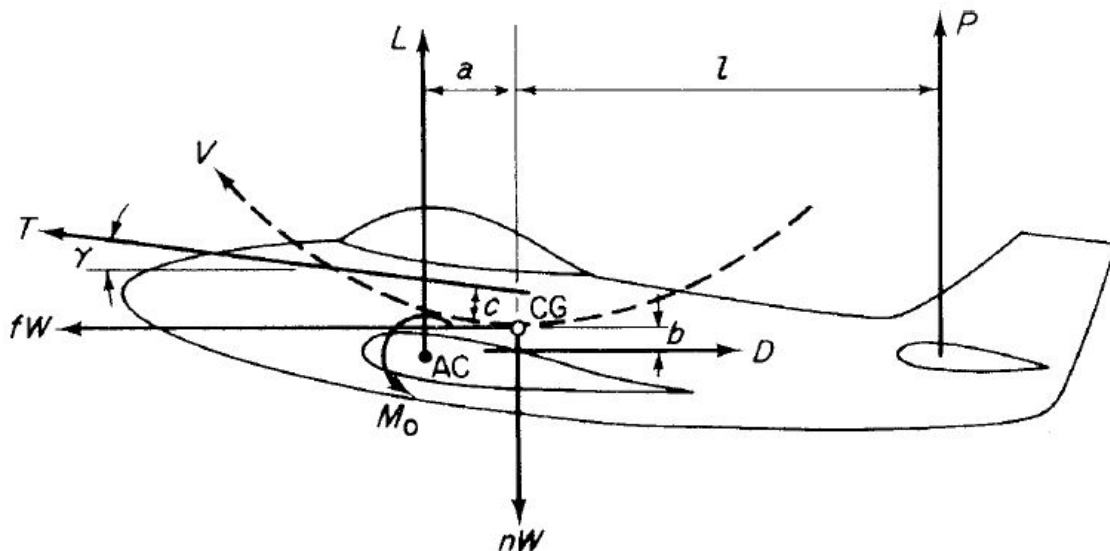


Figure 1.12 Aircraft loads in a pull-out from a dive.

For vertical equilibrium of the aircraft, we have, referring to Fig. 13.7 where the aircraft is shown at the lowest point of the pull-out

$$L + P + T \sin \gamma - nW = 0 \quad (7)$$

For horizontal equilibrium,

$$T \cos \gamma + fW - D = 0 \quad (8)$$

and for pitching moment equilibrium about the aircraft's CG,

$$La - Db - Tc - M_0 - Pl = 0 \quad (9)$$

Equation (9) contains no terms representing the effect of pitching acceleration of the aircraft; this is assumed to be negligible at this stage.

Again, the method of successive approximation is found to be most convenient for the solution of Eqs. (7, 8 and 9). There is, however, a difference to the procedure described for the steady level flight case. The engine thrust T is no longer directly related to the drag D , as the latter changes during the maneuver. Generally, the thrust is regarded as remaining constant and equal to the value appropriate to conditions before the maneuver began.

Gust Loads

The movements of the air in turbulence are generally known as gusts and produce changes in wing incidence, thereby subjecting the aircraft to sudden or gradual increases or decreases in lift from which normal accelerations result. These may be critical for large, high-speed aircraft and may possibly cause higher loads than control initiated maneuvers.

At the present time, two approaches are employed in gust analysis. **One method**, which has been in use for a considerable number of years, determines the aircraft response and loads due to a single or —discrete— gust of a given profile. This profile is defined as a distribution of vertical gust velocity over a given finite length or given period of time.

Early airworthiness requirements specified an instantaneous application of gust velocity u , resulting in the —sharp-edged— gust of Fig. 1.13 (a). Calculations of normal acceleration and aircraft response were based on the assumptions that the aircraft's flight is undisturbed while the aircraft passes from still air into the moving air of the gust and during the time taken for the gust loads to build up; that the aerodynamic forces on the aircraft are determined by the instantaneous incidence of the particular lifting surface; and finally that the aircraft's structure is rigid. The second assumption here relating the aerodynamic force on a lifting surface to its instantaneous incidence neglects the fact that in a disturbance such as a gust there is a gradual growth of circulation and hence of lift to a steady state value (Wagner effect). This, in general, leads to an overestimation of the upward acceleration of an aircraft and therefore of gust loads.

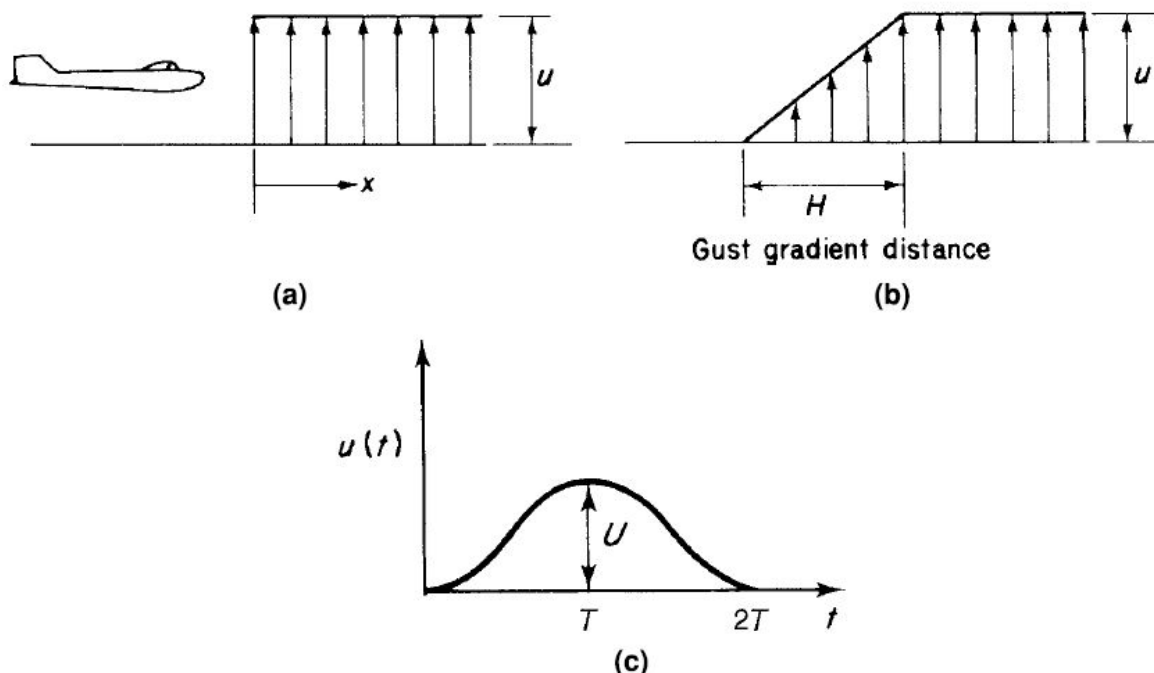


Figure 1.13 (a) Sharp-edged gust; (b) graded gust; (c) 1-cosine gust.

The —sharp-edged‖ gust was replaced when it was realized that the gust velocity built up to a maximum over a period of time. Airworthiness requirements were modified on the assumption that the gust velocity increased linearly to a maximum value over a specified gust gradient distance H . Hence, the —graded‖ gust of Fig. 1.13 (b). In the United Kingdom H is taken as 30.5 m. Since, as far as the aircraft is concerned, the gust velocity builds up to a maximum over a period of time, it is no longer allowable to ignore the change of flight path as the aircraft enters the gust. By the time the gust has attained its maximum value, the aircraft has developed a vertical component of velocity and, in addition, may be pitching, depending on its longitudinal stability characteristics. The effect of the former is to reduce the severity of the gust, whereas the latter may either increase or decrease the loads involved. To evaluate the corresponding gust loads, the designer may either calculate the complete motion of the aircraft during the disturbance and hence obtain the gust loads or replace the —graded‖ gust by an equivalent —sharp-edged‖ gust, producing approximately the same effect. We shall discuss the latter procedure in greater detail later.

The calculation of the complete response of the aircraft to a —graded‖ gust may be obtained from its response to a —sharp-edged‖ or —step‖ gust, by treating the former as comprising a large number of small —steps‖ and superimposing the responses to each of these. Such a process is known as **convolution** or **Duhamel integration**. This treatment is desirable for large or unorthodox aircraft where aeroelastic (structural flexibility) effects on gust loads may be

appreciable or unknown. In such cases, the assumption of a rigid aircraft may lead to an underestimation of gust loads. The equations of motion are therefore modified to allow for aeroelastic in addition to aerodynamic effects. For small and medium-sized aircraft having orthodox aerodynamic features, the equivalent —sharp-edged|| gust procedure is satisfactory.

Although the —graded|| or —ramp|| gust is used as a basis for gust load calculations, other shapes of gust profile are in current use. Typical of these is the —l-cosine|| gust of Fig. 13.11(c), where the gust velocity u is given by $u(t) = (U/2)[l - \cos(\pi t/T)]$. Again, the aircraft response is determined by superimposing the responses to each of a large number of small steps.

ENERGY METHODS

Many structures which are statically indeterminate—in other words, they cannot be analyzed by the application of the equations of statically equilibrium alone—may be conveniently analyzed using an energy approach.

Energy methods provide comparatively simple solutions for deflection problems which are not readily solved by more elementary means.

Generally, as we shall see, modern analysis uses the methods of *total complementary energy* and *total potential energy* (TPE). Either method may be used to solve a particular problem, although as a general rule deflections are more easily found using complementary energy and forces by potential energy.

Although energy methods are applicable to a wide range of structural problems and may even be used as indirect methods of forming equations of equilibrium or compatibility we shall be concerned in this chapter with the solution of deflection problems and the analysis of statically indeterminate structures. We shall also include some methods restricted to the solution of linear systems: the *unit load method*, the *principle of superposition*, and the *reciprocal theorem*.

STRAIN ENERGY AND COMPLEMENTARY ENERGY

Figure 1.14 (a) shows a structural member subjected to a steadily increasing load P . As the member extends, the load P does *work*, and from the *law of conservation of energy*, this *work* is stored in the member as **strain energy**. A typical load-deflection curve for a member possessing nonlinear elastic characteristics is shown in Fig. 1.14 (b). The strain energy U produced by a load P and corresponding extension y is then

$$U = \int_0^y P dy \quad (10)$$

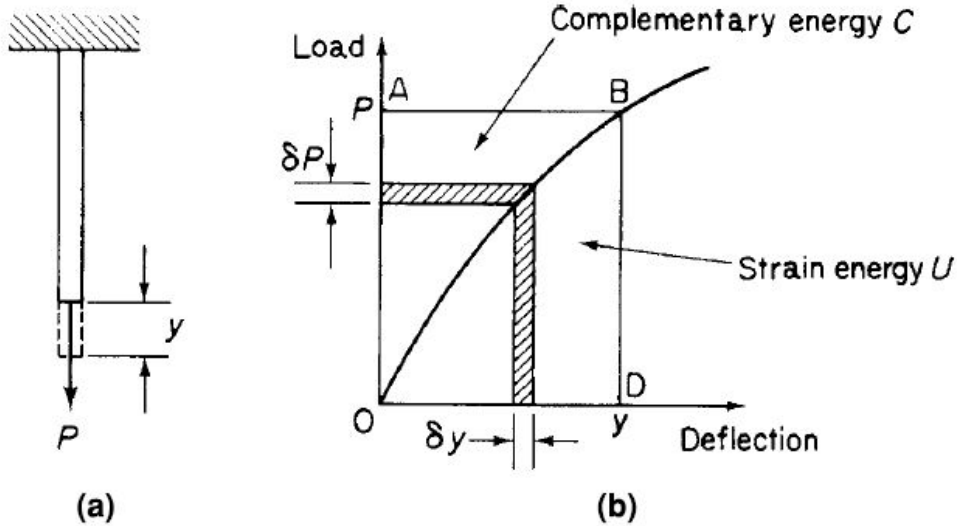


Figure 1.14 (a) Strain energy of a member subjected to simple tension; (b) load–deflection curve for a nonlinearly elastic member.

and is clearly represented by the area OBD under the load–deflection curve. Engesser (1889) called the area OBA above the curve the *complementary energy* C , and from Fig. 1.14 (b),

$$C = \int_0^P y dP \quad (11)$$

Complementary energy, as opposed to strain energy, has no physical meaning, being purely a convenient mathematical quantity. However, it is possible to show that complementary energy obeys the law of conservation of energy in the type of situation usually arising in engineering structures so that its use as an energy method is valid.

Differentiation of Eqs. (10) and (11) with respect to y and P , respectively, gives

$$\frac{dU}{dy} = P \quad \frac{dC}{dP} = y$$

Bearing these relationships in mind, we can now consider the interchangeability of strain and complementary energy. Suppose that the curve of Fig. 1.14 (b) is represented by the function

$$P = by^n$$

where the coefficient b and exponent n are constants. Then,

$$U = \int_0^y P dy = \frac{1}{n} \int_0^P \left(\frac{P}{b}\right)^{1/n} dP$$

$$C = \int_0^P y dP = n \int_0^y by^n dy$$

Hence,

$$\frac{dU}{dy} = P \quad \frac{dU}{dP} = \frac{1}{n} \left(\frac{P}{b}\right)^{1/n} = \frac{1}{n} y \quad (12)$$

$$\frac{dC}{dP} = y \quad \frac{dC}{dy} = bny^n = nP \quad (13)$$

When $n = 1$,

$$\left. \begin{aligned} \frac{dU}{dy} &= \frac{dC}{dy} = P \\ \frac{dU}{dP} &= \frac{dC}{dP} = y \end{aligned} \right\} \quad (14)$$

and the strain and complementary energies are completely interchangeable. Such a condition is found in a linearly elastic member; its related load-deflection curve is shown in Fig. 1.15. Clearly, area OBD(U) is equal to area OBA(C).

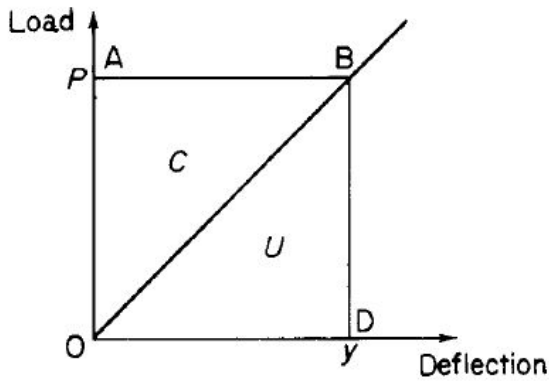


Figure 1.15 Load–deflection curve for a linearly elastic member.

It will be observed that the latter of Eqs. (14) is in the form of what is commonly known as **Castigliano's first theorem**, in which the differential of the strain energy U of a structure with respect to a load is equated to the deflection of the load. To be mathematically correct, however, it is the differential of the complementary energy C which should be equated to deflection (compare Eqs. (12) and (13)).

Application to Deflection Problems

Generally, deflection problems are most readily solved by the complementary energy approach, although for linearly elastic systems there is no difference between the methods of complementary and potential energy, since, as we have seen, complementary and strain energy then becomes completely interchangeable. We shall illustrate the method by reference to the deflections of frames and beams which may or may not possess linear elasticity. Let us suppose that we want to find the deflection Δ_2 of the load P_2 in the simple pin-jointed framework consisting, say, of k members and supporting loads P_1, P_2, \dots, P_n , as shown in Fig. 1.16.

The total complementary energy of the framework is given by

$$C = \sum_{i=1}^k \int_0^{F_i} \lambda_i dF_i - \sum_{r=1}^n \Delta_r P_r$$

(15) (Refer Section 5.2, T.H.G. Megson)

where λ_i is the extension of the i th member, F_i is the force in the i th member, and r is the corresponding displacement of the r th load P_r .

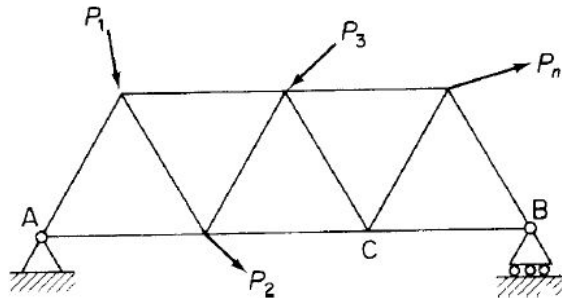


Figure 1.16 Determination of the deflection of a point on a framework by the method of complementary energy.

From the principle of the stationary value of the total complementary energy,

$$\frac{\partial C}{\partial P_2} = \sum_{i=1}^k \lambda_i \frac{\partial F_i}{\partial P_2} - \Delta_2 = 0 \quad (16)$$

from which

$$\Delta_2 = \sum_{i=1}^k \lambda_i \frac{\partial F_i}{\partial P_2} \quad (17)$$

Equation (16) is seen to be identical to the principle of virtual forces in which virtual forces δF and δP act through real displacements λ and. Clearly, the partial derivatives with respect to P_2 of the constant loads P_1, P_2, \dots, P_n vanish, leaving the required deflection Δ_2 as the unknown. At this stage, before Δ_2 can be evaluated, the load-displacement characteristics of the members must be known. For linear elasticity,

$$\lambda_i = \frac{F_i L_i}{A_i E_i}$$

where L_i , A_i , and E_i are the length, the cross-sectional area, and the modulus of elasticity of the i th member, respectively. On the other hand, if the load-displacement relationship is of a nonlinear form, say,

$$F_i = b(\lambda_i)^c$$

in which b and c are known, then Eq. (17) becomes

$$\Delta_2 = \sum_{i=1}^k \left(\frac{F_i}{b} \right)^{1/c} \frac{\partial F_i}{\partial P_2}$$

The computation of Δ_2 is best accomplished in tabular form, but before the procedure is illustrated by an example, some aspects of the solution merit discussion.

UNIT LOAD METHOD

For a linearly elastic structure, the method may be streamlined as follows. Consider the framework of Fig. 5.3 in which we require, say, to find the vertical deflection of the point C. We would place a vertical dummy load P_f at C and write down the total complementary energy of the framework, that is,

$$C = \sum_{i=1}^k \int_0^{F_i} \lambda_i dF_i - \sum_{r=1}^n \Delta_r P_r$$

For a stationary value of C,

$$\frac{\partial C}{\partial P_f} = \sum_{i=1}^k \lambda_i \frac{\partial F_i}{\partial P_f} - \Delta_C = 0$$

from which

$$\Delta_C = \sum_{i=1}^k \lambda_i \frac{\partial F_i}{\partial P_f} \text{ as before} \quad (18)$$

If instead of the arbitrary dummy load P_f we had placed a unit load at C, then the load in the i th linearly elastic member would be

$$F_i = \frac{\partial F_i}{\partial P_f} 1$$

Therefore, the term $\partial F_i / \partial P_f$ in Eq. (5.19) is equal to the load in the i th member due to a unit load at C, and Eq. (5.19) may be written as

$$\Delta_C = \sum_{i=1}^k \frac{F_{i,0} F_{i,1} L_i}{A_i E_i}$$

where $F_{i,0}$ is the force in the i th member due to the actual loading and $F_{i,1}$ is the force in the i th member due to a unit load placed at the position and in the direction of the required deflection.

Similar expressions for deflection due to bending and torsion of linear structures follow from the well-known relationships between bending and rotation and torsion and rotation. Hence, for a member of length L and flexural and torsional rigidities EI and GJ , respectively,

$$\Delta_{B.M} = \int_L \frac{M_0 M_1}{EI} dz \quad \Delta_T = \int_L \frac{T_0 T_1}{GJ} dz$$

where M_0 is the bending moment at any section produced by the actual loading and M_1 is the bending moment at any section due to a unit load applied at the position and in the direction of the required deflection. The same applies to torsion.

FLEXIBILITY METHOD

An alternative approach to the solution of statically indeterminate beams and frames is to release the structure—that is, remove redundant members or supports—until the structure becomes statically determinate. The displacement of some point in the released structure is then determined by, say, the unit load method. The actual loads on the structure are removed and unknown forces applied to the points where the structure has been released; the displacement at the point produced by these unknown forces must, from compatibility, be the same as that in the released structure. The unknown forces are then obtained; this approach is known as the *flexibility method*.

TOTAL POTENTIAL ENERGY

In the spring–mass system shown in its unstrained position in Fig. 5.23(a), we normally define the potential energy of the mass as the product of its weight, Mg , and its height, h , above some arbitrarily fixed datum. In other words, it possesses energy by virtue of its position. After deflection to an equilibrium state (Fig. 5.23(b)), the mass has lost an amount of potential energy equal to Mgy . Thus, we may associate deflection with a loss of potential energy. Alternatively, we may argue that the gravitational force acting on the mass does work during its displacement, resulting in a loss of energy. Applying this reasoning to the elastic system of Fig. 1.14 (a) and assuming that the potential energy of the system is zero in the unloaded state, then the loss of potential energy of the load P as it produces a deflection y is Py .

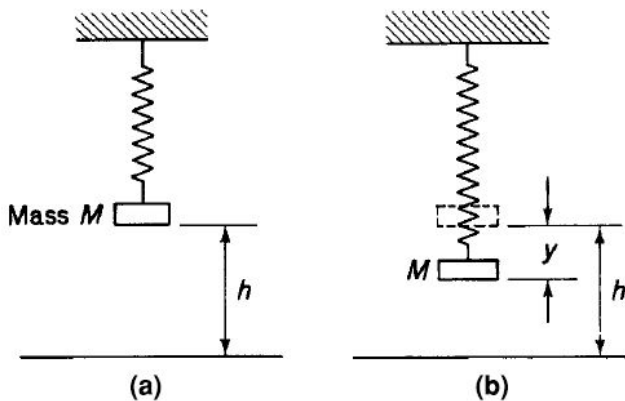


Figure 1.17 (a) Potential energy of a spring–mass system and (b) loss in potential energy due to change in position.

Thus, the potential energy V of P in the deflected equilibrium state is given by

$$V = -Py$$

We now define the TPE of a system in its deflected equilibrium state as the sum of its internal or strain energy and the potential energy of the applied external forces. Hence, for the single member–force configuration of Fig. 1.14 (a),

$$\text{TPE} = U + V = \int_0^y P dy - Py$$

For a general system consisting of loads P_1, P_2, \dots, P_n producing corresponding displacements (i.e., displacements in the directions of the loads; see Section 5.10, T.H.G. Megson) $\Delta_1, \Delta_2, \dots, \Delta_n$, the potential energy of all the loads is

$$V = \sum_{r=1}^n V_r = \sum_{r=1}^n (-P_r \Delta_r)$$

and the TPE of the system is given by

$$\text{TPE} = U + V = U + \sum_{r=1}^n (-P_r \Delta_r)$$

The Principle of the Stationary Value of the Total Potential Energy

Let us now consider an elastic body in equilibrium under a series of external loads, P_1, P_2, \dots, P_n , and suppose that we impose small virtual displacements $\delta\Delta_1, \delta\Delta_2, \dots, \delta\Delta_n$ in the directions of the loads. The virtual work done by the loads is then

$$\sum_{r=1}^n P_r \delta \Delta_r$$

This work will be accompanied by an increment of strain energy δU in the elastic body, since by specifying virtual displacements of the loads we automatically impose virtual displacements on the particles of the body itself, as the body is continuous and is assumed to remain so. This increment in strain energy may be regarded as negative virtual work done by the particles so that the total work done during the virtual displacement is

$$-\delta U + \sum_{r=1}^n P_r \delta \Delta_r$$

The body is in equilibrium under the applied loads so that by the principle of virtual work the preceding expression must be equal to zero. Hence

$$\delta U - \sum_{r=1}^n P_r \delta \Delta_r = 0$$

The loads P_r remain constant during the virtual displacement; therefore, the above equation may be written

$$\delta U - \delta \sum_{r=1}^n P_r \Delta_r = 0$$

or,

$$\delta(U + V) = 0$$

Thus, the total potential energy of an elastic system has a stationary value for all small displacements if the system is in equilibrium.

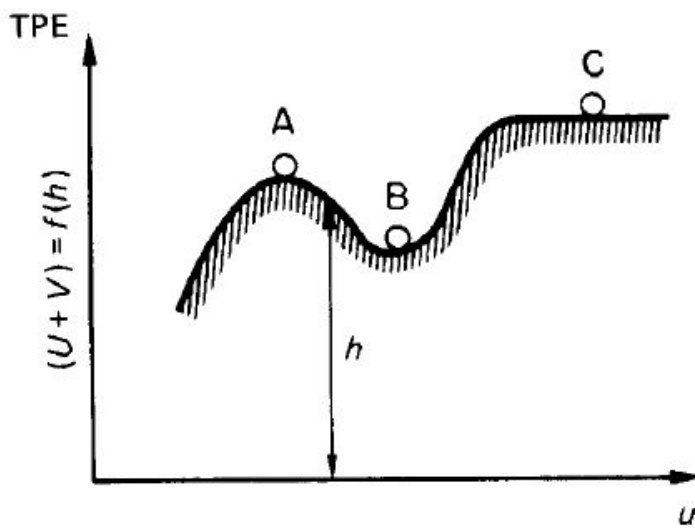


Figure 1.18 States of equilibrium of a particle.

Principle of Superposition

An extremely useful principle used in the analysis of linearly elastic structures is that of superposition. The principle states that if the displacements at all points in an elastic body are proportional to the forces producing them—that is, the body is linearly elastic—the effect on such a body of a number of forces is the sum of the effects of the forces applied separately. We shall make immediate use of the principle in the derivation of the reciprocal theorem in the following section.

It may also be shown that if the stationary value is a minimum, the equilibrium is stable. A qualitative demonstration of this fact is sufficient for our purposes, although mathematical proofs exist. In Fig. 1.18, the positions A , B , and C of a particle correspond to different equilibrium states. The TPE of the particle in each of its three positions is proportional to its height h above

some arbitrary datum, since we are considering a single particle for which the strain energy is zero. Clearly at each position, the first-order variation, $\partial(U+V)/\partial u$, is zero (indicating equilibrium), but only at B where the TPE is a minimum is the equilibrium stable. At A and C, we have unstable and neutral equilibrium, respectively.

To summarize, the principle of the stationary value of the *TPE* may be stated as follows:

The total potential energy of an elastic system has a stationary value for all small displacements when the system is in equilibrium; further, the equilibrium is stable if the stationary value is a minimum.

This principle may often be used in the approximate analysis of structures where an exact analysis does not exist. When suppose that the displaced form of the beam is unknown and must be assumed; this approach is called the **Rayleigh–Ritz method**.

THE RECIPROCAL THEOREM

The reciprocal theorem is an exceptionally powerful method of analysis of linearly elastic structures and is accredited in turn to Maxwell, Betti, and Rayleigh. However, before we establish the theorem, we first consider a useful property of linearly elastic systems resulting from the principle of superposition. The principle enables us to express the deflection of any point in a structure in terms of a constant coefficient and the applied loads. For example, a load P_1 applied at a point 1 in a linearly elastic body produces a deflection Δ_1 at the point given by

$$\Delta_1 = a_{11}P_1$$

in which the influence or flexibility coefficient a_{11} is defined as the deflection at the point 1 in the direction of P_1 , produced by a unit load at the point 1 applied in the direction of P_1 . Clearly, if the body supports a system of loads such as those shown in Fig. 1.18, each of the loads P_1, P_2, \dots, P_n contributes to the deflection at the point 1.

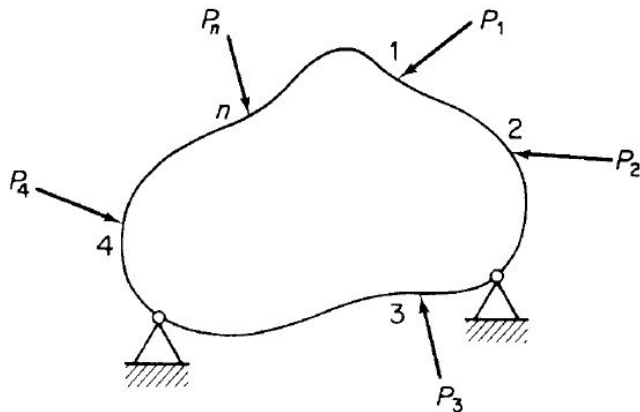


Figure 1.18 Linearly elastic body subjected to loads $P_1, P_2, P_3, \dots, P_n$.

Thus, the corresponding deflection Δ_1 at the point 1 (i.e., the total deflection in the direction of P_1 produced by all the loads) is then

$$\Delta_1 = a_{11}P_1 + a_{12}P_2 + \dots + a_{1n}P_n$$

where a_{12} is the deflection at the point 1 in the direction of P_1 , produced by a unit load at the point 2 in the direction of the load P_2 , and so on.

The corresponding deflections at the points of application of the complete system of loads are then

$$\left. \begin{aligned} \Delta_1 &= a_{11}P_1 + a_{12}P_2 + a_{13}P_3 + \dots + a_{1n}P_n \\ \Delta_2 &= a_{21}P_1 + a_{22}P_2 + a_{23}P_3 + \dots + a_{2n}P_n \\ \Delta_3 &= a_{31}P_1 + a_{32}P_2 + a_{33}P_3 + \dots + a_{3n}P_n \\ &\vdots \\ \Delta_n &= a_{n1}P_1 + a_{n2}P_2 + a_{n3}P_3 + \dots + a_{nn}P_n \end{aligned} \right\}$$

or, in matrix form

$$\begin{bmatrix} \Delta_1 \\ \Delta_2 \\ \Delta_3 \\ \vdots \\ \Delta_n \end{bmatrix} = \begin{bmatrix} a_{11} & a_{12} & a_{13} & \dots & a_{1n} \\ a_{21} & a_{22} & a_{23} & \dots & a_{2n} \\ a_{31} & a_{32} & a_{33} & \dots & a_{3n} \\ \vdots & \vdots & \vdots & & \vdots \\ a_{n1} & a_{n2} & a_{n3} & \dots & a_{nn} \end{bmatrix} \begin{bmatrix} P_1 \\ P_2 \\ P_3 \\ \vdots \\ P_n \end{bmatrix}$$

which may be written in shorthand matrix notation as

$$\{\Delta\} = [A]\{P\}$$

Suppose now that an elastic body is subjected to a gradually applied force P_1 at a point 1, and then, while P_1 remains in position, a force P_2 is gradually applied at another point 2. The total strain energy U of the body is given by

$$U_1 = \frac{P_1}{2}(a_{11}P_1) + \frac{P_2}{2}(a_{22}P_2) + P_1(a_{12}P_2)$$

The third term on the right-hand side of the above equation results from the additional work done by P_1 as it is displaced through a further distance $a_{12}P_2$ by the action of P_2 . If we now remove the loads and apply P_2 followed by P_1 , we have

$$U_2 = \frac{P_2}{2}(a_{22}P_2) + \frac{P_1}{2}(a_{11}P_1) + P_2(a_{21}P_1)$$

By the principle of superposition, the strain energy stored is independent of the order in which the loads are applied. Hence

$$U_1 = U_2$$

and it follows that

$$a_{12} = a_{21}$$

Thus, in its simplest form the reciprocal theorem states that

The deflection at a point 1 in a given direction due to a unit load at a point 2 in a second direction is equal to the deflection at the point 2 in the second direction due to a unit load at the point 1 in the first direction.

In a similar manner, we derive the relationship between moments and rotations, thus

The rotation at a point 1 due to a unit moment at a point 2 is equal to the rotation at the point 2 produced by a unit moment at the point 1.

Finally, we have

The rotation at a point 1 due to a unit load at a point 2 is numerically equal to the deflection at the point 2 in the direction of the unit load due to a unit moment at the point 1.

UNIT-II

THIN PLATE THEORY, STRUCTURAL INSTABILITY

BENDING OF THIN PLATES

Generally, we define a thin plate as a sheet of material whose thickness is small compared with its other dimensions but which is capable of resisting bending in addition to membrane forces. Such a plate forms a basic part of an aircraft structure, being, for example, the area of stressed skin bounded by adjacent stringers and ribs in a wing structure or by adjacent stringers and frames in a fuselage.

In this chapter, we shall investigate the effect of a variety of loading and support conditions on the small deflection of rectangular plates. Two approaches are presented: an —exact theory based on the solution of a differential equation and an energy method relying on the principle of the stationary value of the total potential energy of the plate and its applied loading.

PURE BENDING OF THIN PLATES

The thin rectangular plate of Fig. 2.1 is subjected to pure bending moments of intensity M_x and M_y per unit length uniformly distributed along its edges. The former bending moment is applied along the edges parallel to the y axis, and the latter along the edges parallel to the x axis. We shall assume that these bending moments are positive when they produce compression at the upper surface of the plate and tension at the lower.

If we further assume that the displacement of the plate in a direction parallel to the z axis is small compared with its thickness t and that sections which are plane before bending remain plane after bending, then, as in the case of simple beam theory, the middle plane of the plate does not deform during the bending and is therefore a *neutral plane*. We take the neutral plane as the reference plane for our system of axes.

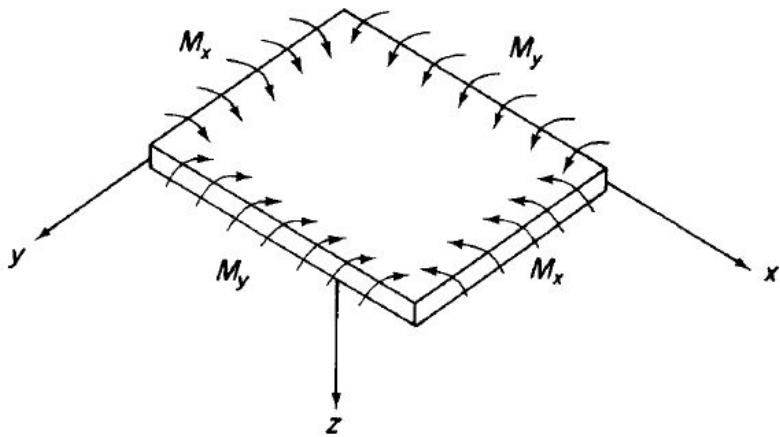


Figure 2.1 Plate subjected to pure bending.

Let us consider an element of the plate of side $\delta x \delta y$ and having a depth equal to the thickness t of the plate as shown in Fig. 2.2(a). Suppose that the radii of curvature of the neutral plane n are ρ_x and ρ_y in the xz and yz planes, respectively (Fig. 2.2(b)). Positive curvature of the plate corresponds to the positive bending moments, which produce displacements in the positive direction of the z or downward axis. Again, as in simple beam theory, the direct strains ε_x and ε_y corresponding to direct stresses

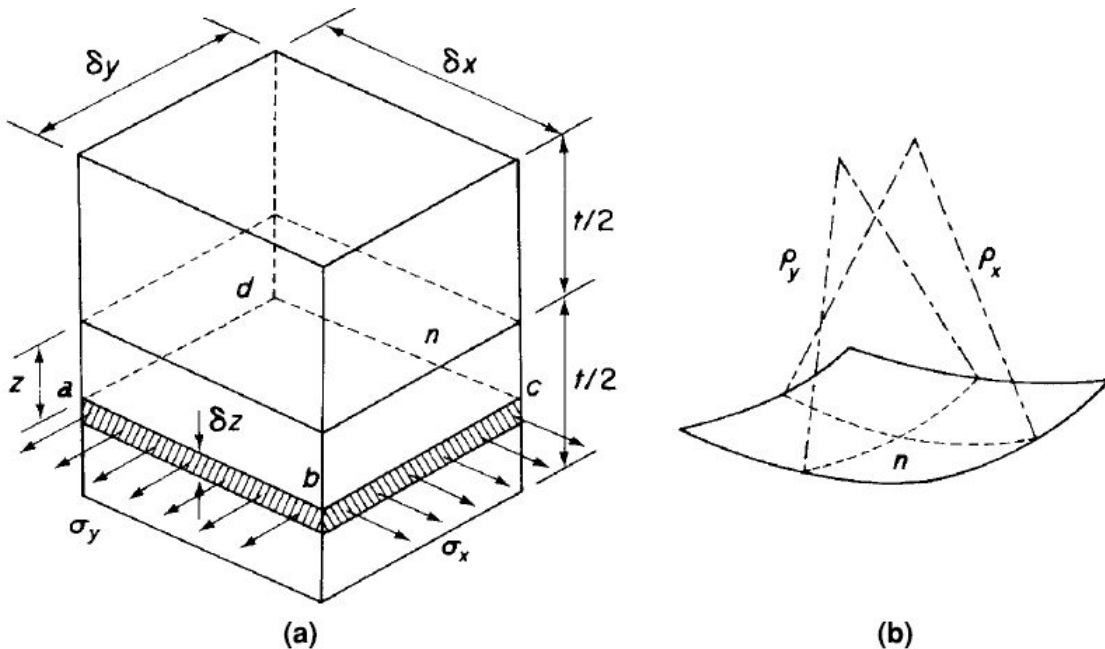


Figure 2.2 (a) Direct stress on lamina of plate element; (b) radii of curvature of neutral plane.

ζ_x and ζ_y of an elemental lamina of thickness δz a distance z below the neutral plane are given by

$$\varepsilon_x = \frac{z}{\rho_x} \quad \varepsilon_y = \frac{z}{\rho_y} \quad (2.1)$$

We know

$$\varepsilon_x = \frac{1}{E}(\sigma_x - \nu\sigma_y) \quad \varepsilon_y = \frac{1}{E}(\sigma_y - \nu\sigma_x) \quad (2.2)$$

Substituting for ε_x and ε_y from Eqs. (2.1) into (2.2) and rearranging gives

$$\left. \begin{aligned} \sigma_x &= \frac{Ez}{1-\nu^2} \left(\frac{1}{\rho_x} + \frac{\nu}{\rho_y} \right) \\ \sigma_y &= \frac{Ez}{1-\nu^2} \left(\frac{1}{\rho_y} + \frac{\nu}{\rho_x} \right) \end{aligned} \right\} \quad (2.3)$$

As would be expected from our assumption of plane sections remaining plane, the direct stresses vary linearly across the thickness of the plate, their magnitudes depending on the curvatures (i.e., bending moments) of the plate. The internal direct stress distribution on each vertical surface of the element must be in equilibrium with the applied bending moments. Thus,

$$M_x \delta y = \int_{-t/2}^{t/2} \sigma_x z \delta y dz$$

and

$$M_y \delta x = \int_{-t/2}^{t/2} \sigma_y z \delta x dz$$

Substituting for ζ_x and ζ_y from Eqs. (2.3) gives

$$M_x = \int_{-t/2}^{t/2} \frac{Ez^2}{1-\nu^2} \left(\frac{1}{\rho_x} + \frac{\nu}{\rho_y} \right) dz$$

$$M_y = \int_{-t/2}^{t/2} \frac{Ez^2}{1-\nu^2} \left(\frac{1}{\rho_y} + \frac{\nu}{\rho_x} \right) dz$$

Let

$$D = \int_{-t/2}^{t/2} \frac{Ez^2}{1-\nu^2} dz = \frac{Et^3}{12(1-\nu^2)}$$

Then,

$$M_x = D \left(\frac{1}{\rho_x} + \frac{\nu}{\rho_y} \right) \quad (2.5)$$

$$M_y = D \left(\frac{1}{\rho_y} + \frac{\nu}{\rho_x} \right) \quad (2.6)$$

in which D is known as the flexural rigidity of the plate.

If w is the deflection of any point on the plate in the z direction, then we may relate w to the curvature of the plate in the same manner as the well-known expression for beam curvature. Hence

$$\frac{1}{\rho_x} = -\frac{\partial^2 w}{\partial x^2} \quad \frac{1}{\rho_y} = -\frac{\partial^2 w}{\partial y^2}$$

the negative signs resulting from the fact that the centers of curvature occur above the plate in which region z is negative. Equations (2.5) and (2.6) then become

$$M_x = -D \left(\frac{\partial^2 w}{\partial x^2} + \nu \frac{\partial^2 w}{\partial y^2} \right) \quad (2.7)$$

$$M_y = -D \left(\frac{\partial^2 w}{\partial y^2} + \nu \frac{\partial^2 w}{\partial x^2} \right) \quad (2.8)$$

Equations (2.7) and (2.8) define the deflected shape of the plate provided that M_x and M_y are known. If either M_x or M_y is zero, then

$$\frac{\partial^2 w}{\partial x^2} = -\nu \frac{\partial^2 w}{\partial y^2} \quad \text{or} \quad \frac{\partial^2 w}{\partial y^2} = -\nu \frac{\partial^2 w}{\partial x^2}$$

and the plate has curvatures of opposite signs. The case of $M_y = 0$ is illustrated in Fig. 2.3. A surface possessing two curvatures of opposite sign is known as an anticlastic surface, as opposed to a synclastic surface, which has curvatures of the same sign. Further, if $M_x = M_y = M$, then from Eqs. (2.5) and (2.6)

$$\frac{1}{\rho_x} = \frac{1}{\rho_y} = \frac{1}{\rho}$$

Therefore, the deformed shape of the plate is spherical and of curvature

$$\frac{1}{\rho} = \frac{M}{D(1 + \nu)} \quad (2.9)$$

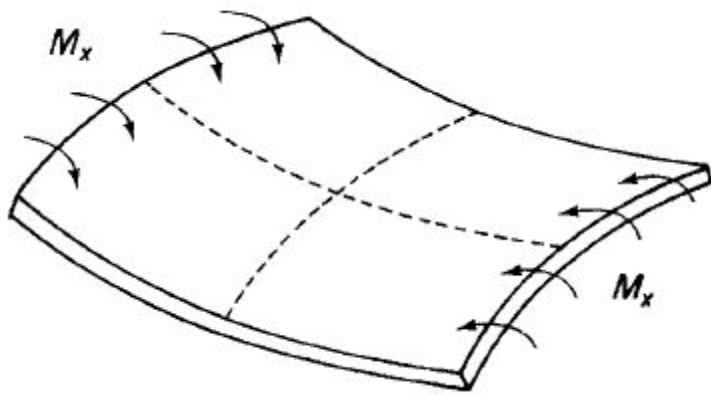


Figure 2.3 Anticlastic bending.

PLATES SUBJECTED TO BENDING AND TWISTING

In general, the bending moments applied to the plate will not be in planes perpendicular to its edges. Such bending moments, however, may be resolved in the normal manner into tangential and perpendicular components, as shown in Fig. 2.4. The perpendicular components are seen to be M_x and M_y as before, while the tangential components M_{xy} and M_{yx} (again these are moments per unit length) produce twisting of the plate about axes parallel to the x and y axes. The system of suffixes and the sign convention for these twisting moments must be clearly understood to avoid confusion. M_{xy} is a twisting moment intensity in a vertical x plane parallel to the y axis, whereas M_{yx} is a twisting moment intensity in a vertical y plane

parallel to the x axis. Note that the first suffix gives the direction of the axis of the twisting moment. We also define positive twisting moments as being clockwise when viewed along their axes in directions parallel to the positive directions of the corresponding x or y axis. In Fig. 2.4, therefore, all moment intensities are positive.

Since the twisting moments are tangential moments or torques, they are resisted by a system of horizontal shear stresses τ_{xy} , as shown in Fig. 2.6. From a consideration of complementary shear stresses (see Fig. 2.6), $M_{xy} = -M_{yx}$, so that we may represent a general moment application to the plate in terms of M_x , M_y , and M_{xy} as shown in Fig. 2.5(a).

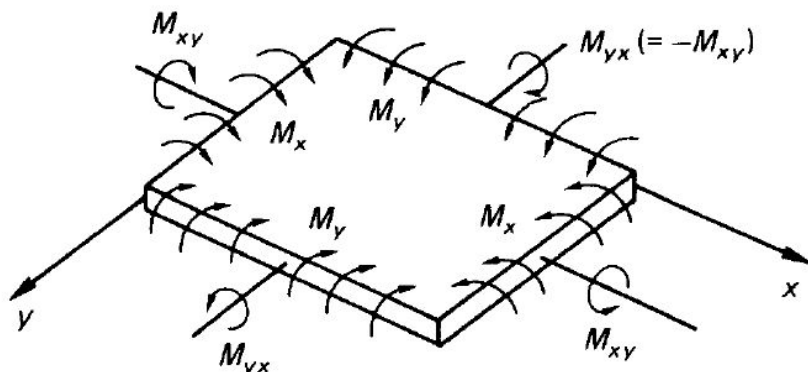


Figure 2.4 Plate subjected to bending and twisting.

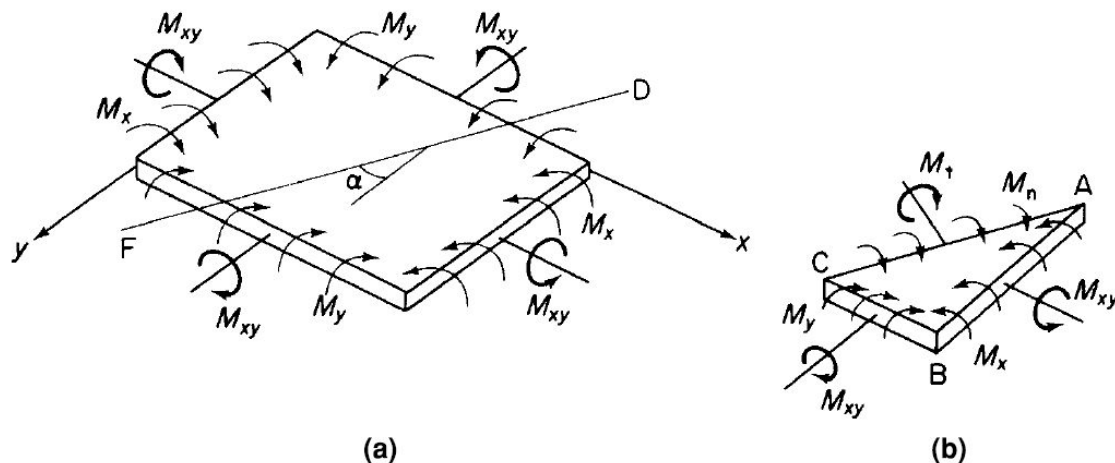


Figure 2.5 (a) Plate subjected to bending and twisting; (b) tangential and normal moments on an arbitrary plane.

These moments produce tangential and normal moments, M_t and M_n , on an arbitrarily chosen diagonal plane FD. We may express these moment intensities (in an analogous fashion to the complex stress systems of Section 1.6) in terms of M_x , M_y , and M_{xy} . Thus, for equilibrium of the triangular element ABC of Fig. 2.5(b) in a plane perpendicular to AC

$$M_n AC = M_x AB \cos \alpha + M_y BC \sin \alpha - M_{xy} AB \sin \alpha - M_{xy} BC \cos \alpha$$

giving

$$M_n = M_x \cos^2 \alpha + M_y \sin^2 \alpha - M_{xy} \sin 2\alpha \quad (2.10)$$

Similarly, for equilibrium in a plane parallel to CA

$$M_t AC = M_x AB \sin \alpha - M_y BC \cos \alpha + M_{xy} AB \cos \alpha - M_{xy} BC \sin \alpha$$

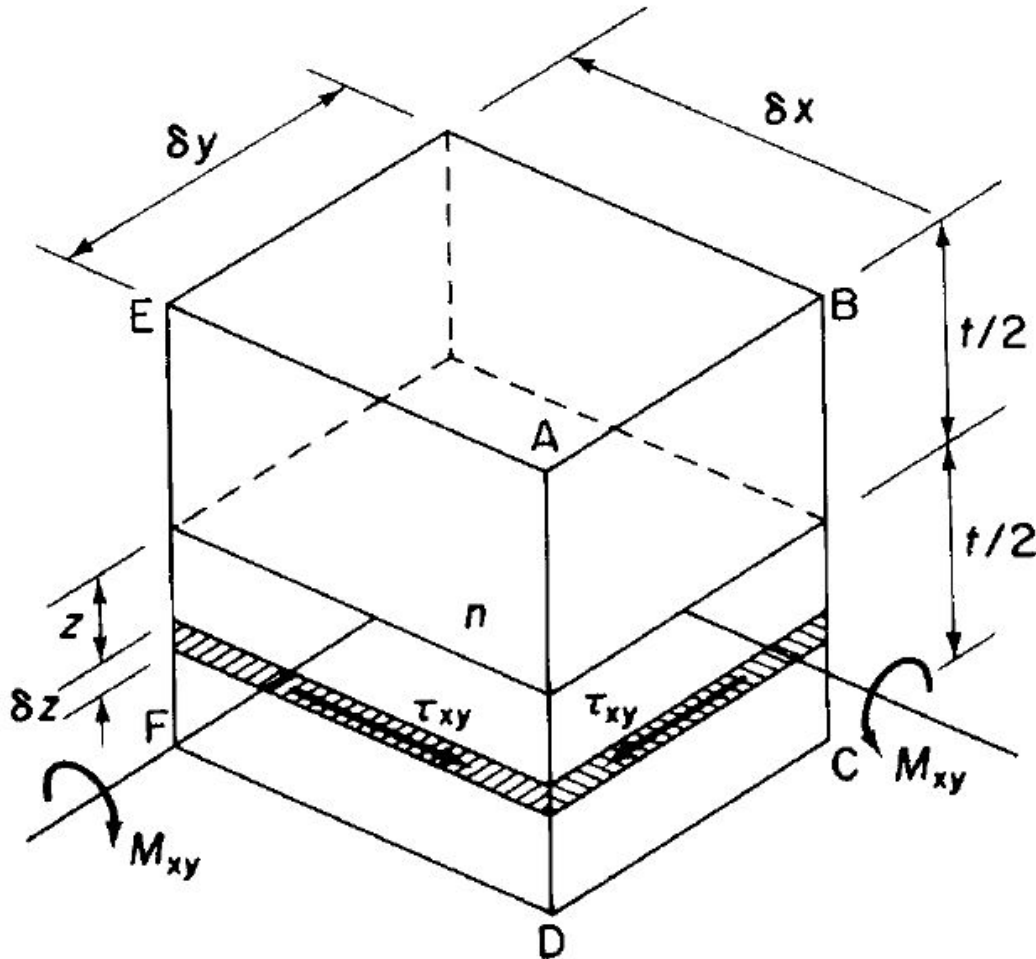


Figure 2.6 Complementary shear stresses due to twisting moments M_{xy} .

or

$$M_t = \frac{(M_x - M_y)}{2} \sin 2\alpha + M_{xy} \cos 2\alpha \quad (2.11)$$

We observe from Eq. (2.11) that there are two values of α , differing by 90° and given by

$$\tan 2\alpha = -\frac{2M_{xy}}{M_x - M_y}$$

for which $M_t=0$, leaving normal moments of intensity M_n on two mutually perpendicular planes. These moments are termed *principal moments*, and their corresponding curvatures are called *principal curvatures*. For a plate subjected to pure bending and twisting in which M_x , M_y , and M_{xy} are invariable throughout the plate, the principal moments are the algebraically greatest and least moments in the plate. It follows that there are no shear stresses on these planes and that the corresponding direct stresses, for a given value of z and moment intensity, are the algebraically greatest and least values of direct stress in the plate.

Let us now return to the loaded plate of Fig. 2.5(a). We have established, in Eqs. (2.7) and (2.8), the relationships between the bending moment intensities M_x and M_y and the deflection w of the plate. The next step is to relate the twisting moment M_{xy} to w . From the principle of superposition, we may consider M_{xy} acting separately from M_x and M_y . As stated previously, M_{xy} is resisted by a system of horizontal complementary shear stresses on the vertical faces of sections taken throughout the thickness of the plate parallel to the x and y axes. Consider an element of the plate formed by such sections, as shown in Fig. 2.6. The complementary shear stresses on a lamina of the element a distance z below the neutral plane are, in accordance with the sign convention of Section 1.2, τ_{xy} (Refer T.H.G. megson). Therefore, on the face ABCD

$$M_{xy}\delta y = - \int_{-t/2}^{t/2} \tau_{xy}\delta yz dz$$

and on the face ADFE

$$M_{xy}\delta x = - \int_{-t/2}^{t/2} \tau_{xy}\delta xz dz$$

giving

$$M_{xy} = - \int_{-t/2}^{t/2} \tau_{xy}z dz$$

or in terms of the shear strain γ_{xy} and modulus of rigidity G

$$M_{xy} = -G \int_{-t/2}^{t/2} \gamma_{xy}z dz \quad (2.12)$$

the shear strain γ_{xy} is given by

$$\gamma_{xy} = \frac{\partial v}{\partial x} + \frac{\partial u}{\partial y}$$

We require, of course, to express γ_{xy} in terms of the deflection w of the plate; this may be accomplished as follows. An element taken through the thickness of the plate will suffer rotations equal to $\partial w / \partial x$ and

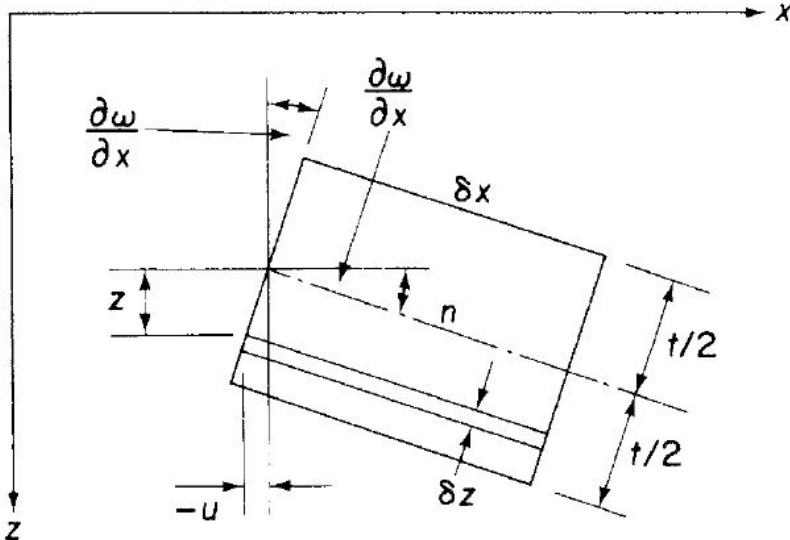


Figure 2.7 Determination of shear strain γ_{xy} .

$\partial w / \partial y$ in the xz and yz planes, respectively. Considering the rotation of such an element in the xz plane, as shown in Fig. 2.7, we see that the displacement u in the x direction of a point a distance z below the neutral plane is

$$u = -\frac{\partial w}{\partial x} z$$

Similarly, the displacement v in the y direction is

$$v = -\frac{\partial w}{\partial y} z$$

Hence, substituting for u and v in the expression for γ_{xy} , we have

$$\gamma_{xy} = -2z \frac{\partial^2 w}{\partial x \partial y} \quad (2.13)$$

from which Eq. 2.12

$$M_{xy} = G \int_{-t/2}^{t/2} 2z^2 \frac{\partial^2 w}{\partial x \partial y} dz$$

or

$$M_{xy} = \frac{Gt^3}{6} \frac{\partial^2 w}{\partial x \partial y}$$

Replacing G by the expression $E/2(1+\nu)$

$$M_{xy} = \frac{Et^3}{12(1+\nu)} \frac{\partial^2 w}{\partial x \partial y}$$

Multiplying the numerator and denominator of this equation by the factor $(1-\nu)$ yields

$$M_{xy} = D(1-\nu) \frac{\partial^2 w}{\partial x \partial y}$$

(2.14)

Equations (2.7), (2.8), and (2.14) relate the bending and twisting moments to the plate deflection and are analogous to the bending moment-curvature relationship for a simple beam.

PLATES SUBJECT TO A DISTRIBUTED TRANSVERSE LOAD

The relationships between bending and twisting moments and plate deflection are now employed in establishing the general differential equation for the solution of a thin rectangular plate, supporting a distributed transverse load of intensity q per unit area (see Fig. 2.8). The distributed load may, in general, vary over the surface of the plate and is, therefore, a function of x and y . We assume, as in the preceding analysis, that the middle plane of the plate is the neutral plane and that the plate deforms such that plane sections remain plane after bending. This latter assumption introduces an apparent inconsistency in the theory. For plane sections to remain plane, the shear strains γ_{xz} and γ_{yz} must be zero. However, the transverse load produces transverse shear forces (and therefore stresses) as shown in Fig. 2.9. We therefore assume that although $\gamma_{xz} = \gamma_{xz}/G$ and $\gamma_{yz} = \gamma_{yz}/G$ are negligible, the corresponding shear forces are of the same order of magnitude as the applied load q and the moments M_x , M_y , and M_{xy} . This assumption is analogous to that made in a slender beam theory in which shear strains are ignored.

The element of plate shown in Fig. 2.9 supports bending and twisting moments as previously described and, in addition, vertical shear forces Q_x and Q_y per unit length on faces perpendicular to the x and y axes, respectively. The variation of shear stresses τ_{xz} and τ_{yz} along the small edges δx , δy of the element is neglected, and the resultant shear forces $Q_x \delta y$ and $Q_y \delta x$ are assumed to act through the

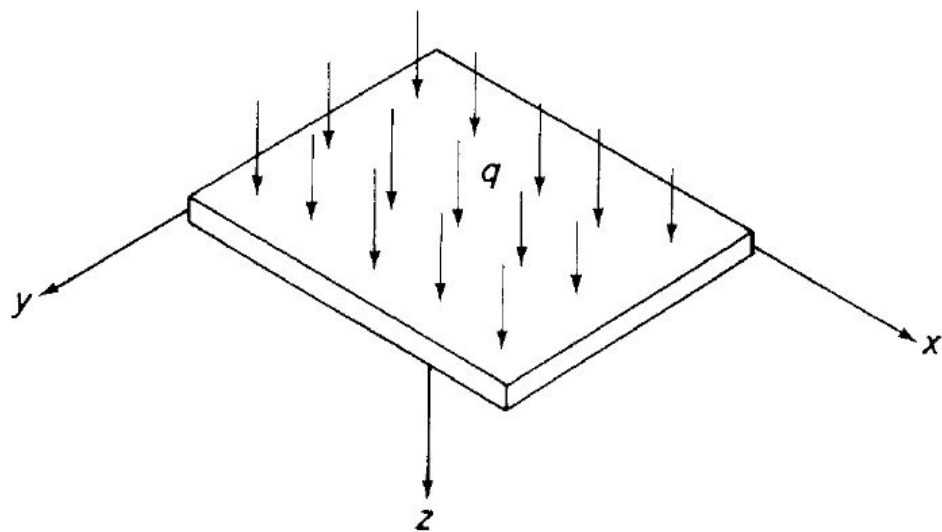


Figure 2.8 Plate supporting a distributed transverse load.

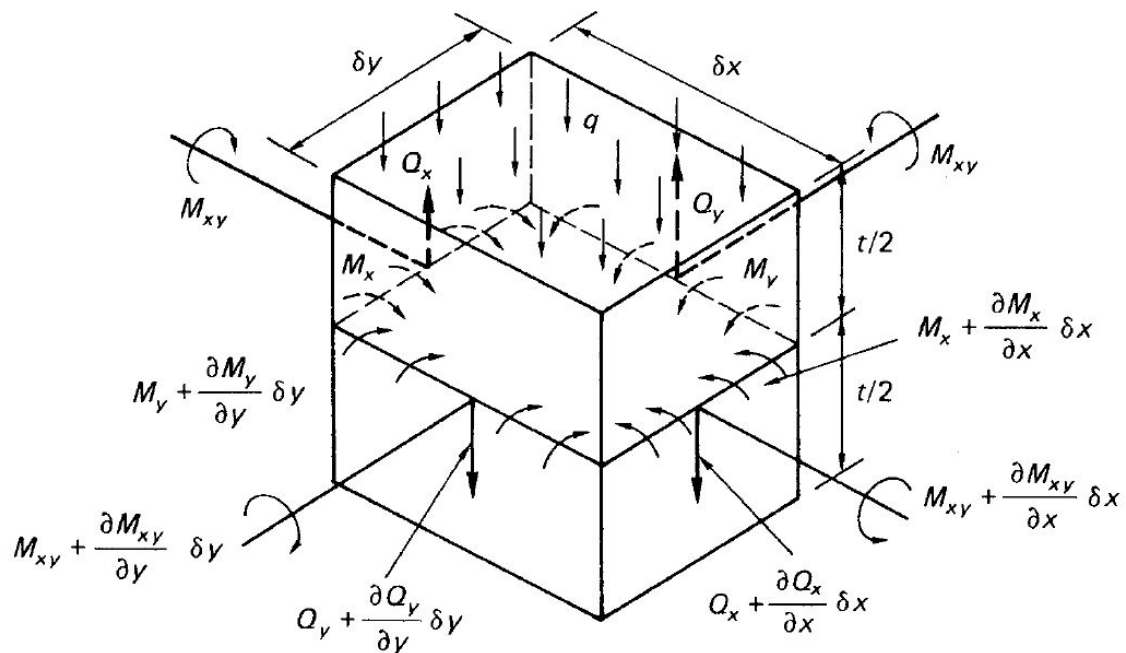


Figure 2.9 Plate element subjected to bending, twisting, and transverse loads.

centroid of the faces of the element. From the previous sections,

$$M_x = \int_{-t/2}^{t/2} \sigma_x z dz \quad M_y = \int_{-t/2}^{t/2} \sigma_y z dz \quad M_{xy} = (-M_{yx}) = - \int_{-t/2}^{t/2} \tau_{xy} z dz$$

In a similar fashion,

$$Q_x = \int_{-t/2}^{t/2} \tau_{xz} dz \quad Q_y = \int_{-t/2}^{t/2} \tau_{yz} dz$$
(2.15)

For equilibrium of the element parallel to Oz and assuming that the weight of the plate is included in q

$$\left(Q_x + \frac{\partial Q_x}{\partial x} \delta x\right) \delta y - Q_x \delta y + \left(Q_y + \frac{\partial Q_y}{\partial y} \delta y\right) \delta x - Q_y \delta x + q \delta x \delta y = 0$$

or, after simplification,

$$\frac{\partial Q_x}{\partial x} + \frac{\partial Q_y}{\partial y} + q = 0$$
(2.16)

Taking moments about the x axis

$$M_{xy} \delta y - \left(M_{xy} + \frac{\partial M_{xy}}{\partial x} \delta x\right) \delta y - M_y \delta x + \left(M_y + \frac{\partial M_y}{\partial y} \delta y\right) \delta x - \left(Q_y + \frac{\partial Q_y}{\partial y} \delta y\right) \delta x \delta y + Q_x \frac{\delta y^2}{2} - \left(Q_x + \frac{\partial Q_x}{\partial x} \delta x\right) \frac{\delta y^2}{2} - q \delta x \frac{\delta y^2}{2} = 0$$

Simplifying this equation and neglecting small quantities of a higher order than those retained give

$$(2.17) \quad \frac{\partial M_{xy}}{\partial x} - \frac{\partial M_y}{\partial y} + Q_y = 0$$

Similarly, taking moments about the y axis, we have

$$\frac{\partial M_{xy}}{\partial y} - \frac{\partial M_x}{\partial x} + Q_x = 0 \quad (2.18)$$

Substituting in Eq. (2.16) for Q_x and Q_y from Eqs. (2.18) and (2.17), we obtain

$$\frac{\partial^2 M_x}{\partial x^2} - \frac{\partial^2 M_{xy}}{\partial x \partial y} + \frac{\partial^2 M_y}{\partial y^2} - \frac{\partial^2 M_{xy}}{\partial x \partial y} = -q$$

or

$$\frac{\partial^2 M_x}{\partial x^2} - 2 \frac{\partial^2 M_{xy}}{\partial x \partial y} + \frac{\partial^2 M_y}{\partial y^2} = -q \quad (2.19)$$

Replacing M_x , M_{xy} , and M_y in Eq. (2.19) from Eqs. (2.7), (2.14), and (2.8) gives

$$\frac{\partial^4 w}{\partial x^4} + 2 \frac{\partial^4 w}{\partial x^2 \partial y^2} + \frac{\partial^4 w}{\partial y^4} = \frac{q}{D} \quad (2.20)$$

This equation may also be written as

$$\left(\frac{\partial^2}{\partial x^2} + \frac{\partial^2}{\partial y^2} \right) \left(\frac{\partial^2 w}{\partial x^2} + \frac{\partial^2 w}{\partial y^2} \right) w = \frac{q}{D}$$

or

$$\left(\frac{\partial^2}{\partial x^2} + \frac{\partial^2}{\partial y^2} \right)^2 w = \frac{q}{D}$$

The operator $(\partial^2/\partial x^2 + \partial^2/\partial y^2)$ is the well-known Laplace operator in two dimensions and is sometimes written as ∇^2 . Thus,

$$(\nabla^2)^2 w = \frac{q}{D}$$

Generally, the transverse distributed load q is a function of x and y so that the determination of the deflected form of the plate reduces to obtaining a solution of Eq. (2.20), which satisfies the known boundary conditions of the problem. The bending and twisting moments follow from Eqs. (2.7), (2.8), and (2.14), and the shear forces per unit length Q_x and Q_y are found from Eqs. (2.17) and (2.18) by substitution for M_x , M_y , and M_{xy} in terms of the deflection w of the plate; thus,

$$Q_x = \frac{\partial M_x}{\partial x} - \frac{\partial M_{xy}}{\partial y} = -D \frac{\partial}{\partial x} \left(\frac{\partial^2 w}{\partial x^2} + \frac{\partial^2 w}{\partial y^2} \right) \quad (2.21)$$

$$Q_y = \frac{\partial M_y}{\partial y} - \frac{\partial M_{xy}}{\partial x} = -D \frac{\partial}{\partial y} \left(\frac{\partial^2 w}{\partial x^2} + \frac{\partial^2 w}{\partial y^2} \right) \quad (2.22)$$

Direct and shear stresses are then calculated from the relevant expressions relating them to M_x , M_y , M_{xy} , Q_x , and Q_y . Before discussing the solution of Eq. (2.20) for particular cases, we shall establish boundary conditions for various types of edge support.

COMBINED BENDING AND IN-PLANE LOADING OF A THIN RECTANGULAR PLATE

So far our discussion has been limited to small deflections of thin plates produced by different forms of transverse loading. In these cases, we assumed that the middle or neutral plane of the plate remained unstressed. Additional in-plane tensile, compressive, or shear loads will produce stresses in the middle plane, and these, if of sufficient magnitude, will affect the bending of the plate. Where the in-plane stresses are small compared with the critical buckling stresses, it is sufficient to consider the two systems separately; the total stresses are then obtained by superposition. On the other hand, if the in-plane stresses are not small, then their effect on the bending of the plate must be considered.

The elevation and plan of a small element $\delta x \delta y$ of the middle plane of a thin deflected plate are shown in Fig. 2.12. Direct and shear forces per unit length produced by the in-plane loads are given the notation N_x , N_y , and N_{xy} and are assumed to be acting in positive senses in the directions shown. Since there are no resultant forces in the x or y directions from the transverse loads (see Fig. 2.9), we need only to include the in-plane loads shown in Fig. 2.12 when considering the equilibrium of the element in these directions. For equilibrium parallel to Ox ,

$$\begin{aligned} & \left(N_x + \frac{\partial N_x}{\partial x} \delta x \right) \delta y \cos \left(\frac{\partial w}{\partial x} + \frac{\partial^2 w}{\partial x^2} \delta x \right) - N_x \delta y \cos \frac{\partial w}{\partial x} \\ & + \left(N_{yx} + \frac{\partial N_{yx}}{\partial y} \delta y \right) \delta x - N_{yx} \delta x = 0 \end{aligned}$$

For small deflections, $\partial w / \partial x$ and $(\partial w / \partial x) + (\partial^2 w / \partial x^2) \delta x$ are small, and the cosines of these angles are therefore approximately equal to one. The equilibrium equation thus simplifies to

$$\frac{\partial N_x}{\partial x} + \frac{\partial N_{yx}}{\partial y} = 0 \quad (2.23)$$

Similarly, for equilibrium in the

y direction, we have

$$\frac{\partial N_y}{\partial y} + \frac{\partial N_{xy}}{\partial x} = 0 \quad (2.24)$$

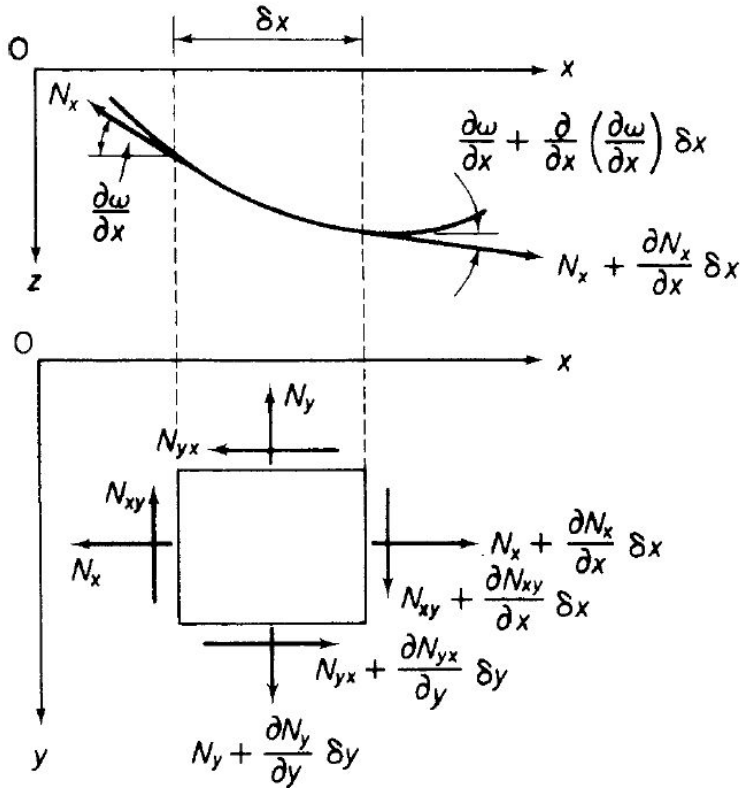


Figure 2.12 In-plane forces on plate element.

Note that the components of the in-plane shear loads per unit length are, to a first order of approximation, the value of the shear load multiplied by the projection of the element on the relevant axis.

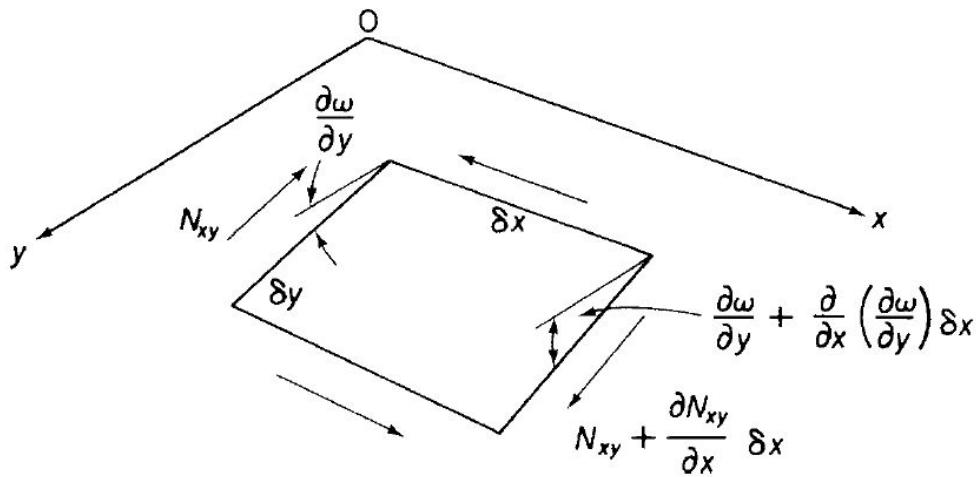


Figure 2.13 Component of shear loads in the z direction.

The determination of the contribution of the shear loads to the equilibrium of the element in the z direction is complicated by the fact that the element possesses curvature in both xz and yz planes. Therefore, from Fig. 7.13, the component in the z direction due to the N_{xy} shear loads only is

$$\left(N_{xy} + \frac{\partial N_{xy}}{\partial x} \delta x \right) \delta y \left(\frac{\partial w}{\partial y} + \frac{\partial^2 w}{\partial x \partial y} \delta x \right) - N_{xy} \delta y \frac{\partial w}{\partial y}$$

or

$$N_{xy} \frac{\partial^2 w}{\partial x \partial y} \delta x \delta y + \frac{\partial N_{xy}}{\partial x} \frac{\partial w}{\partial y} \delta x \delta y$$

neglecting terms of a lower order. Similarly, the contribution of N_{yx} is

$$N_{yx} \frac{\partial^2 w}{\partial x \partial y} \delta x \delta y + \frac{\partial N_{yx}}{\partial y} \frac{\partial w}{\partial x} \delta x \delta y$$

The components arising from the direct forces per unit length are readily obtained from Fig. 2.12, namely,

$$\left(N_x + \frac{\partial N_x}{\partial x} \delta x \right) \delta y \left(\frac{\partial w}{\partial x} + \frac{\partial^2 w}{\partial x^2} \delta x \right) - N_x \delta y \frac{\partial w}{\partial x}$$

or

$$N_x \frac{\partial^2 w}{\partial x^2} \delta x \delta y + \frac{\partial N_x}{\partial x} \frac{\partial w}{\partial x} \delta x \delta y$$

and similarly

$$N_y \frac{\partial^2 w}{\partial y^2} \delta x \delta y + \frac{\partial N_y}{\partial y} \frac{\partial w}{\partial y} \delta x \delta y$$

The total force in the z direction is found from the summation of these expressions and is

$$\begin{aligned} & N_x \frac{\partial^2 w}{\partial x^2} \delta x \delta y + \frac{\partial N_x}{\partial x} \frac{\partial w}{\partial x} \delta x \delta y + N_y \frac{\partial^2 w}{\partial y^2} \delta x \delta y + \frac{\partial N_y}{\partial y} \frac{\partial w}{\partial y} \delta x \delta y \\ & + \frac{\partial N_{xy}}{\partial x} \frac{\partial w}{\partial y} \delta x \delta y + 2N_{xy} \frac{\partial^2 w}{\partial x \partial y} \delta x \delta y + \frac{\partial N_{xy}}{\partial y} \frac{\partial w}{\partial x} \delta x \delta y \end{aligned}$$

in which N_{yx} is equal to and is replaced by N_{xy} . Using Eqs. (2.23) and (2.24), we reduce this expression to

$$\left(N_x \frac{\partial^2 w}{\partial x^2} + N_y \frac{\partial^2 w}{\partial y^2} + 2N_{xy} \frac{\partial^2 w}{\partial x \partial y} \right) \delta x \delta y$$

Therefore, the governing differential equation for a thin plate supporting transverse and in-plane loads is,

$$\frac{\partial^4 w}{\partial x^4} + 2 \frac{\partial^4 w}{\partial x^2 \partial y^2} + \frac{\partial^4 w}{\partial y^4} = \frac{1}{D} \left(q + N_x \frac{\partial^2 w}{\partial x^2} + N_y \frac{\partial^2 w}{\partial y^2} + 2N_{xy} \frac{\partial^2 w}{\partial x \partial y} \right)$$

BENDING OF THIN PLATES HAVING A SMALL INITIAL CURVATURE

Suppose that a thin plate has an initial curvature so that the deflection of any point in its middle plane is w_0 . We assume that w_0 is small compared with the thickness of the plate. The application of transverse and in-plane loads will cause the plate to deflect a further amount w_1 so that the total deflection is then $w = w_0 + w_1$. However, in the derivation of Eq. (2.25), we note that the left-hand side was obtained from expressions for bending moments which themselves depend on the change of curvature. We therefore use the deflection w_1 on the left-hand side, not w . The effect on bending of the in-plane forces depends on the total deflection w so that we write Eq. (2.25)

$$\begin{aligned} & \frac{\partial^4 w_1}{\partial x^4} + 2 \frac{\partial^4 w_1}{\partial x^2 \partial y^2} + \frac{\partial^4 w_1}{\partial y^4} \\ &= \frac{1}{D} \left[q + N_x \frac{\partial^2 (w_0 + w_1)}{\partial x^2} + N_y \frac{\partial^2 (w_0 + w_1)}{\partial y^2} + 2N_{xy} \frac{\partial^2 (w_0 + w_1)}{\partial x \partial y} \right] \end{aligned} \quad (2.26)$$

The effect of an initial curvature on deflection is therefore equivalent to the application of a transverse load of intensity

$$N_x \frac{\partial^2 w_0}{\partial x^2} + N_y \frac{\partial^2 w_0}{\partial y^2} + 2N_{xy} \frac{\partial^2 w_0}{\partial x \partial y}$$

Thus, in-plane loads alone produce bending, provided there is an initial curvature.

Assuming that the initial form of the deflected plate is

$$w_0 = \sum_{m=1}^{\infty} \sum_{n=1}^{\infty} A_{mn} \sin \frac{m\pi x}{a} \sin \frac{n\pi y}{b} \quad (2.27)$$

then by substitution in Eq. (7.34), we find that if N_x is compressive and $N_y = N_{xy} = 0$,

$$w_1 = \sum_{m=1}^{\infty} \sum_{n=1}^{\infty} B_{mn} \sin \frac{m\pi x}{a} \sin \frac{n\pi y}{b} \quad (2.28)$$

where

ENERGY METHOD FOR THE BENDING OF THIN PLATES

Two types of solution are obtainable for thin plate bending problems by the application of the principle of the stationary value of the total potential energy of the plate and its external loading. The first, in which the form of the deflected shape of the plate is known, produces an exact solution; the second, the Rayleigh-Ritz method, assumes an approximate deflected shape in the form of a series having a finite number of terms chosen to satisfy the boundary conditions of the problem and also to give the kind of deflection pattern expected.

Strain Energy Produced by Bending and Twisting

In thin plate analysis, we are concerned with deflections normal to the loaded surface of the plate. These, as in the case of slender beams, are assumed to be primarily due to bending action so that the effects of shear strain and shortening or stretching of the middle plane of the plate are ignored. Therefore, it is sufficient for us to calculate the strain energy produced by bending and twisting only as this will be applicable, for the reason of the preceding assumption, to all loading cases. It must be remembered that we are only neglecting the contributions of shear and direct strains on the deflection of the plate; the stresses producing them must not be ignored.

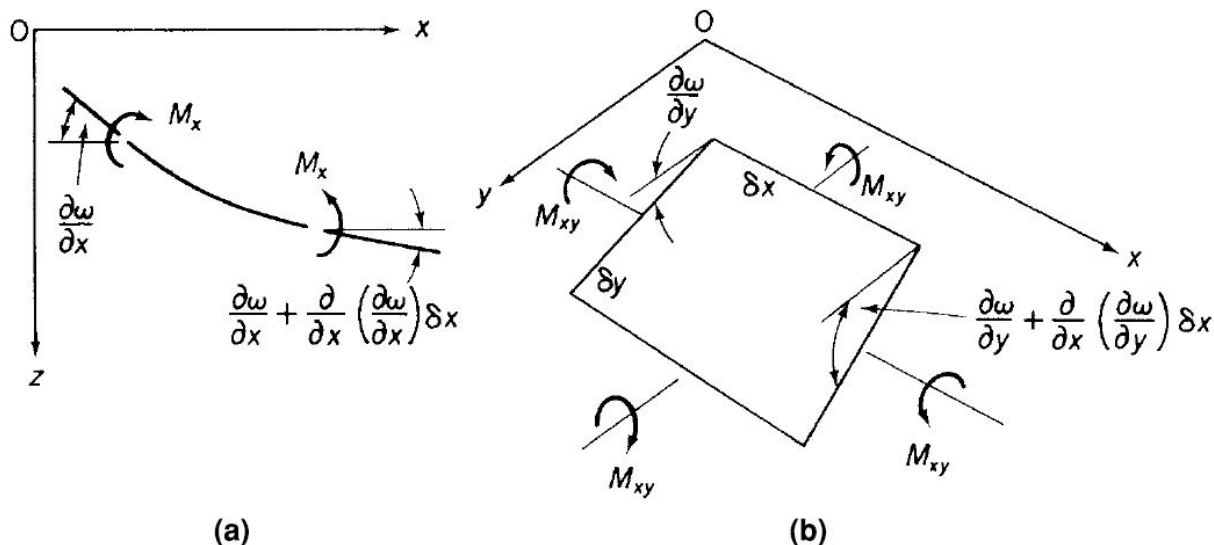


Figure 2.14 (a) Strain energy of element due to bending; (b) strain energy due to twisting.

Consider the element $\delta x \times \delta y$ of a thin plate $a \times b$ shown in elevation in the xz -plane in Fig. 2.14(a). Bending moments M_x per unit length applied to its δy edge produce a change in slope between its ends equal to $(\partial^2 w / \partial x^2) \delta x$. However, since we regard the moments M_x as positive in the sense shown, then this change in slope, or relative rotation, of the ends of the element is negative as the slope decreases with increasing x . The bending strain energy due to M_x is then

$$\frac{1}{2}M_x\delta y \left(-\frac{\partial^2 w}{\partial x^2} \delta x \right)$$

Similarly, in the yz plane the contribution of M_y to the bending strain energy is

$$\frac{1}{2}M_y\delta x \left(-\frac{\partial^2 w}{\partial y^2} \delta y \right)$$

The strain energy due to the twisting moment per unit length, M_{xy} , applied to the δy edges of the element, is obtained from Fig. 7.14(b). The relative rotation of the δy edges is $(\partial^2 w / \partial x \partial y) \delta x$ so that the corresponding strain energy is

$$\frac{1}{2}M_{xy}\delta y \frac{\partial^2 w}{\partial x \partial y} \delta x$$

Finally, the contribution of the twisting moment M_{xy} on the δx edges is, in a similar fashion,

$$\frac{1}{2}M_{xy}\delta x \frac{\partial^2 w}{\partial x \partial y} \delta y$$

The total strain energy of the element from bending and twisting is thus

$$\frac{1}{2} \left(-M_x \frac{\partial^2 w}{\partial x^2} - M_y \frac{\partial^2 w}{\partial y^2} + 2M_{xy} \frac{\partial^2 w}{\partial x \partial y} \right) \delta x \delta y$$

Substitution for M_x , M_y , and M_{xy} from Eqs. (7.7), (7.8), and (7.14) gives the total strain energy of the element as

$$\frac{D}{2} \left[\left(\frac{\partial^2 w}{\partial x^2} \right)^2 + \left(\frac{\partial^2 w}{\partial y^2} \right)^2 + 2\nu \frac{\partial^2 w}{\partial x^2} \frac{\partial^2 w}{\partial y^2} + 2(1-\nu) \left(\frac{\partial^2 w}{\partial x \partial y} \right)^2 \right] \delta x \delta y$$

which on rearranging becomes

$$\frac{D}{2} \left\{ \left(\frac{\partial^2 w}{\partial x^2} + \frac{\partial^2 w}{\partial y^2} \right)^2 - 2(1-\nu) \left[\frac{\partial^2 w}{\partial x^2} \frac{\partial^2 w}{\partial y^2} - \left(\frac{\partial^2 w}{\partial x \partial y} \right)^2 \right] \right\} \delta x \delta y$$

Hence, the total strain energy U of the rectangular plate $a \times b$ is

$$U = \frac{D}{2} \int_0^a \int_0^b \left\{ \left(\frac{\partial^2 w}{\partial x^2} + \frac{\partial^2 w}{\partial y^2} \right)^2 - 2(1-\nu) \left[\frac{\partial^2 w}{\partial x^2} \frac{\partial^2 w}{\partial y^2} - \left(\frac{\partial^2 w}{\partial x \partial y} \right)^2 \right] \right\} dx dy \quad (2.29)$$

Note that if the plate is subject to pure bending only, then $M_{xy}=0$, and $\partial^2 w / \partial x \partial y = 0$, so that Eq. (2.29) simplifies to

$$U = \frac{D}{2} \int_0^a \int_0^b \left[\left(\frac{\partial^2 w}{\partial x^2} \right)^2 + \left(\frac{\partial^2 w}{\partial y^2} \right)^2 + 2\nu \frac{\partial^2 w}{\partial x^2} \frac{\partial^2 w}{\partial y^2} \right] dx dy \quad (2.30)$$

BUCKLING OF THIN PLATES

A thin plate may buckle in a variety of modes depending on its dimensions, the loading, and the method of support. Usually, however, buckling loads are much lower than those likely to cause failure in the material of the plate. The simplest form of buckling arises when compressive loads are applied to simply supported opposite edges and the unloaded edges are free, as shown in Fig. 9.1. A thin plate in this configuration behaves in exactly the same way as a pin-ended column so that the critical load is that predicted by the Euler theory. Once this critical load is reached, the plate is incapable of supporting any further load. This is not the case, however, when the unloaded edges are supported against displacement out of the xy -plane. Buckling, for such plates, takes the form of a bulging displacement of the central region of the plate, while the parts adjacent to the supported edges remain straight. These parts enable the plate to resist higher loads, which is an important factor in aircraft design.

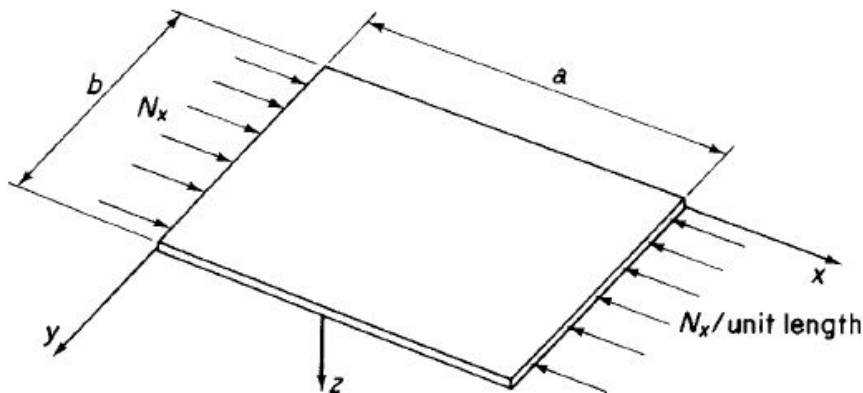


Figure 2.15 Buckling of a thin flat plate.

At this stage, we are not concerned with this postbuckling behavior but rather with the prediction of the critical load which causes the initial bulging of the central area of the plate. For the analysis, we may conveniently use the method of total potential energy, since we have already, derived expressions for strain and potential energy corresponding to various load and support configurations. In these expressions, we assumed that the displacement of the plate comprises bending deflections only and that these are small compared with the thickness of the plate. These restrictions therefore apply in the subsequent theory.

First, we consider the relatively simple case of the thin plate of Fig. 2.15, loaded as shown, but simply supported along all four edges. We have seen that its true deflected shape may be represented by the infinite double trigonometrical series

$$w = \sum_{m=1}^{\infty} \sum_{n=1}^{\infty} A_{mn} \sin \frac{m\pi x}{a} \sin \frac{n\pi y}{b}$$

Also, the total potential energy of the plate is

$$\begin{aligned} U + V = & \frac{1}{2} \int_0^a \int_0^b \left[D \left\{ \left(\frac{\partial^2 w}{\partial x^2} + \frac{\partial^2 w}{\partial y^2} \right)^2 \right. \right. \\ & \left. \left. - 2(1-\nu) \left[\frac{\partial^2 w}{\partial x^2} \frac{\partial^2 w}{\partial y^2} - \left(\frac{\partial^2 w}{\partial x \partial y} \right)^2 \right] \right\} - N_x \left(\frac{\partial w}{\partial x} \right)^2 \right] dx dy \end{aligned} \quad (2.31)$$

The integration of Eq. (9.1) on substituting for w is similar

Thus,

$$U + V = \frac{\pi^4 abD}{8} \sum_{m=1}^{\infty} \sum_{n=1}^{\infty} A_{mn}^2 \left(\frac{m^2}{a^2} + \frac{n^2}{b^2} \right) - \frac{\pi^2 b}{8a} N_x \sum_{m=1}^{\infty} \sum_{n=1}^{\infty} m^2 A_{mn}^2 \quad (2.32)$$

The total potential energy of the plate has a stationary value in the neutral equilibrium of its buckled state (i.e., $N_x = N_{x,CR}$). Therefore, differentiating Eq. (2.32) with respect to each unknown coefficient A_{mn} , we have

$$\frac{\partial(U + V)}{\partial A_{mn}} = \frac{\pi^4 abD}{4} A_{mn} \left(\frac{m^2}{a^2} + \frac{n^2}{b^2} \right)^2 - \frac{\pi^2 b}{4a} N_{x,CR} m^2 A_{mn} = 0$$

and for a nontrivial solution

$$N_{x,CR} = \pi^2 a^2 D \frac{1}{m^2} \left(\frac{m^2}{a^2} + \frac{n^2}{b^2} \right)^2 \quad (2.33)$$

We observe from Eq. (2.33) that each term in the infinite series for displacement corresponds, as in the case of a column, to a different value of critical load (note the problem is an eigenvalue problem). The lowest value of critical load evolves from some critical combination of integer's m and n —that is, the number of half-waves in the x and y directions, and the plate dimensions. Clearly $n = 1$ gives a minimum value so that no matter what the values of m, a , and b , the plate buckles into a half sine wave in the y direction. Thus, we may write Eq. (2.33) as minimum value so that no matter what the values of m, a , and b , the plate buckles into a half sine wave in the y direction. Thus, we may write Eq. (2.33) as

$$N_{x,CR} = \pi^2 a^2 D \frac{1}{m^2} \left(\frac{m^2}{a^2} + \frac{1}{b^2} \right)^2$$

or

$$N_{x,CR} = \frac{k\pi^2 D}{b^2} \quad (2.24)$$

where the plate *buckling coefficient k* is given by the minimum value of

$$k = \left(\frac{mb}{a} + \frac{a}{mb} \right)^2 \quad (2.25)$$

for a given value of a/b . To determine the minimum value of k for a given value of a/b , we plot k as a function of a/b for different values of m as shown by the dotted curves in Fig. 2.16. The minimum value of k is obtained from the lower envelope of the curves shown solid in the figure.

It can be seen that m varies with the ratio a/b and that k and the buckling load are a minimum when $k = 4$ at values of $a/b = 1, 2, 3, \dots$. As a/b becomes large, k approaches 4 so that long narrow plates tend to buckle into a series of squares.

The transition from one buckling mode to the next may be found by equating values of k for the m and $m+1$ curves. Hence,

$$\frac{mb}{a} + \frac{a}{mb} = \frac{(m+1)b}{a} + \frac{a}{(m+1)b}$$

giving

$$\frac{a}{b} = \sqrt{m(m+1)}$$

Substituting $m = 1$, we have $a/b = \sqrt{2} = 1.414$, and for $m = 2, a/b = \sqrt{6} = 2.45$, and so on.

For a given value of a/b , the critical stress, $\zeta_{CR} = N_{x,CR}/t$,

$$\sigma_{CR} = \frac{k\pi^2 E}{12(1-\nu^2)} \left(\frac{t}{b} \right)^2 \quad (2.26)$$

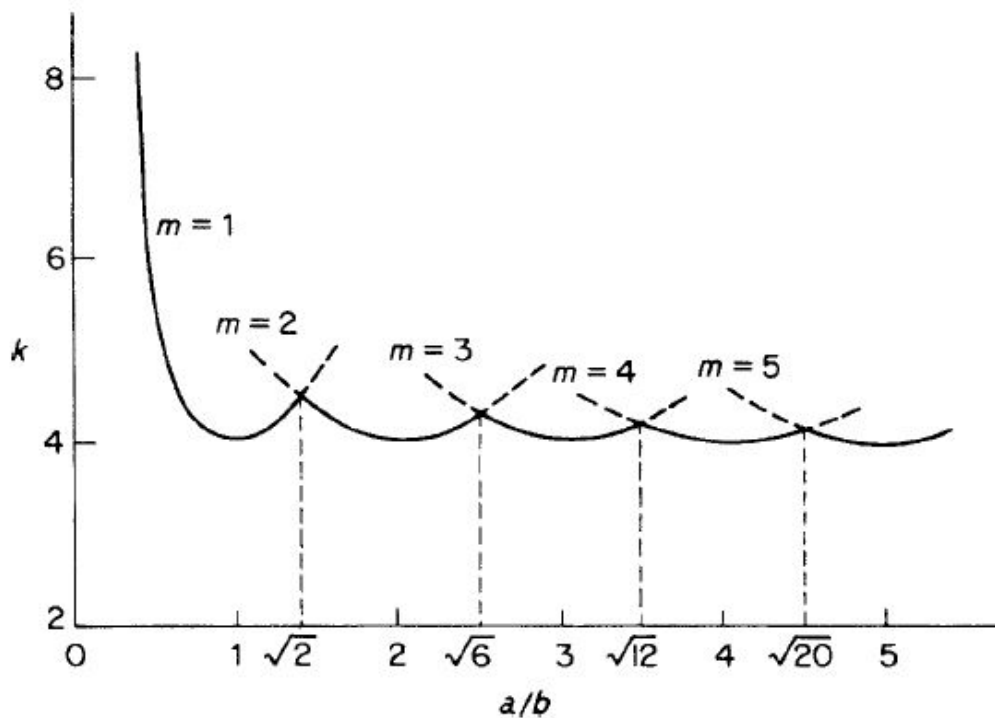


Figure 2.16 Buckling coefficient k for simply supported plates.

In general, the critical stress for a uniform rectangular plate, with various edge supports and loaded by constant or linearly varying in-plane direct forces (N_x, N_y) or constant shear forces (N_{xy}) along its edges, is given by Eq. (2.26). The value of k remains a function of a/b but also depends on the type of loading and edge support.

INELASTIC BUCKLING OF PLATES

For plates having small values of b/t , the critical stress may exceed the elastic limit of the material of the plate. In such a situation, Eq. (2.26) is no longer applicable, since, as we saw in the case of columns, E becomes dependent on stress, as does Poisson's ratio ν . These effects are usually included in a plasticity correction factor ε so that Eq. (2.26) becomes

$$\sigma_{CR} = \frac{\eta k \pi^2 E}{12(1 - \nu^2)} \left(\frac{t}{b}\right)^2 \quad (2.27)$$

Where E and ν are elastic values of Young's modulus and Poisson's ratio. In the linearly elastic region, $\varepsilon = 1$. The derivation of a general expression for ε is

$$\eta = \frac{1 - v_e^2}{1 - v_p^2} \frac{E_s}{E} \left[\frac{1}{2} + \frac{1}{2} \left(\frac{1}{4} + \frac{3}{4} \frac{E_t}{E_s} \right)^{\frac{1}{2}} \right]$$

where E_t and E_s are the tangent modulus and secant modulus (stress/strain) of the plate in the inelastic region and v_e and v_p are Poisson's ratio in the elastic and inelastic ranges.

EXPERIMENTAL DETERMINATION OF CRITICAL LOAD FOR A FLAT PLATE

The displacement of an initially curved plate from the zero load position was found to be

$$w_1 = \sum_{m=1}^{\infty} \sum_{n=1}^{\infty} B_{mn} \sin \frac{m\pi x}{a} \sin \frac{n\pi y}{b}$$

where

$$B_{mn} = \frac{A_{mn} N_x}{\frac{\pi^2 D}{a^2} \left(m + \frac{n^2 a^2}{mb^2} \right)^2 - N_x}$$

We see that the coefficients B_{mn} increase with an increase of compressive load intensity N_x . It follows that when N_x approaches the critical value, $N_{x,CR}$, the term in the series corresponding to the buckled shape of the plate becomes the most significant. For a square plate, $n = 1$ and $m = 1$ give a minimum value of critical load so that at the center of the plate

$$w_1 = \frac{A_{11} N_x}{N_{x,CR} - N_x}$$

or rearranging

$$w_1 = N_{x,CR} \frac{w_1}{N_x} - A_{11}$$

Thus, a graph of w_1 plotted against w_1/N_x will have a slope, in the region of the critical load, equal to $N_{x,CR}$.

LOCAL INSTABILITY

Thin-walled columns are encountered in aircraft structures in the shape of longitudinal stiffeners, which are normally fabricated by extrusion processes or by forming from a flat sheet. A variety of cross sections are used, although each is usually composed of flat plate elements arranged to form angle, channel, Z-, or —top hat— sections, as shown in Fig. 2.17. We see that the plate elements fall into two distinct categories: flanges which have a free unloaded edge and webs which are supported by the adjacent plate elements on both unloaded edges.

In local instability, the flanges and webs buckle like plates, with a resulting change in the crosssection of the column. The wavelength of the buckle is of the order of the widths of the plate elements, and the corresponding critical stress is generally independent of the length of the column when the length is equal to or greater than three times the width of the largest plate element in the column cross section.

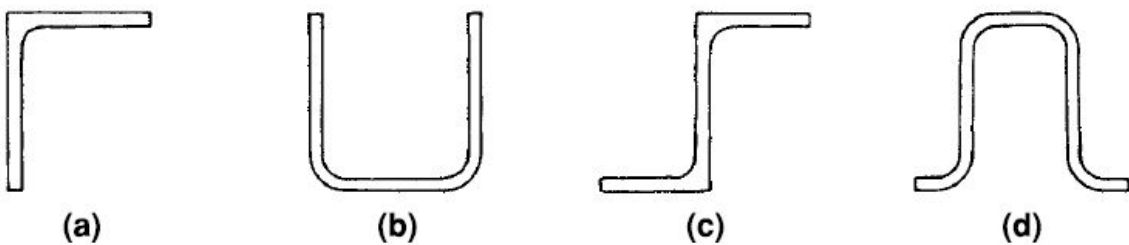


Figure 2.17 (a) Extruded angle; (b) formed channel; (c) extruded Z; (d) formed —top hat.||

Buckling occurs when the weakest plate element, usually a flange, reaches its critical stress, although in some cases all the elements reach their critical stresses simultaneously. When this occurs, the rotational restraint provided by adjacent elements to one another disappears, and the elements behave as though they are simply supported along their common edges. These cases are the simplest to analyze and are found where the cross section of the column is an equal-legged angle, T-, cruciform, or a square tube of constant thickness. Values of local critical stress for columns possessing these types of section may be found using Eq. (9.7) and an appropriate value of k . For example, k for a cruciform section column is obtained from Fig. 9.3(a) for a plate which is simply supported on three sides with one edge free and has $a/b > 3$. Hence, $k = 0.43$, and if the section buckles elastically, then $\varepsilon = 1$ and

$$\sigma_{CR} = 0.388E \left(\frac{t}{b} \right)^2 \quad (\nu = 0.3)$$

It must be appreciated that the calculation of local buckling stresses is generally complicated with no particular method gaining universal acceptance, much of the information available being experimental.

INSTABILITY OF STIFFENED PANELS

Stiffeners in earlier types of stiffened panel possessed a relatively high degree of strength compared with the thin skin resulting in the skin buckling at a much lower stress level than the stiffeners. Such panels may be analyzed by assuming that the stiffeners provide simply supported edge conditions to a series of flat plates.

A more efficient structure is obtained by adjusting the stiffener sections so that buckling occurs in both stiffeners and skin at about the same stress. This is achieved by a construction involving closely spaced stiffeners of comparable thickness to the skin. Since their critical stresses are nearly the same, there is an appreciable interaction at buckling between skin and stiffeners so that the complete panel must be considered a unit. However, caution must be exercised, since it is possible for the two simultaneous critical loads to interact and reduce the actual critical load of the structure. Various modes of buckling are possible, including primary buckling, where the wavelength is of the order of the panel length, and local buckling, with wavelengths of the order of the width of the plate elements of the skin or stiffeners. A discussion of the various buckling modes of panels having Z-section stiffeners has been given by Argyris and Dunne. Elements of the skin or stiffeners. A discussion of the various buckling modes of panels having Z-section stiffeners has been given by Argyris and Dunne.

For detailed work on stiffened panels, reference should be made to as much as possible of the

Preceding works. The literature is, however, extensive so that here we represent a relatively simple approach suggested by Gerard. Figure 2.18 represents a panel of width w stiffened by longitudinal members which may be flats (as shown), Z-, I-, channel, or —top hat sections. It is possible for the panel to behave as an Euler column, its cross section being that shown in Fig. 2.18. If the equivalent length of the panel

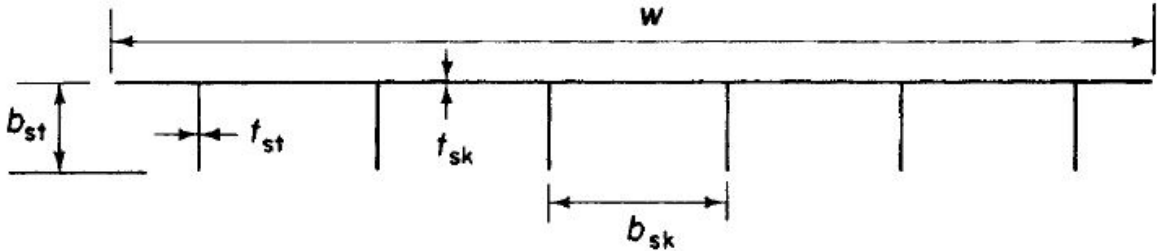


Figure 2.18 Stiffened panel.

acting as a column is l_e , then the Euler critical stress is

$$\sigma_{CR,E} = \frac{\pi^2 E}{(l_e/r)^2}$$

$$\sigma_{CR} = \frac{\eta k \pi^2 E}{12(1 - \nu^2)} \left(\frac{t}{b}\right)^2$$

$$\sigma_{CR} = \frac{4\pi^2 E}{12(1 - \nu^2)} \left(\frac{t_{sk}}{b_{sk}}\right)^2$$

$$\sigma_{CR} = \frac{0.43\pi^2 E}{12(1 - \nu^2)} \left(\frac{t_{st}}{b_{st}}\right)^2$$

The compressive load is applied to the panel over its complete cross section. To relate this load to an applied compressive stress σ_A acting on each element of the cross section, we divide the load per unit width, say N_x , by an equivalent skin thickness \bar{t} , hence

$$\sigma_A = \frac{N_x}{\bar{t}}$$

where

$$\bar{t} = \frac{A_{st}}{b_{sk}} + t_{sk}$$

and A_{st} is the stiffener area.

FAILURE STRESS IN PLATES AND STIFFENED PANELS

Gerard proposes a semiempirical solution for flat plates supported on all four edges. After elastic buckling occurs, theory and experiment indicate that the average compressive stress, ζ_a , in the plate and the unloaded edge stress, ζ_e , are related by the following expression:

$$\frac{\bar{\sigma}_a}{\sigma_{CR}} = \alpha_1 \left(\frac{\sigma_e}{\sigma_{CR}} \right)^n$$

$$\sigma_{CR} = \frac{k\pi^2 E}{12(1-\nu^2)} \left(\frac{t}{b} \right)^2$$

$$\frac{\bar{\sigma}_f}{\sigma_{cy}} = \alpha_1 \left(\frac{\sigma_{CR}}{\sigma_{cy}} \right)^{1-n}$$

$$\frac{\alpha_1 \pi^{2(1-n)}}{[12(1-\nu^2)]^{1-n}} = \alpha$$

yield

$$\frac{\bar{\sigma}_f}{\sigma_{cy}} = \alpha k^{1-n} \left[\frac{t}{b} \left(\frac{E}{\sigma_{cy}} \right)^{\frac{1}{2}} \right]^{2(1-n)}$$

or, in a simplified form,

$$\frac{\bar{\sigma}_f}{\sigma_{cy}} = \beta \left[\frac{t}{b} \left(\frac{E}{\sigma_{cy}} \right)^{\frac{1}{2}} \right]^m$$

where $\beta = \alpha k m / 2$.

Experiments on simply supported flat plates and square tubes of various aluminum and magnesium alloys and steel show that $\beta = 1.42$ and $m = 0.85$ fit the results within ± 10 percent up to the yield strength. Corresponding values for long, clamped, flat plates are $\beta = 1.80$, $m = 0.85$.

Gerard extended the preceding method to the prediction of local failure stresses for the plate elements of thin-walled columns. Equation becomes

$$\frac{\bar{\sigma}_f}{\sigma_{cy}} = \beta_g \left[\left(\frac{gt^2}{A} \right) \left(\frac{E}{\sigma_{cy}} \right)^{\frac{1}{2}} \right]^m$$

$$\frac{\bar{\sigma}_f}{\sigma_{cy}} = \beta_g \left[\frac{gt_{sk}t_{st}}{A} \left(\frac{E}{\bar{\sigma}_{cy}} \right)^{\frac{1}{2}} \right]^m$$

where t_{sk} and t_{st} are the skin and stiffener thicknesses, respectively. A weighted yield stress $\bar{\sigma}_{cy}$ is used for a panel in which the material of the skin and stiffener have different yield stresses; thus,

$$\bar{\sigma}_{cy} = \frac{\sigma_{cy} + \sigma_{cy,sk}[(\bar{t}/t_{st}) - 1]}{\bar{t}/t_{st}}$$

where \bar{t} is the average or equivalent skin thickness previously defined. The parameter g is obtained in a similar manner to that for a thin-walled column, except that the number of cuts in the skin and the

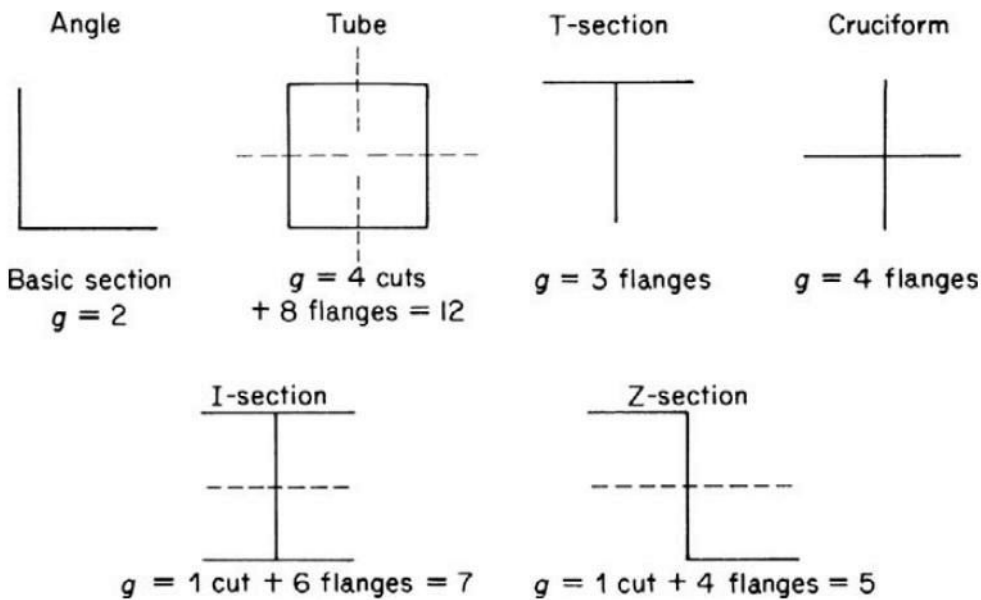


Figure 2.19 Determination of empirical constant g .

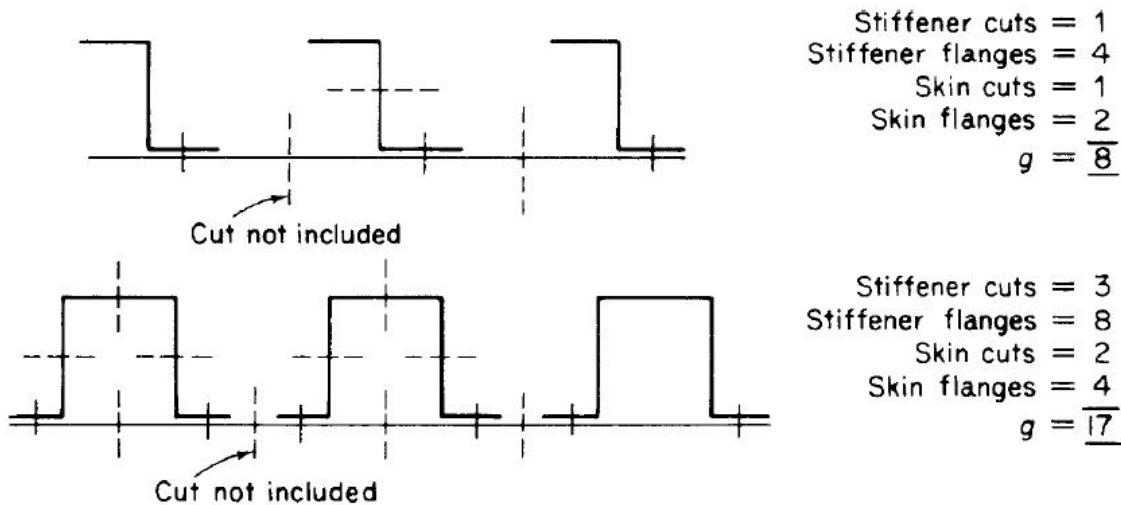


Figure 2.20 Determination of g for two types of stiffener/skin combinations.

TENSION FIELD BEAMS

The spars of aircraft wings usually comprise an upper and a lower flange connected by thin, stiffened webs. These webs are often of such a thickness that they buckle under shear stresses at a fraction of their ultimate load. The form of the buckle is shown in Fig. 2.21 (a), where the web of the beam buckles under the action of internal diagonal compressive stresses produced by shear, leaving a wrinkled web capable of supporting diagonal tension only in a direction perpendicular to that of the buckle; the beam is then said to be a *complete tension field beam*.

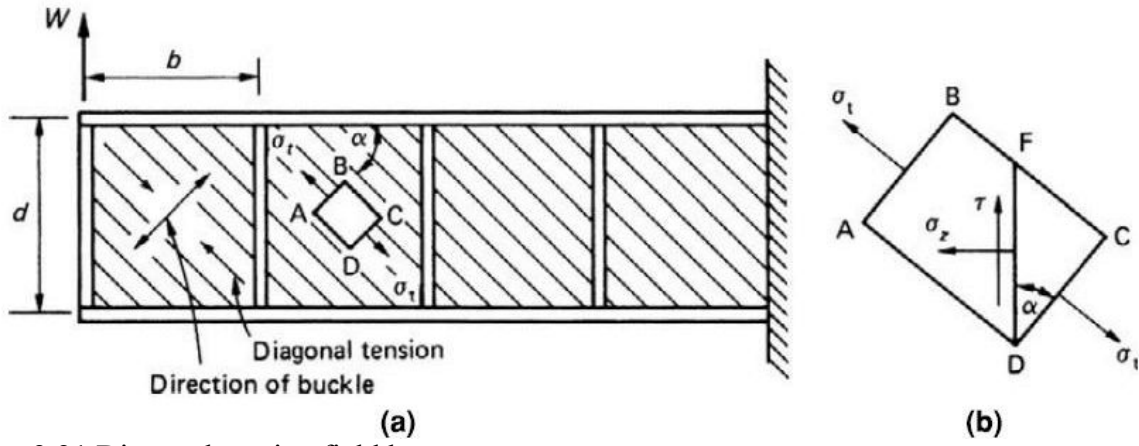


Figure 2.21 Diagonal tension field beam.

Complete Diagonal Tension

The theory presented here is due to Wagner. The beam shown in Fig. 2.21 (a) has concentrated flange areas having a depth d between their centroids and vertical stiffeners which are spaced uniformly along the length of the beam. It is assumed that the flanges resist the internal bending moment at any section of the beam, while the web, of thickness t , resists the vertical shear force. The effect of this assumption is to produce a uniform shear stress distribution through the depth of the web (see Section 19.3, T.H.G. Megson) at any section. Therefore, at a section of the beam where the shear force is S , the shear stress η is given by

$$\tau = \frac{S}{td}$$

Consider now an element ABCD of the web in a panel of the beam, as shown in Fig. 2.21(a). The element is subjected to tensile stresses, ζ_t , produced by the diagonal tension on the planes AB and CD; the angle of the diagonal tension is α . On a vertical plane FD in the element, the shear stress is η and the direct stress is ζ_z . Now, considering the equilibrium of the element FCD (Fig. 2.21(b)) and resolving forces vertically, we have (see Section 1.6, T.H.G. Megson)

$$\sigma_t CDt \sin \alpha = \tau FDt$$

which gives

$$\sigma_t = \frac{\tau}{\sin \alpha \cos \alpha} = \frac{2\tau}{\sin 2\alpha}$$

or, substituting for η from Eq. (9.14) and noting that in this case $S = W$ at all sections of the beam,

$$\sigma_t = \frac{2W}{td \sin 2\alpha}$$

Further, resolving forces horizontally for the element FCD,

$$\sigma_z FDt = \sigma_t CDt \cos \alpha$$

which gives

$$\sigma_z = \sigma_t \cos^2 \alpha$$

or, substituting for σ_t from Eq. (9.15),

$$\sigma_z = \frac{\tau}{\tan \alpha}$$

or, for this particular beam, from Eq. (9.14)

$$\sigma_z = \frac{W}{td \tan \alpha}$$

Since η and ζt are constant through the depth of the beam, it follows that ζz is constant through the depth of the beam.

The direct loads in the flanges are found by considering a length z of the beam, as shown in Fig. 2.22. On the plane mm , there are direct and shear stresses ζz and η acting in the web, together with direct loads FT and FB in the top and bottom flanges, respectively. FT and FB are produced by a combination of the bending moment Wz at the section plus the compressive action (ζz) of the diagonal tension. Taking moments about the bottom flange,

$$Wz = FTd - \frac{\sigma_z td^2}{2}$$

$$FT = \frac{Wz}{d} + \frac{W}{2 \tan \alpha}$$

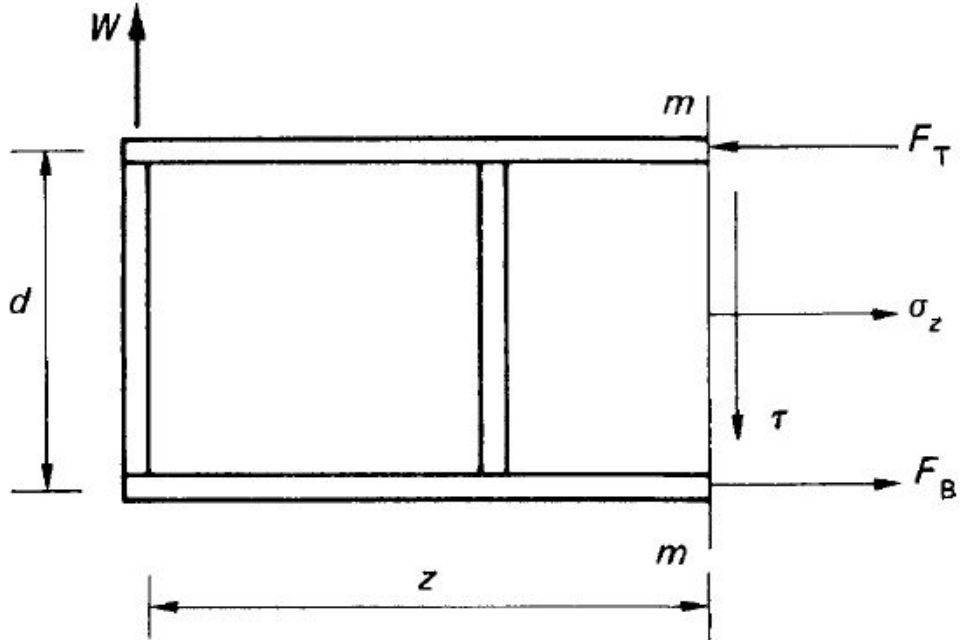


Figure 2.22 Determination of flange forces.

Now, resolving forces horizontally,

$$F_B - F_T + \sigma_z td = 0$$

which gives, on substituting for σ_z and F_T from Eqs. (9.18) and (9.19),

$$F_B = \frac{Wz}{d} - \frac{W}{2\tan\alpha}$$

$$\sigma_y H C t = \sigma_t C D t \sin \alpha$$

which gives

$$\sigma_y = \sigma_t \sin^2 \alpha$$

Substituting for σ_t from Eq. (9.15),

$$\sigma_y = \tau \tan \alpha$$

or, from Eq. (9.14), in which $S = W$

$$\sigma_y = \frac{W}{td} \tan \alpha$$

The tensile stresses ζ on horizontal planes in the web of the beam cause compression in the vertical stiffeners. Each stiffener may be assumed to support half of each adjacent panel in the beam so that the

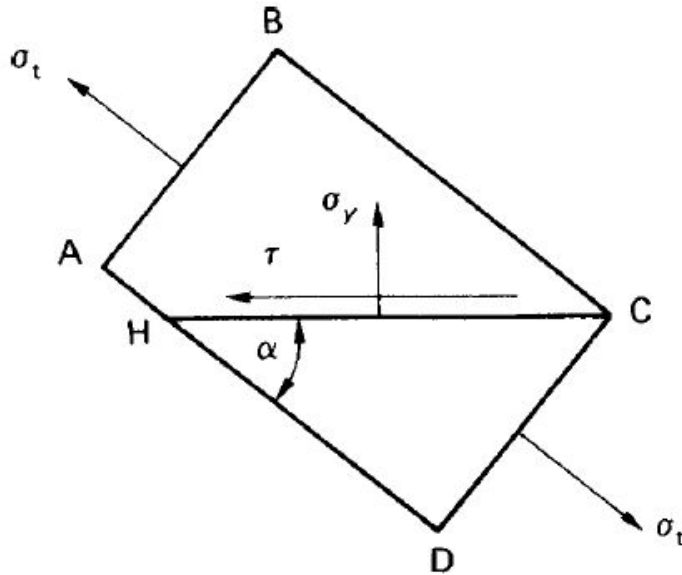


Figure 2.23 Stress system on a horizontal plane in the beam web.

compressive load P in a stiffener is given by

$$P = \sigma_y t b$$

which becomes, from Eq. (9.22),

$$P = \frac{Wb}{d} \tan \alpha$$

If the load P is sufficiently high, the stiffeners will buckle. Tests indicate that they buckle as columns of equivalent length

$$\left. \begin{array}{ll} l_e = d / \sqrt{4 - 2b/d} & \text{for } b < 1.5d \\ l_e = d & \text{for } b > 1.5d \end{array} \right\}$$

or

In addition to causing compression in the stiffeners, the direct stress σ_y produces bending of the beam flanges between the stiffeners, as shown in Fig. 2.24. Each flange acts as a continuous beam carrying a uniformly distributed load of intensity σ_{yt} . The maximum bending moment in a continuous beam with ends fixed against rotation occurs at a support and is $wL^2/12$, in which w is the load intensity and L is the beam span. In this case, therefore, the maximum bending moment M_{max} occurs at a stiffener and is given by

$$M_{max} = \frac{\sigma_y t b^2}{12}$$

$$M_{\max} = \frac{Wb^2 \tan \alpha}{12d}$$

Midway between the stiffeners this bending moment reduces to $Wb^2 \tan \alpha / 24d$.

The angle α adjusts itself such that the total strain energy of the beam is a minimum. If it is assumed that the flanges and stiffeners are rigid, then the strain energy comprises the shear strain energy of the web only and $\alpha = 45^\circ$. In practice, both flanges and stiffeners deform so that α is somewhat less than 45° , usually of the order of 40° and, in the type of beam common to aircraft structures, rarely below 38° . For beams having all components made of the same material, the condition of minimum strain energy leads to various equivalent expressions for α , one of which is

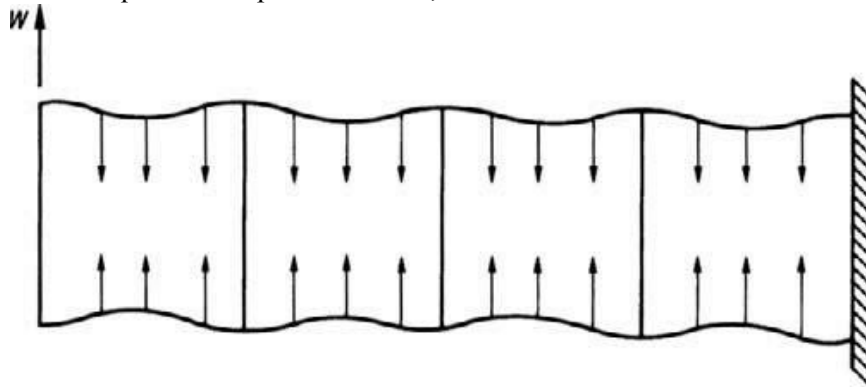


Figure 2.24 Bending of flanges due to web stress.

$$\tan^2 \alpha = \frac{\sigma_t + \sigma_F}{\sigma_t + \sigma_S}$$

in which ζF and ζS are the uniform direct *compressive* stresses induced by the diagonal tension in the flanges and stiffeners, respectively. Thus,

$$\sigma_F = \frac{W}{2A_F \tan \alpha}$$

in which A_F is the cross-sectional area of each flange. Also,

$$\sigma_S = \frac{Wb}{A_S d} \tan \alpha$$

An alternative expression for α , again derived from a consideration of the total strain energy of the beam, is

$$\tan^4 \alpha = \frac{1 + td/2A_F}{1 + tb/A_S}$$

Incomplete Diagonal Tension

In modern aircraft structures, beams having extremely thin webs are rare. They retain, after buckling, some of their ability to support loads so that even near failure they are in a state of stress somewhere between that of pure diagonal tension and the prebuckling stress. Such a beam is described as an *incomplete diagonal tension field beam* and may be analyzed by semiempirical theory as follows. It is assumed that the nominal web shear η ($= S/td$) may be divided into a —true shear component η_S and a diagonal tension component η_{DT} by writing

$$\tau_{DT} = k\tau, \quad \tau_S = (1 - k)\tau$$

Where k , the *diagonal tension factor*, is a measure of the degree to which the diagonal tension is developed. A completely unbuckled web has $k = 0$, whereas $k = 1$ for a web in complete diagonal tension. The value of k corresponding to a web having a critical shear stress η_{CR} is given by the empirical expression

$$k = \tanh\left(0.5 \log \frac{\tau}{\tau_{CR}}\right)$$

The ratio η/η_{CR} is known as the *loading ratio* or *buckling stress ratio*. The buckling stress η_{CR} may be calculated from the formula

$$\tau_{CR,elastic} = k_{ss} E \left(\frac{t}{b} \right)^2 \left[R_d + \frac{1}{2} (R_b - R_d) \left(\frac{b}{d} \right)^3 \right]$$

Where k_{ss} is the coefficient for a plate with simply supported edges, and R_d and R_b are empirical restraint coefficients for the vertical and horizontal edges of the web panel, respectively. Graphs giving k_{ss} , R_d , and R_b are reproduced in the study of Kuhn.

The stress equations are modified in the light of these assumptions and may be rewritten in terms of the applied shear stress η as

$$\sigma_F = \frac{k\tau \cot \alpha}{(2A_F/td) + 0.5(1 - k)}$$

$$\sigma_S = \frac{k\tau \tan \alpha}{(A_S/tb) + 0.5(1 - k)}$$

Further, the web stress ζ_t given, becomes two direct stresses: ζ_1 along the direction of α given by

$$\sigma_1 = \frac{2k\tau}{\sin 2\alpha} + \tau(1 - k) \sin 2\alpha$$

$$\sigma_2 = -\tau(1 - k) \sin 2\alpha$$

while the effective lengths for the calculation of stiffener buckling loads become

or

	$l_e = d_s / \sqrt{1 + k^2(3 - 2b/d_s)}$	for $b < 1.5d$
	$l_e = d_s$	for $b > 1.5d$

In some cases, beams taper along their lengths, in which case the flange loads are no longer horizontal but have vertical components which reduce the shear load carried by the web, where d is the depth of the beam at the section considered, we have, resolving forces vertically,

$$W - (F_T + F_B) \sin \beta - \sigma_t (d \cos \alpha) \sin \alpha = 0$$

For horizontal equilibrium,

$$(F_T - F_B) \cos \beta - \sigma_t t d \cos^2 \alpha = 0$$

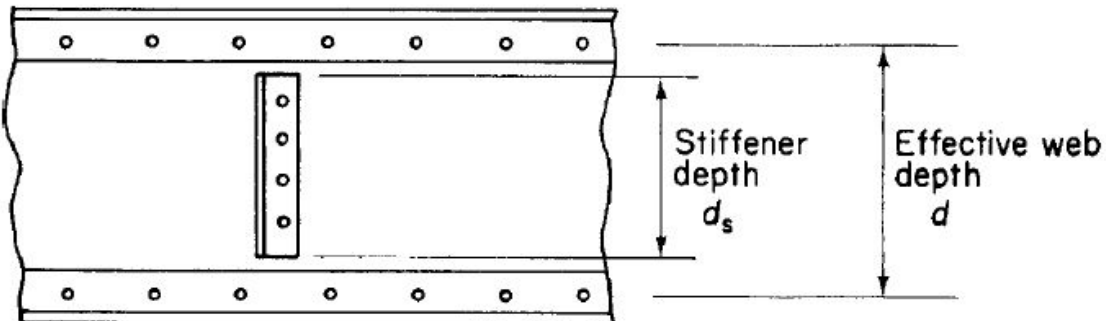


Figure 2.25 Calculation of stiffener buckling load.

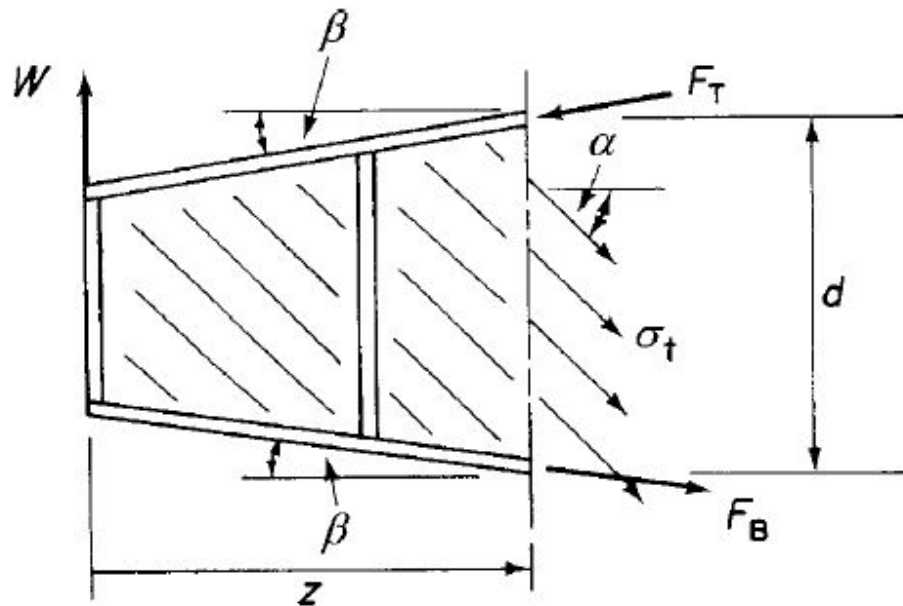


Figure 2.26 Effect of taper on diagonal tension field beam calculations.

Taking moments about B,

$$Wz - F_T d \cos \beta + \frac{1}{2} \sigma_t t d^2 \cos^2 \alpha = 0$$

$$\sigma_t = \frac{2W}{td \sin 2\alpha} \left(1 - \frac{2z}{d} \tan \beta \right)$$

$$F_T = \frac{W}{d \cos \beta} \left[z + \frac{d \cot \alpha}{2} \left(1 - \frac{2z}{d} \tan \beta \right) \right]$$

$$F_B = \frac{W}{d \cos \beta} \left[z - \frac{d \cot \alpha}{2} \left(1 - \frac{2z}{d} \tan \beta \right) \right]$$

$$P = \frac{Wb}{d} \tan \alpha \left(1 - \frac{2z}{d} \tan \beta \right)$$

Also, the shear force S at any section of the beam is

$$S = W - (F_T + F_B) \sin \beta$$

$$S = W \left(1 - \frac{2z}{d} \tan \beta \right)$$

Post buckling Behavior

It is possible, if the beam flanges are relatively light, for failure due to yielding to occur in the beam flanges after the web has buckled so that plastic hinges form and a failure mechanism. This postbuckling behavior was investigated by Evans et al. [Ref. 14], who developed a design method for beams subjected to bending and shear. It is their method of analysis which is presented here.

Suppose that the panel AXBZ in Fig. 2.27 has collapsed due to a shear load S and a bending moment M ; plastic hinges have formed at W, X, Y, and Z. In the initial stages of loading, the web remains perfectly flat until it reaches its critical stresses: η_{cr} in shear and ζ_{crb} in bending. The values of these

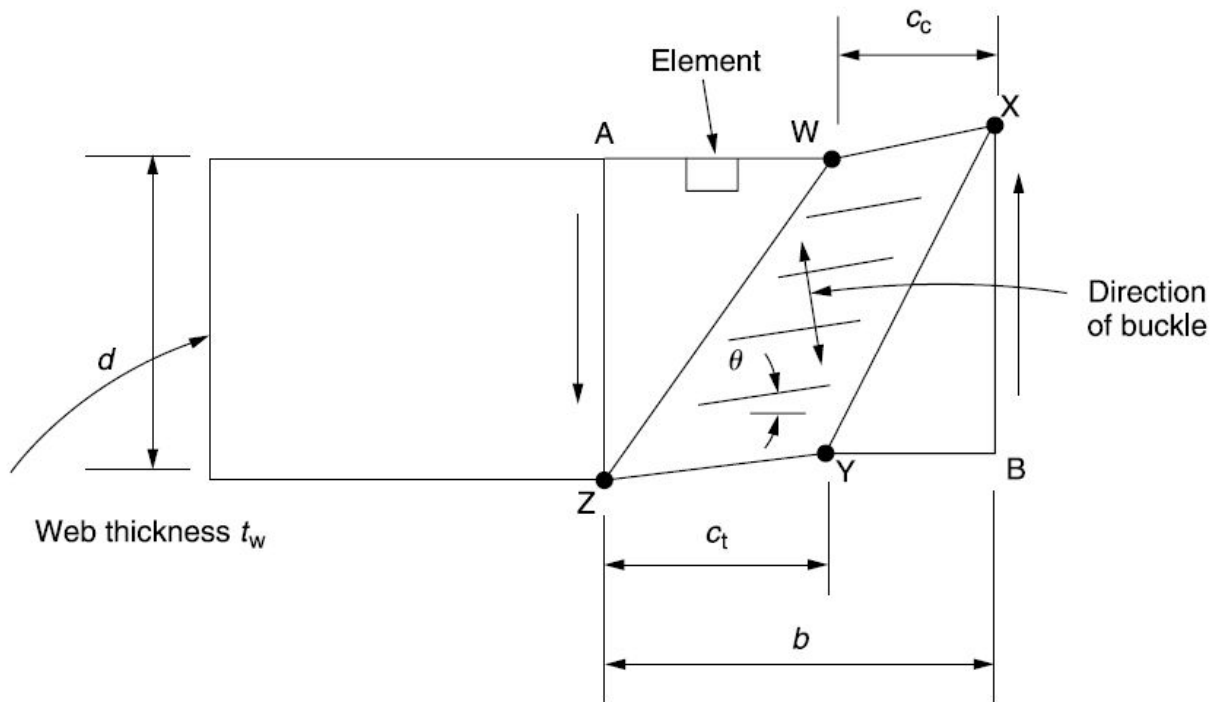


Figure 2.27 Collapse mechanism of a panel of a tension field beam.

stresses may be found approximately from

$$\left(\frac{\sigma_{mb}}{\sigma_{crb}}\right)^2 + \left(\frac{\tau_m}{\tau_{cr}}\right)^2 = 1$$

Where ζ_{crb} is the critical value of bending stress with $S = 0$, $M = 0$, and η_{cr} is the critical value of shear stress when $S = 0$ and $M = 0$. Once the critical stress is reached, the web starts to buckle and cannot carry any increase in compressive stress so that, any additional load is carried by tension field action. It is assumed that the shear and bending stresses remain at their critical values η_m and ζ_{mb} and that there are *additional* stresses ζ_t which are inclined at an angle ζ to the horizontal and which carry any increases in the applied load. At collapse—that is, at ultimate load conditions—the additional stress ζ_t reaches its maximum value $\zeta_{t(max)}$, and the panel is in the collapsed state shown in Fig. 2.27.

Consider now the small rectangular element on the edge AW of the panel before collapse. The stresses acting on the element are shown in Fig. 2.28 (a). The stresses on planes parallel to and perpendicular to the direction of the buckle may be found by considering the equilibrium of triangular elements within this rectangular element. Initially, we shall consider the triangular element CDE which is subjected to the stress system shown in Fig. 2.28 (b) and is in equilibrium under the action of the forces corresponding to these stresses. Note that the edge CE of the element is parallel to the direction of the buckle in the web.

For equilibrium of the element in a direction perpendicular to CE

$$\sigma_\xi CE + \sigma_{mb} ED \cos \theta - \tau_m ED \sin \theta - \tau_m DC \cos \theta = 0$$

Dividing by CE and rearranging, we have

$$\sigma_\xi = -\sigma_{mb} \cos^2 \theta + \tau_m \sin 2\theta$$

Similarly, by considering the equilibrium of the element in the direction EC, we have

$$\tau_{\eta\xi} = -\frac{\sigma_{mb}}{2} \sin 2\theta - \tau_m \cos 2\theta$$

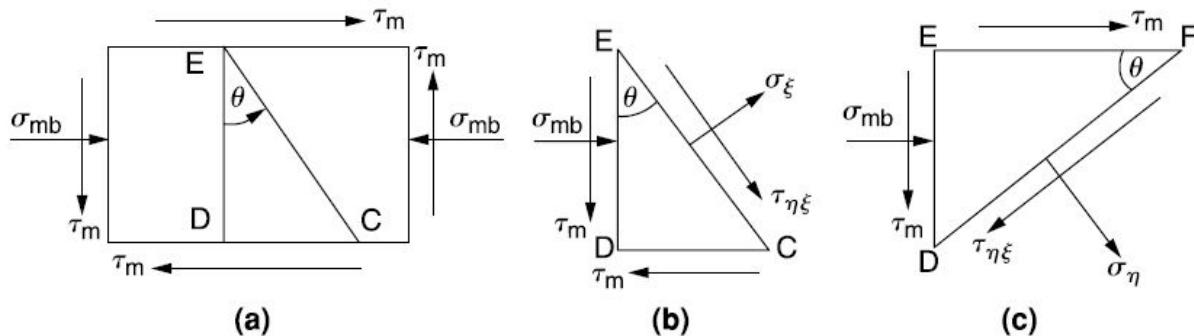


Figure 2.28 Determination of stresses on planes parallel and perpendicular to the plane of the buckle.

Further, the direct stress ζ on the plane FD (Fig. 2.28 (c)) which is perpendicular to the plane of the buckle is found from the equilibrium of the element FED. Then,

$$\sigma_\eta FD + \sigma_{mb} ED \sin \theta + \tau_m EF \sin \theta + \tau_m DE \cos \theta = 0$$

Dividing by FD and rearranging give

$$\sigma_\eta = -\sigma_{mb} \sin^2 \theta - \tau_m \sin 2\theta$$

Note that the shear stress on this plane forms a complementary shear stress system with $\eta_{\xi\eta}$. The failure condition is reached by adding $\zeta_{t(\max)}$ to ζ_ξ and using the von Mises theory of elastic failure , that is,

$$\sigma_y^2 = \sigma_1^2 + \sigma_2^2 - \sigma_1 \sigma_2 + 3\tau^2$$

Where σ_y is the yield stress of the material, ζ_1 and ζ_2 are the direct stresses acting on two mutually perpendicular planes, and η is the shear stress acting on the same two planes. Hence, when the yield stress in the web is ζ_{yw} , failure occurs when

$$\sigma_{yw}^2 = (\sigma_\xi + \sigma_{t(\max)})^2 + \sigma_\eta^2 - \sigma_\eta (\sigma_\xi + \sigma_{t(\max)}) + 3\tau_{\xi\eta}^2$$

$$\sigma_{t(\max)} = -\frac{1}{2}A + \frac{1}{2}[A^2 - 4(\sigma_{mb}^2 + 3\tau_m^2 - \sigma_{yw}^2)]^{\frac{1}{2}}$$

$$A = 3\tau_m \sin 2\theta + \sigma_{mb} \sin^2 \theta - 2\sigma_{mb} \cos^2 \theta$$

These equations have been derived for a point on the edge of the panel but are applicable to any point within its boundary. Therefore, the resultant force F_w corresponding to the tension field in the web may be calculated and its line of action determined.

If the average stresses in the compression and tension flanges are ζ_{cf} and ζ_{tf} and the yield stress of the flanges is ζ_{yf} , the reduced plastic moments in the flanges are

$$M'_{pc} = M_{pc} \left[1 - \left(\frac{\sigma_{cf}}{\sigma_{yf}} \right)^2 \right] \quad (\text{compression flange})$$

$$M'_{pt} = M_{pt} \left[1 - \left(\frac{\sigma_{tf}}{\sigma_{yf}} \right)^2 \right] \quad (\text{tension flange})$$

The position of each plastic hinge may be found by considering the equilibrium of a length of flange and using the principle of virtual work. In Fig. 2.29, the length WX of the upper flange of the beam is given a virtual displacement θ . The work done by the shear force at X is equal to the energy absorbed by the plastic hinges at W and X and the work done *against* the tension field stress $\zeta_{t(\max)}$. Suppose that the average value of the tension field stress is ζ_{tc} —that is, the stress at the midpoint of WX .

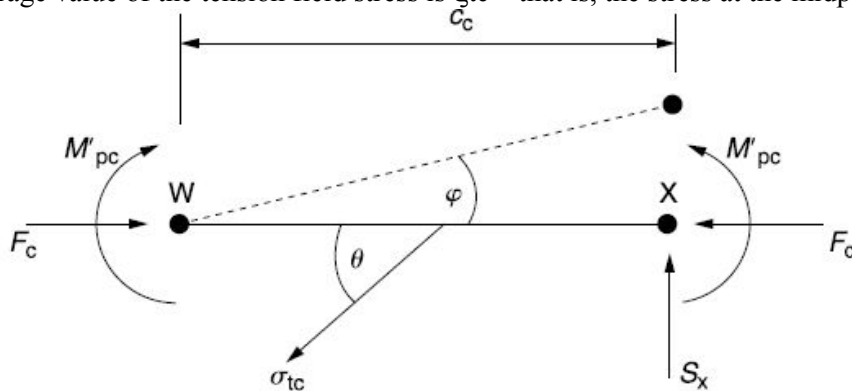


Figure 2.29 Determination of plastic hinge position.

Then,

$$S_x c_c \phi = 2M'_{pc} \phi + \sigma_{tc} t_w \sin^2 \theta \frac{c_c^2}{2} \phi$$

The minimum value of S_x is obtained by differentiating with respect to c_c , that is,

$$\frac{dS_x}{dc_c} = -2 \frac{M'_{pc}}{c_c^2} + \sigma_{tc} t_w \frac{\sin^2 \theta}{2} = 0$$

which gives

$$c_c^2 = \frac{4M'_{pc}}{\sigma_{tc} t_w \sin^2 \theta}$$

Similarly, in the tension flange,

$$c_t^2 = \frac{4M'_{pt}}{\sigma_{tf} t_w \sin^2 \theta}$$

Clearly, for the plastic hinges to occur within a flange, both c_c and c_t must be less than b . Therefore,

$$M'_{pc} < \frac{t_w b^2 \sin^2 \theta}{4} \sigma_{tc}$$

The average axial stress in the compression flange between W and X is obtained by considering the equilibrium of half of the length of WX, then

$$F_c = \sigma_{cf} A_{cf} + \sigma_{tc} t_w \frac{c_c}{2} \sin \theta \cos \theta + \tau_m t_w \frac{c_c}{2}$$

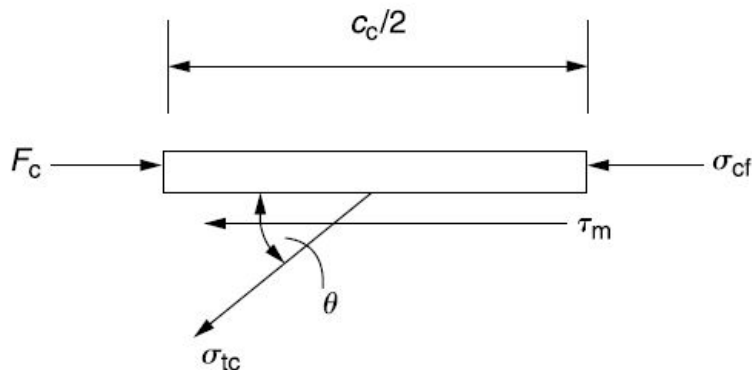


Figure 2.30 Determination of flange stress.

from which

$$\sigma_{cf} = \frac{F_c - \frac{1}{2}(\sigma_{tc} \sin \theta \cos \theta + \tau_m)t_w c_c}{A_{cf}}$$

Where F_c is the force in the compression flange at W and A_{cf} is the cross-sectional area of the compression flange.

Similarly, for the tension flange,

$$\sigma_{tf} = \frac{F_t + \frac{1}{2}(\sigma_{tt} \sin \theta \cos \theta + \tau_m)t_w c_t}{A_{tf}}$$

The forces F_c and F_t are found by considering the equilibrium of the beam to the right of WY(Fig. 2.31). Then, resolving vertically and noting that $S_{cr} = \eta_m t_w d$,

$$S_{ult} = F_w \sin \theta + \tau_m t_w d + \sum W_n$$

Resolving horizontally and noting that $H_{cr} = \tau_m t_w (b - c_c - c_t)$,

$$F_c - F_t = F_w \cos \theta - \tau_m t_w (b - c_c - c_t)$$

Taking moments about O, we have

$$\begin{aligned} F_c + F_t &= \frac{2}{d} \left[S_{ult} \left(s + \frac{b + c_c - c_t}{2} \right) + M'_{pt} - M'_{pc} \right. \\ &\quad \left. + F_w q - M_w - \sum_n W_n z_n \right] \end{aligned}$$

where W_1 to W_n are external loads applied to the beam to the right of WY and M_w is the bending moment in the web when it has buckled and become a tension field, that is,

$$M_w = \frac{\sigma_{mb} b d^2}{b}$$

The flange forces are then

$$\begin{aligned} F_c &= \frac{S_{ult}}{2d} (d \cot \theta + 2s + b + c_c - c_t) \\ &\quad + \frac{1}{d} \left(M'_{pt} - M'_{pc} + F_w q - M_w - \sum_n W_n z_n \right) \\ &\quad - \frac{1}{2} \tau_m t_w (d \cot \theta + b - c_c - c_t) \end{aligned}$$

$$\begin{aligned}
F_t &= \frac{S_{ult}}{2d} (d \cot \theta + 2s + b + c_c - c_t) \\
&\quad + \frac{1}{d} \left(M'_{pt} - M'_{pc} - F_w q - M_w - \sum_n W_n z_n \right) \\
&\quad + \frac{1}{2} \tau_m t_w (d \cot \theta + b - c_c - c_t)
\end{aligned}$$

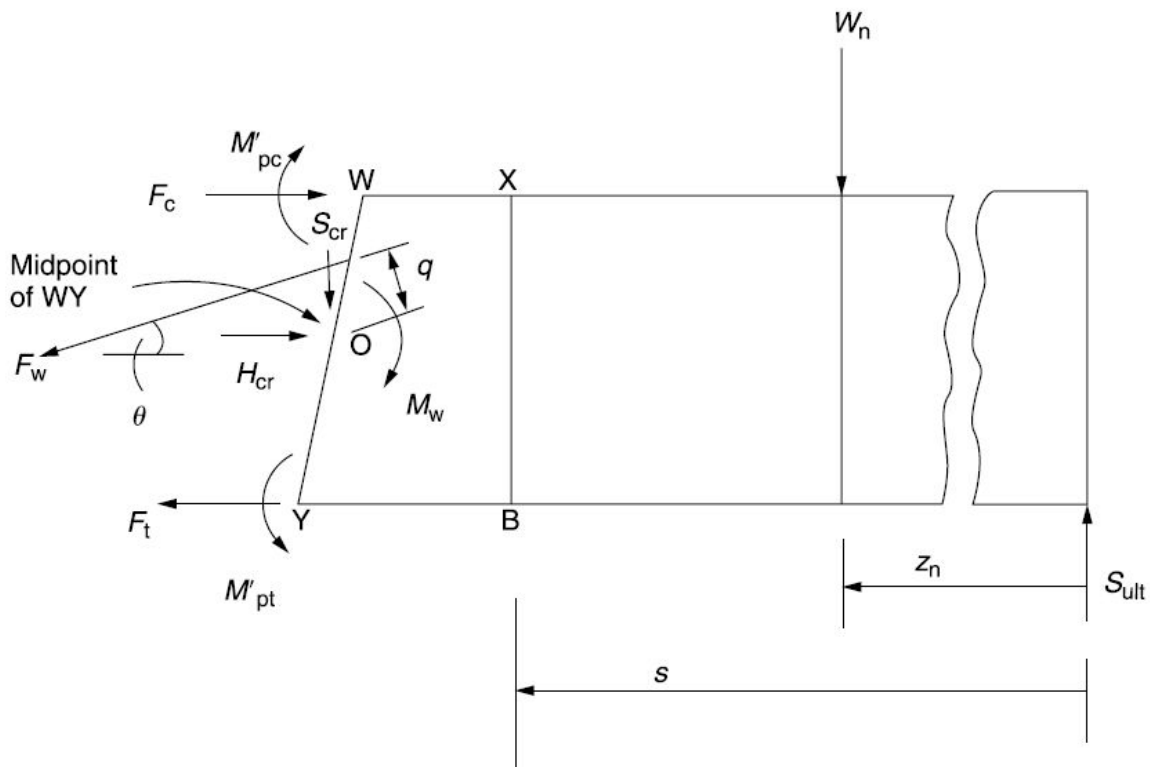


Figure 2.31 Determination of flange forces.

Evans et al. adopted an iterative procedure for solving in which an initial value of ζ was assumed and ζ_{cf} and ζ_{tf} were taken to be zero. Then, c_c and c_t were calculated, and approximate values of F_c and F_t are found, giving better estimates for ζ_{cf} and ζ_{tf} . The procedure was then repeated until the required accuracy was obtained.

UNIT-III

BENDING, SHEAR AND TORSION OF THIN WALLED BEAMS

UNSYMMETRICAL BENDING

The value of direct stress at a point in the cross section of a beam subjected to bending depends on the position of the point, the applied loading, and the geometric properties of the cross section. It follows that it is of no consequence whether the cross section is open or closed. We, therefore, derive the theory for a beam of arbitrary cross section and then discuss its application to thin-walled open and closed section beams subjected to bending moments.

The assumptions are identical to those made for symmetrical bending. However, before we derive an expression for the direct stress distribution in a beam subjected to bending, we shall establish sign conventions for moments, forces, and displacements; investigate the effect of choice of section on the positive directions of these parameters, and discuss the determination of the components of a bending moment applied in any longitudinal plane.

Sign Conventions and Notation

Forces, moments, and displacements are referred to an arbitrary system of axes $Oxyz$, of which Oz is parallel to the longitudinal axis of the beam and Oxy are axes in the plane of the cross section. We assign the symbols M , S , P , T , and w to bending moment, shear force, axial or direct load, torque, and distributed load intensity, respectively, with suffixes where appropriate to indicate sense or direction. Thus, M_x is a bending moment about the x axis, S_x is a shear force in the x direction, and so on. Figure 3.1 shows positive directions and senses for the above loads and moments applied externally to a beam and also the positive directions of the components of displacement u , v , and w of any point in the beam cross section parallel to the x , y , and z axes, respectively. A further condition defining the signs of the bending moments M_x and M_y is that they are positive when they induce tension in the positive xy quadrant of the beam cross section.

If we refer internal forces and moments to that face of a section which is seen when viewed in the direction zO , and then, as shown in Fig. 3.2, positive internal forces and moments are in the same direction and sense as the externally applied loads, whereas on the opposite face they form an opposing system. The former system, which we shall use, has the advantage that direct and shear loads are always positive in the positive directions of the appropriate axes whether they are internal loads or not. It must be realized, though, that internal stress resultants then become equivalent to externally applied forces and moments and are not in equilibrium with them.

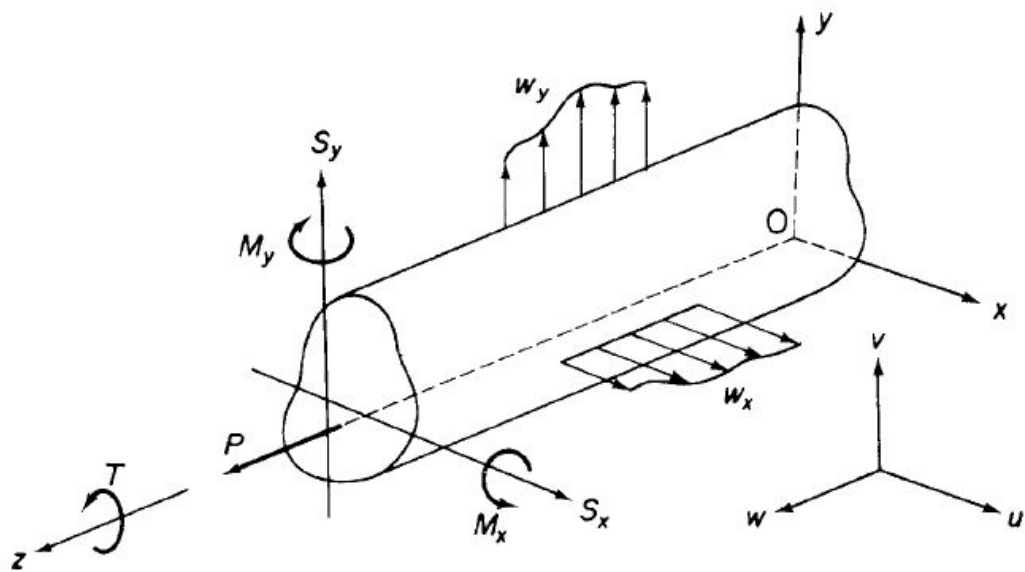


Figure 3.1 Notation and sign convention for forces, moments, and displacements.

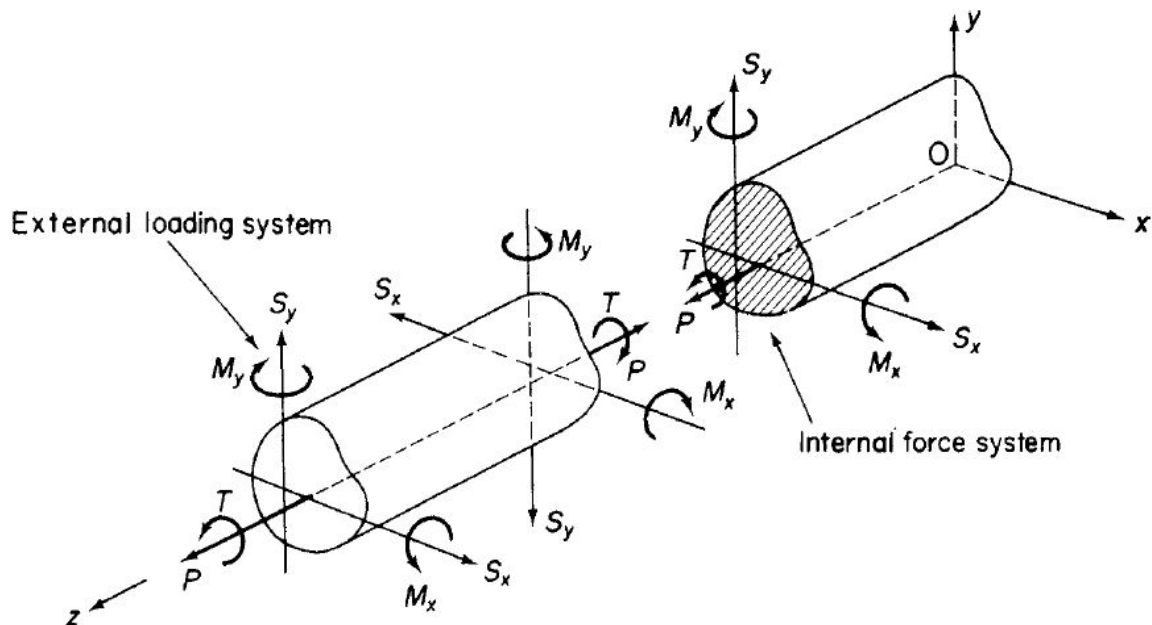


Figure 3.2 Internal force system.

Resolution of Bending Moments

A bending moment M applied in any longitudinal plane parallel to the z axis may be resolved into components M_x and M_y by the normal rules of vectors. However, a visual appreciation of the situation is often helpful. Referring to Fig. 3.3, we see that a bending moment M in a plane at an angle ζ to Ox may have components of differing sign depending on the size of ζ . In both cases, for the sense of

M shown

$$M_x = M \sin \theta$$

$$M_y = M \cos \theta$$

which give, for $\zeta < \pi/2$, M_x and M_y positive and for $\zeta > \pi/2$, M_x positive and M_y negative.

Direct Stress Distribution due to Bending

Consider a beam having the arbitrary cross section shown in Fig. 3.4(a). The beam supports bending moments M_x and M_y and bends about some axis in its cross section which is therefore an axis of zero stress or a *neutral axis* (NA). Let us suppose that the origin of axes coincides with the centroid C of the cross section and that the neutral axis is a distance p from C. The direct stress σ_z on an element of area δA at a point (x, y) and a distance ξ from the neutral axis is,

$$\sigma_z = E \varepsilon_z$$

If the beam is bent to a radius of curvature ρ about the neutral axis at this particular section then, since plane sections are assumed to remain plane after bending, and by a comparison with symmetrical bending theory

$$\varepsilon_z = \frac{\xi}{\rho}$$

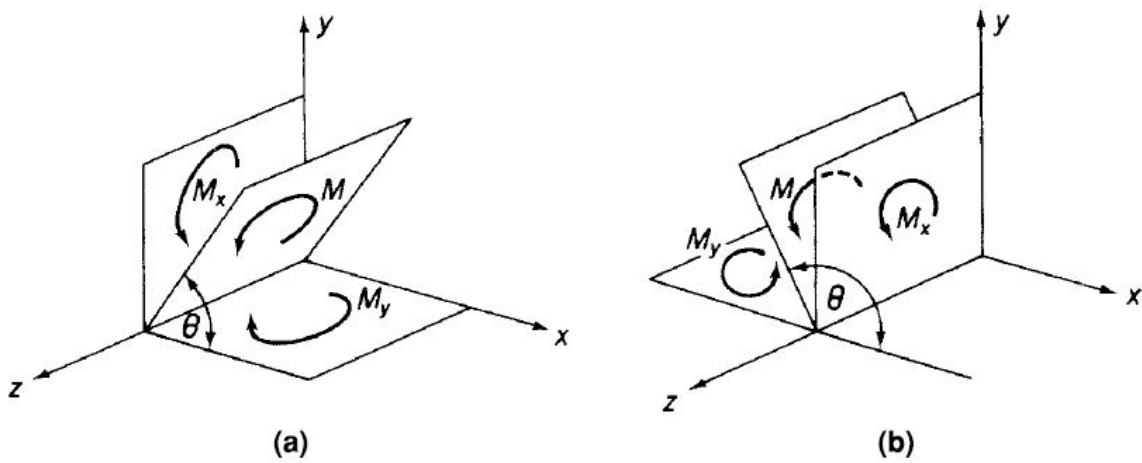


Figure 3.3 Resolution of bending moments: (a) $\zeta < 90^\circ$ and (b) $\zeta > 90^\circ$.

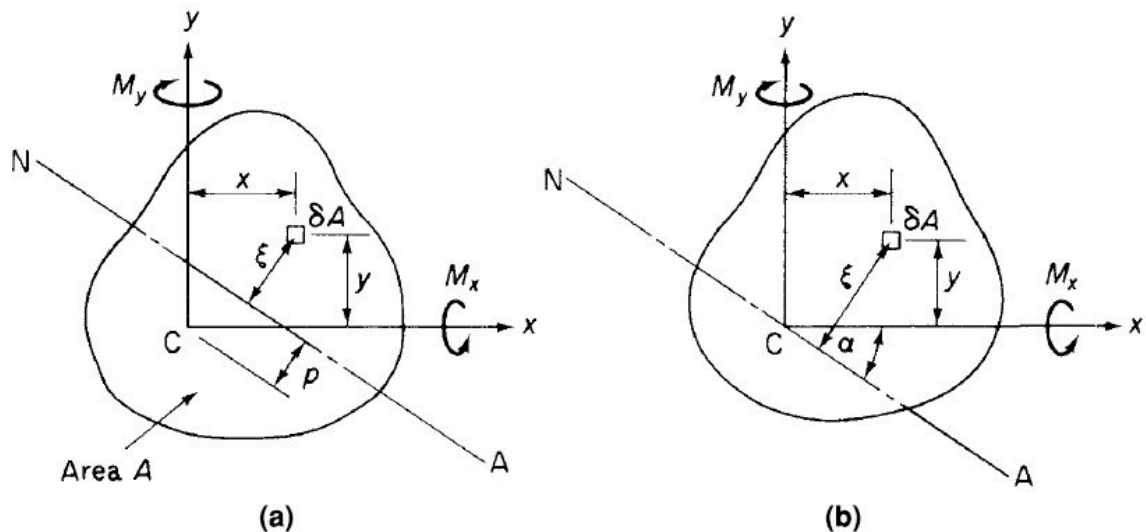


Figure 3.4 Determination of neutral axis position and direct stress due to bending.

we have

$$\sigma_z = \frac{E\xi}{\rho}$$

The beam supports pure bending moments so that the resultant normal load on any section must be zero. Hence,

$$\int_A \sigma_z dA = 0$$

Therefore, replacing σ_z in this equation from Eq. (15.14) and cancelling the constant E/ρ gives

$$\int_A \xi dA = 0$$

Suppose that the inclination of the neutral axis to Cx is α (measured clockwise from Cx), then

$$\xi = x \sin \alpha + y \cos \alpha$$

$$\sigma_z = \frac{E}{\rho} (x \sin \alpha + y \cos \alpha)$$

The moment resultants of the internal direct stress distribution have the same sense as the applied moments M_x and M_y . Therefore,

$$M_x = \int_A \sigma_z y dA, \quad M_y = \int_A \sigma_z x dA$$

$$I_{xx} = \int_A y^2 dA, \quad I_{yy} = \int_A x^2 dA, \quad I_{xy} = \int_A xy dA$$

gives

$$M_x = \frac{E \sin \alpha}{\rho} I_{xy} + \frac{E \cos \alpha}{\rho} I_{xx}, \quad M_y = \frac{E \sin \alpha}{\rho} I_{yy} + \frac{E \cos \alpha}{\rho} I_{xy}$$

or, in matrix form

$$\begin{Bmatrix} M_x \\ M_y \end{Bmatrix} = \frac{E}{\rho} \begin{bmatrix} I_{xy} & I_{xx} \\ I_{yy} & I_{xy} \end{bmatrix} \begin{Bmatrix} \sin \alpha \\ \cos \alpha \end{Bmatrix}$$

from which

$$\frac{E}{\rho} \begin{Bmatrix} \sin \alpha \\ \cos \alpha \end{Bmatrix} = \begin{bmatrix} I_{xy} & I_{xx} \\ I_{yy} & I_{xy} \end{bmatrix}^{-1} \begin{Bmatrix} M_x \\ M_y \end{Bmatrix}$$

that is,

$$\frac{E}{\rho} \begin{Bmatrix} \sin \alpha \\ \cos \alpha \end{Bmatrix} = \frac{1}{I_{xx}I_{yy} - I_{xy}^2} \begin{bmatrix} -I_{xy} & I_{xx} \\ I_{yy} & -I_{xy} \end{bmatrix} \begin{Bmatrix} M_x \\ M_y \end{Bmatrix}$$

so that,

$$\sigma_z = \left(\frac{M_y I_{xx} - M_x I_{xy}}{I_{xx} I_{yy} - I_{xy}^2} \right)_x + \left(\frac{M_x I_{yy} - M_y I_{xy}}{I_{xx} I_{yy} - I_{xy}^2} \right)_y \quad (3.1)$$

Alternatively, Eq. (3.1) may be rearranged in the form

$$\sigma_z = \frac{M_x (I_{yy}y - I_{xy}x)}{I_{xx}I_{yy} - I_{xy}^2} + \frac{M_y (I_{xx}x - I_{xy}y)}{I_{xx}I_{yy} - I_{xy}^2} \quad (3.2)$$

From Eq. (3.2) it can be seen that if, say, $M_y=0$, the moment M_x produces a stress which varies with Both x and y ; similarly for M_y if $M_x=0$.

In the case where the beam cross section has *either* (or both) Cx or Cy as an axis of symmetry, the product second moment of area I_{xy} is zero and Cx and Cy are *principal axes*. Equation (3.2) then reduces to

$$\sigma_z = \frac{M_x}{I_{xx}}y + \frac{M_y}{I_{yy}}x \quad (3.3)$$

Further, if either M_y or M_x is zero, then

$$\sigma_z = \frac{M_x}{I_{xx}}y \quad \text{or} \quad \sigma_z = \frac{M_y}{I_{yy}}x \quad (3.4)$$

Position of the Neutral Axis

The neutral axis always passes through the centroid of area of a beam's cross section, but its inclination α to the x axis depends on the form of the applied loading and the geometrical properties of the beam's cross section.

At all points on the neutral axis the direct stress is zero. Therefore, from Eq. (3.1),

$$0 = \left(\frac{M_y I_{xx} - M_x I_{xy}}{I_{xx} I_{yy} - I_{xy}^2} \right) x_{NA} + \left(\frac{M_x I_{yy} - M_y I_{xy}}{I_{xx} I_{yy} - I_{xy}^2} \right) y_{NA},$$

where x_{NA} and y_{NA} are the coordinates of any point on the neutral axis. Hence,

$$\frac{y_{NA}}{x_{NA}} = -\frac{M_y I_{xx} - M_x I_{xy}}{M_x I_{yy} - M_y I_{xy}}$$

or, referring to Fig. 15.12(b) and noting that when α is positive x_{NA} and y_{NA} are of opposite sign

$$\tan \alpha = \frac{M_y I_{xx} - M_x I_{xy}}{M_x I_{yy} - M_y I_{xy}} \quad (3.5)$$

DEFLECTIONS DUE TO BENDING

Suppose that at some section of an unsymmetrical beam the deflection normal to the neutral axis (and therefore an absolute deflection) is δ , as shown in Fig. 3.5. In other words, the centroid C is displaced from its initial position CI through an amount δ to its final position CF. Suppose also that the center of curvature R of the beam at this particular section is on the opposite side of the neutral axis to the direction

of the displacement δ and that the radius of curvature is ρ . For this position of the center of curvature and from the usual approximate expression for curvature,

we have

$$\frac{1}{\rho} = \frac{d^2\zeta}{dz^2}$$

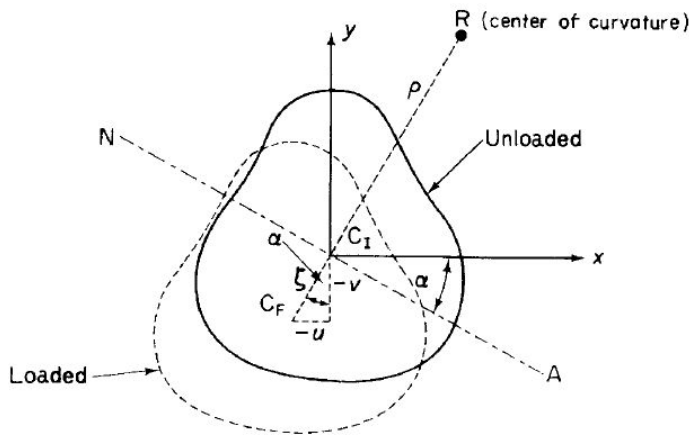


Figure 3.5 Determination of beam deflection due to bending.

The components u and v of δ are in the negative directions of the x and y axes, respectively, so that

$$u = -\zeta \sin \alpha, \quad v = -\zeta \cos \alpha$$

Differentiating above equ. twice with respect to z and then substituting for δ , we

Obtain

$$\frac{\sin \alpha}{\rho} = -\frac{d^2u}{dz^2}, \quad \frac{\cos \alpha}{\rho} = -\frac{d^2v}{dz^2}$$

we see that

$$\frac{1}{\rho} \begin{Bmatrix} \sin \alpha \\ \cos \alpha \end{Bmatrix} = \frac{1}{E(I_{xx}I_{yy} - I_{xy}^2)} \begin{bmatrix} -I_{xy} & I_{xx} \\ I_{yy} & -I_{xy} \end{bmatrix} \begin{Bmatrix} M_x \\ M_y \end{Bmatrix}$$

upon solving we have

$$\begin{Bmatrix} u'' \\ v'' \end{Bmatrix} = \frac{-1}{E(I_{xx}I_{yy} - I_{xy}^2)} \begin{bmatrix} -I_{xy} & I_{xx} \\ I_{yy} & -I_{xy} \end{bmatrix} \begin{Bmatrix} M_x \\ M_y \end{Bmatrix}$$

on rearranging, we get

$$\begin{Bmatrix} M_x \\ M_y \end{Bmatrix} = -E \begin{bmatrix} I_{xy} & I_{xx} \\ I_{yy} & I_{xy} \end{bmatrix} \begin{Bmatrix} u'' \\ v'' \end{Bmatrix}$$

that is

$$\begin{aligned} M_x &= -EI_{xy}u'' - EI_{xx}v'' \\ M_y &= -EI_{yy}u'' - EI_{xy}v'' \end{aligned}$$

For a beam having either Cx or Cy (or both) as an axis of symmetry, $I_{xy}=0$ and Eqs. reduce to

$$u'' = -\frac{M_y}{EI_{yy}}, \quad v'' = -\frac{M_x}{EI_{xx}}$$

Approximations for Thin-Walled Sections

We may exploit the thin-walled nature of aircraft structures to make simplifying assumptions in the determination of stresses and deflections produced by bending. Thus, the thickness t of thin-walled sections is assumed to be small compared with their cross-sectional dimensions so that stresses maybe regarded as being constant across the thickness. Furthermore, we neglect squares and higher powers of t in the computation of sectional properties and take the section to be represented by the midline of its wall. As an illustration of the procedure, we shall consider the channel section of Fig. 3.6(a).

The section is singly symmetric about the x axis so that $I_{xy}=0$. The second moment of area I_{xx} is then given by

$$I_{xx} = 2 \left[\frac{(b+t/2)t^3}{12} + \left(b + \frac{t}{2} \right) th^2 \right] + t \frac{[2(h-t/2)]^3}{12}$$

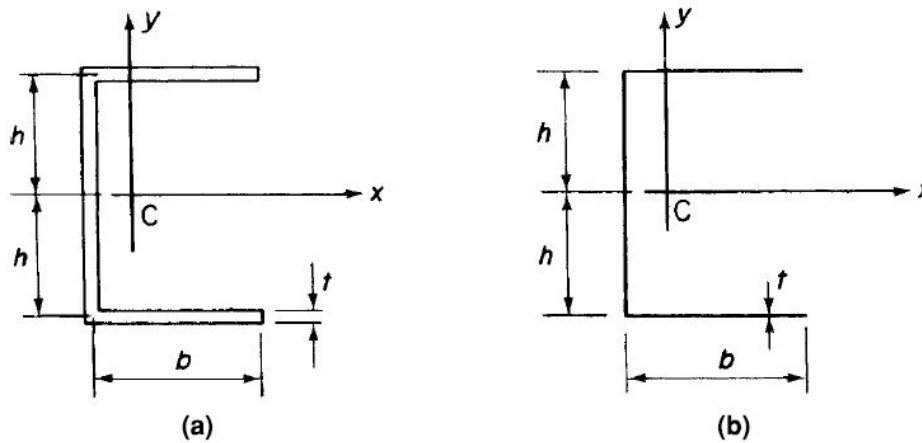


Figure 3.6 (a) Actual thin-walled channel section; (b) approximate representation of section.

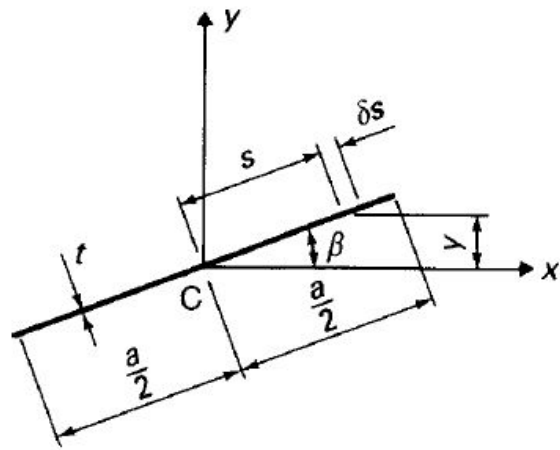


Figure 3.7 Second moments of area of an inclined thin section.

Expanding the cubed term, we have

$$I_{xx} = 2 \left[\frac{(b+t/2)t^3}{12} + \left(b + \frac{t}{2} \right) th^2 \right] + \frac{t}{12} \left[(2)^3 \left(h^3 - 3h^2 \frac{t}{2} + 3h \frac{t^2}{4} - \frac{t^3}{8} \right) \right]$$

which reduces, after powers of t^2 and upward are ignored, to

$$I_{xx} = 2bth^2 + t \frac{(2h)^3}{12}$$

The second moment of area of the section about Cy is obtained in a similar manner.

We see, therefore, that for the purpose of calculating section properties, we may regard the section as being represented by a single line, as shown in Fig. 3.7 (b).

Thin-walled sections frequently have inclined or curved walls which complicate the calculation of section properties. Consider the inclined thin section of Fig. 3.7. Its second moment of area about a horizontal axis through its centroid is given by

$$I_{xx} = 2 \int_0^{a/2} t y^2 ds = 2 \int_0^{a/2} t(s \sin \beta)^2 ds$$

from which

$$I_{xx} = \frac{a^3 t \sin^2 \beta}{12}$$

Similarly,

$$I_{yy} = \frac{a^3 t \cos^2 \beta}{12}$$

The product second moment of area is

$$\begin{aligned} I_{xy} &= 2 \int_0^{a/2} t y ds \\ &= 2 \int_0^{a/2} t(s \cos \beta)(s \sin \beta) ds \end{aligned}$$

which gives

$$I_{xy} = \frac{a^3 t \sin 2\beta}{24}$$

We note here that these expressions are approximate in that their derivation neglects powers of t^2 and upward by ignoring the second moments of area of the element ds about axes through its own centroid. Properties of thin-walled curved sections are found in a similar manner. Thus, I_{xx} for the semicircular section of Fig. 3.8 is

$$I_{xx} = \int_0^{\pi r} ty^2 ds$$

Expressing y and s in terms of a single variable ζ simplifies the integration, so

$$I_{xx} = \int_0^{\pi} t(r \cos \theta)^2 r d\theta$$

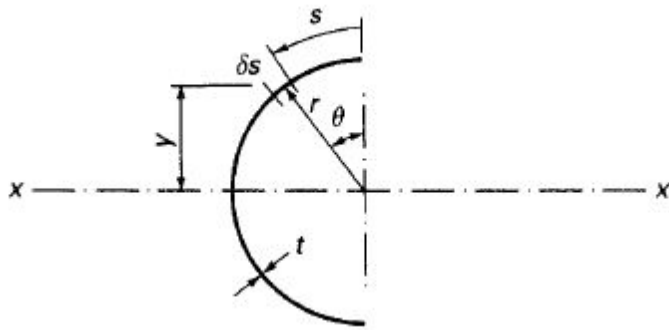


Figure 3.8 Second moment of area of a semicircular section.

from which

$$I_{xx} = \frac{\pi r^3 t}{2}$$

TEMPERATURE EFFECTS

A beam sections in aircraft structures are generally thin walled and do not necessarily have axes of symmetry. We shall now investigate how the effects of temperature on such sections may be determined.

We have seen that the strain produced by a temperature change ΔT is given by

$$\varepsilon = \alpha \Delta T$$

It follows that the direct stress on an element of cross-sectional area δA is

$$\sigma = E \alpha \Delta T \delta A$$

Consider now the beam section shown in Fig. 15.36 and suppose that a temperature variation ΔT is

applied to the complete cross section; that is, ΔT is a function of both x and y .

The total normal force due to the temperature change on the beam cross section is then given by

$$N_T = \int \int_A E\alpha \Delta T dA$$

Further, the moments about the x and y axes are

$$M_{xT} = \int \int_A E\alpha \Delta T y dA$$

$$M_{yT} = \int \int_A E\alpha \Delta T x dA,$$

We have noted that beam sections in aircraft structures are generally thin walled so that Eqs. may be more easily integrated for such sections by dividing them into thin rectangular components as we did when calculating section properties. We then use the Riemann integration technique in which we calculate the contribution of each component to the normal force and moments and sum them to determine each resultant. Equations then become

$$N_T = \sum E\alpha \Delta T A_i$$

$$M_{xT} = \sum E\alpha \Delta T \bar{y}_i A_i$$

$$M_{yT} = \sum E\alpha \Delta T \bar{x}_i A_i$$

in which A_i is the cross-sectional area of a component and x_i and y_i are the coordinates of its centroid.

SHEAR OF THIN WALLED BEAMS

GENERAL STRESS, STRAIN, AND DISPLACEMENT RELATIONSHIPS

In this section, we shall establish the equations of equilibrium and expressions for strain which are necessary for the analysis of open section beams supporting shear loads and closed section beam carrying shear and torsional loads. Generally, in the analysis we assume that axial constraint effects are negligible that the shear stresses normal to the beam surface may be neglected, since they are zero at each surface and the wall is thin, that direct and shear stresses on planes normal to the beam surface are constant across the thickness, and finally that the beam is of uniform section so that the thickness may vary with distance around each section but is constant along the beam. In addition, we ignore squares and higher powers of the thickness t in the calculation of section properties.

The parameter s in the analysis is distance measured around the cross section from some convenient origin. An element $\delta s \times \delta z \times t$ of the beam wall is maintained in equilibrium by a system of direct and shear stresses as shown in Fig. 16.1(a). The direct stress ζ_z is produced by bending moments or by the bending action of shear loads, whereas the shear stresses are due to shear and/or torsion of a closed section beam or shear of an open section beam. The hoop stress ζ_s is usually zero but may be caused,

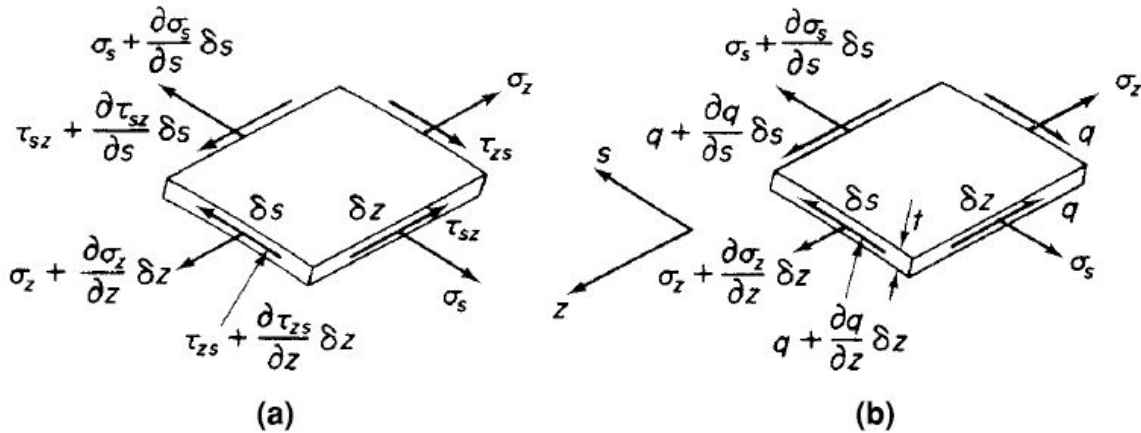


Figure 3.9 (a) General stress system on element of a closed or open section beam; (b) direct stress and shear flow system on the element.

in closed section beams, by internal pressure. Although we have specified that t may vary with s , this variation is small for most thin-walled structures so that we may reasonably make the approximation that t is constant over the length δs . Also, $\eta_{zs} = \eta_{sz} = \eta$, say. However, we shall find it convenient to work in terms of *shear flow* q —that is, shear force per unit length rather than in terms of shear stress. Hence, in Fig. 3.9 (b),

$$q = \tau t$$

and is regarded as being positive in the direction of increasing s .

For equilibrium of the element in the z direction and neglecting body forces

$$\left(\sigma_z + \frac{\partial \sigma_z}{\partial z} \delta z\right) t \delta s - \sigma_z t \delta s + \left(q + \frac{\partial q}{\partial s} \delta s\right) \delta_z - q \delta z = 0$$

which reduces to

$$\frac{\partial q}{\partial s} + t \frac{\partial \sigma_z}{\partial z} = 0$$

$$\frac{\partial q}{\partial z} + t \frac{\partial \sigma_s}{\partial s} = 0$$

The direct stresses ζ_z and ζ_s produce direct strains ε_z and ε_s , while the shear stress η induces a shear strain γ ($=\gamma_z s = \gamma_s z$). We shall now proceed to express these strains in terms of the three components of the displacement of a point in the section wall (see Fig. 3.10). Of these components, v_t is a tangential displacement in the xy plane and is taken to be positive in the direction of increasing s ; v_n is a normal displacement in the xy plane and is positive outward; and w is an axial displacement. We have

$$\varepsilon_z = \frac{\partial w}{\partial z}$$

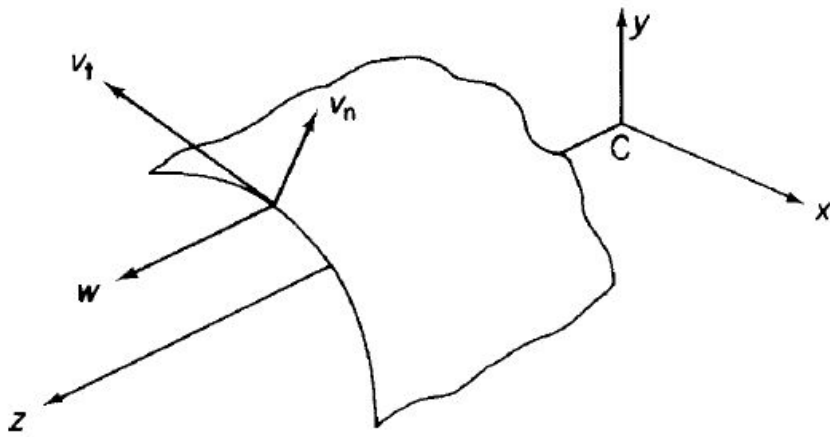


Figure 3.10 Axial, tangential, and normal components of displacement of a point in the beam wall.

It is possible to derive a simple expression for the direct strain ε_s in terms of v_t , v_n , s , and the curvature $1/r$ in the xy -plane of the beam wall. However, as we do not require ε_s in the subsequent analysis, we shall, for brevity, merely quote the expression

$$\varepsilon_s = \frac{\partial v_t}{\partial s} + \frac{v_n}{r}$$

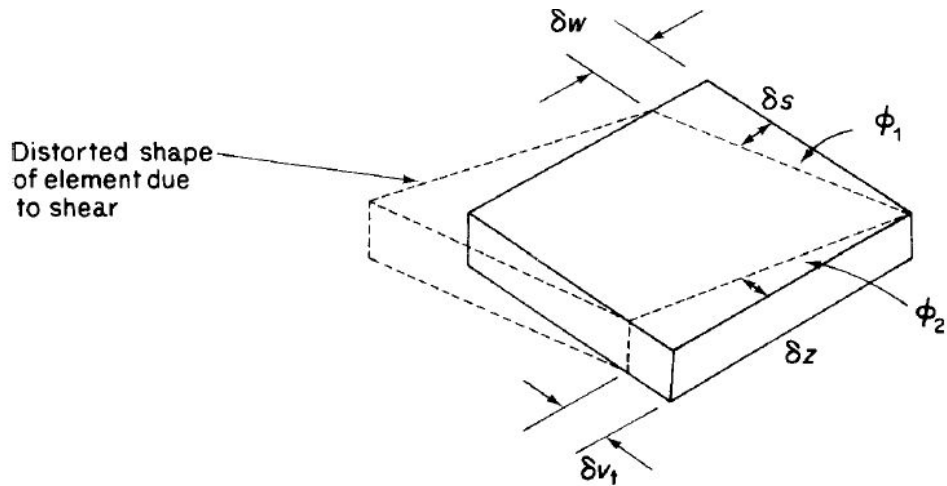


Figure 3.11 Determination of shear strain γ in terms of tangential and axial components of displacement.

The shear strain γ is found in terms of the displacements w and v_t by considering the shear distortion of an element $\delta s \times \delta z$ of the beam wall. From Fig. 3.11, we see that the shear strain is given by

$$\gamma = \phi_1 + \phi_2$$

or, in the limit as both δs and δz tend to zero

$$\gamma = \frac{\partial w}{\partial s} + \frac{\partial v_t}{\partial z}$$

In addition to the assumptions specified in the earlier part of this section, we further assume that during any displacement, the shape of the beam cross section is maintained by a system of closely spaced diaphragms which are rigid in their own plane but are perfectly flexible normal to their own plane (CSR assumption). There is, therefore, no resistance to axial displacement w , and the cross section moves as a rigid body in its own plane, the displacement of any point being completely specified by translations u and v and a rotation ζ (see Fig. 3.12).

At first sight this appears to be a rather sweeping assumption, but for aircraft structures of the thinshell type, whose cross sections are stiffened by ribs or frames positioned at frequent intervals along their lengths, it is a reasonable approximation for the actual behavior of such sections. The tangential displacement v_t of any point N in the wall of either an open or closed section beam is seen from Fig. 3.12 to be

$$v_t = p\theta + u \cos \psi + v \sin \psi$$

where clearly u , v , and ζ are functions of z only (w may be a function of z and s).

The origin O of the axes in Fig. 3.12 has been chosen arbitrarily, and the axes suffer displacements u , v , and ζ . These displacements, in a loading case such as pure torsion, are equivalent to a pure rotation about some point R(x_R , y_R) in the cross section where R is the *center of twist*. Therefore, in Fig. 3.12,

$$v_t = p_R \theta$$

$$p_R = p - x_R \sin \psi + y_R \cos \psi$$

$$v_t = p\theta - x_R \theta \sin \psi + y_R \theta \cos \psi$$

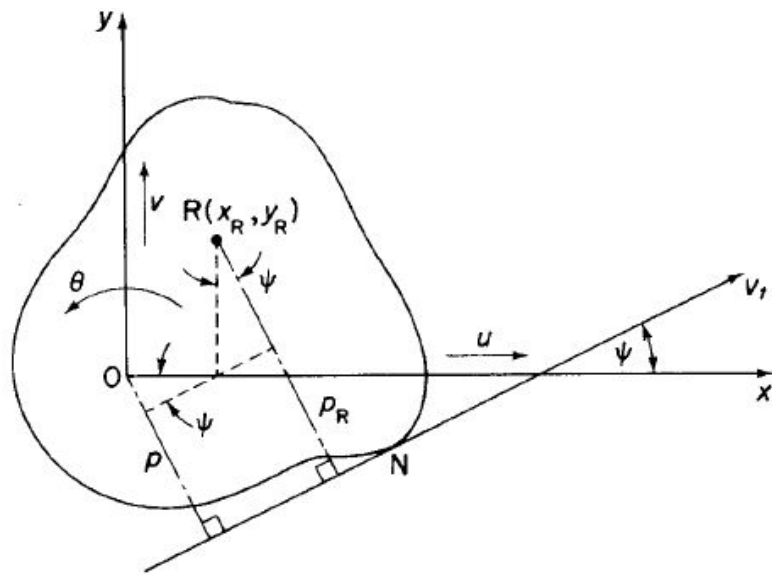


Figure 3.12 Establishment of displacement relationships and position of center of twist of beam (open or closed).

$$\frac{\partial v_t}{\partial z} = p \frac{d\theta}{dz} - x_R \sin \psi \frac{d\theta}{dz} + y_R \cos \psi \frac{d\theta}{dz}$$

$$\frac{\partial v_t}{\partial z} = p \frac{d\theta}{dz} + \frac{du}{dz} \cos \psi + \frac{dv}{dz} \sin \psi$$

$$x_R = -\frac{dv/dz}{d\theta/dz} \quad y_R = \frac{du/dz}{d\theta/dz}$$

SHEAR OF OPEN SECTION BEAMS

The open section beam of arbitrary section shown in Fig. 3.13 supports shear loads S_x and S_y such that there is no twisting of the beam cross section. For this condition to be valid, the shear loads must both pass through a particular point in the cross section known as the *shear center*.

Since there are no hoop stresses in the beam, the shear flows and direct stresses acting on an element of the beam wall are related by

$$\frac{\partial q}{\partial s} + t \frac{\partial \sigma_z}{\partial z} = 0$$

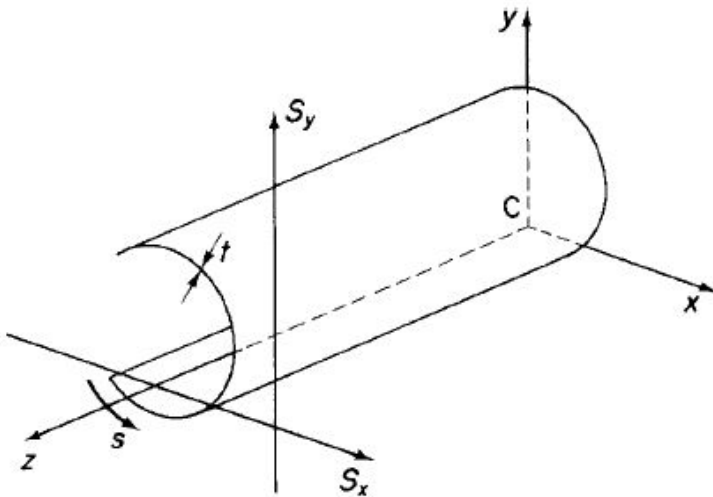


Figure 3.13 Shear loading of open section beam.

$\partial M_y / \partial z = S_x$, and so on—this expression becomes

$$\frac{\partial \sigma_z}{\partial z} = \frac{(S_x I_{xx} - S_y I_{xy})}{I_{xx} I_{yy} - I_{xy}^2} x + \frac{(S_y I_{yy} - S_x I_{xy})}{I_{xx} I_{yy} - I_{xy}^2} y$$

Substituting for $\partial \zeta_z / \partial z$

$$\frac{\partial q}{\partial s} = - \frac{(S_x I_{xx} - S_y I_{xy})}{I_{xx} I_{yy} - I_{xy}^2} tx - \frac{(S_y I_{yy} - S_x I_{xy})}{I_{xx} I_{yy} - I_{xy}^2} ty$$

$$\int_0^s \frac{\partial q}{\partial s} ds = - \left(\frac{S_x I_{xx} - S_y I_{xy}}{I_{xx} I_{yy} - I_{xy}^2} \right) \int_0^s tx ds - \left(\frac{S_y I_{yy} - S_x I_{xy}}{I_{xx} I_{yy} - I_{xy}^2} \right) \int_0^s ty ds$$

$$q_s = - \left(\frac{S_x I_{xx} - S_y I_{xy}}{I_{xx} I_{yy} - I_{xy}^2} \right) \int_0^s tx ds - \left(\frac{S_y I_{yy} - S_x I_{xy}}{I_{xx} I_{yy} - I_{xy}^2} \right) \int_0^s ty ds \quad (3.6)$$

$$q_s = -\frac{S_x}{I_{yy}} \int_0^s t x \, ds - \frac{S_y}{I_{xx}} \int_0^s t y \, ds$$

Shear Center

We have defined the position of the shear center as that point in the cross section through which shear loads produce no twisting. It may be shown by use of the reciprocal theorem that this point is also the center of twist of sections subjected to torsion. There are, however, some important exceptions to this general rule. Clearly, in the majority of practical cases, it is impossible to guarantee that a shear load will act through the shear center of a section. Equally apparent is the fact that any shear load may be represented by the combination of the shear load applied through the shear center and a torque. The stresses produced by the separate actions of torsion and shear may then be added by superposition. It is, therefore, necessary to know the location of the shear center in all types of section or to calculate its position. Where a cross section has an axis of symmetry, the shear center must, of course, lie on this axis. For cruciform or angle sections of the type shown in Fig. 3.14, the shear center is located at the intersection of the sides, since the resultant internal shear loads all pass through these points.

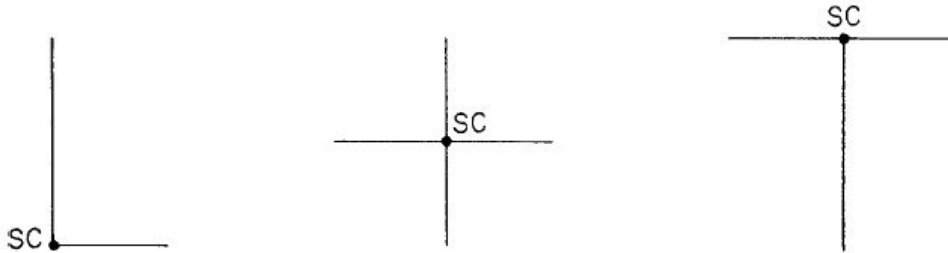


Figure 3.14 Shear center position for type of open section beam shown.

Twist and Warping of Shear-Loaded Closed Section Beams

Shear loads which are not applied through the shear center of a closed section beam cause cross sections to twist and warp; in other words, in addition to rotation, they suffer out of plane axial displacements. Expressions for these quantities may be derived in terms of the shear flow distribution q_s as follows. Since $q = \eta t$ and $\eta = G\gamma$ (see Chapter 1), then we can express q_s in terms of the warping and tangential displacements w and v_t of a point in the beam wall by using Eq. (16.6). Thus,

$$q_s = Gt \left(\frac{\partial w}{\partial s} + \frac{\partial v_t}{\partial z} \right)$$

$$\frac{q_s}{Gt} = \frac{\partial w}{\partial s} + p \frac{d\theta}{dz} + \frac{du}{dz} \cos \psi + \frac{dv}{dz} \sin \psi$$

$$\int_0^s \frac{q_s}{Gt} ds = \int_0^s \frac{\partial w}{\partial s} ds + \frac{d\theta}{dz} \int_0^s p ds + \frac{du}{dz} \int_0^s \cos \psi ds + \frac{dv}{dz} \int_0^s \sin \psi ds$$

or

$$\int_0^s \frac{q_s}{Gt} ds = \int_0^s \frac{\partial w}{\partial s} ds + \frac{d\theta}{dz} \int_0^s p ds + \frac{du}{dz} \int_0^s dx + \frac{dv}{dz} \int_0^s dy$$

$$\int_0^s \frac{q_s}{Gt} ds = (w_s - w_0) + 2A_{Os} \frac{d\theta}{dz} + \frac{du}{dz} (x_s - x_0) + \frac{dv}{dz} (y_s - y_0),$$

$$\oint \frac{q_s}{Gt} ds = 2A \frac{d\theta}{dz}$$

$$\frac{d\theta}{dz} = \frac{1}{2A} \oint \frac{q_s}{Gt} ds$$

$$w_s - w_0 = \int_0^s \frac{q_s}{Gt} ds - \frac{A_{Os}}{A} \oint \frac{q_s}{Gt} ds - \frac{du}{dz} (x_s - x_0) - \frac{dv}{dz} (y_s - y_0)$$

$$w_s - w_0 = \int_0^s \frac{q_s}{Gt} ds - \frac{A_{Os}}{A} \oint \frac{q_s}{Gt} ds - y_R \frac{d\theta}{dz} (x_s - x_0) + x_R \frac{d\theta}{dz} (y_s - y_0)$$

$$w_s - w_0 = \int_0^s \frac{q_s}{Gt} ds - \frac{A_{Os}}{A} \oint \frac{q_s}{Gt} ds$$

In problems involving singly or doubly symmetrical sections, the origin for s may be taken to coincide with a point of zero warping which will occur where an axis of symmetry and the wall of the section intersect. For unsymmetrical sections, the origin for s may be chosen arbitrarily. The resulting warping distribution will have exactly the same form as the actual distribution but will be displaced axially by the unknown warping displacement at the origin for s . This value may be found by referring to the torsion of closed section beams subject to axial constraint. In the analysis of such beams, it is assumed that the direct stress distribution set up by the constraint is directly proportional to the free warping of the section—that is,

$$\sigma = \text{constant} \times w$$

Also, since a pure torque is applied, the resultant of any internal direct stress system must be zero; in other words, it is self-equilibrating. Thus,

$$\text{Resultant axial load} = \oint \sigma t \, ds$$

where σ is the direct stress at any point in the cross section. Then, from the above assumption

$$0 = \oint w t \, ds$$

or

$$0 = \oint (w_s - w_0) t \, ds$$

so that

$$w_0 = \frac{\oint w_s t \, ds}{\oint t \, ds}$$

TORSION OF BEAMS

TORSION OF CLOSED SECTION BEAMS

A closed section beam subjected to a pure torque T as shown in Fig. 13.15 does not, in the absence of an axial constraint, develop a direct stress system. It follows that the equilibrium conditions reduce to $\partial q/\partial s=0$ and $\partial q/\partial z=0$, respectively. These relationships may only be satisfied simultaneously by a constant value of q . We deduce, therefore, that the application of a pure torque to a closed section beam results in the development of a constant shear flow in the beam wall. However, the shear stress η may vary around the cross section, since we allow the wall thickness t to be a function of s . The relationship between the applied torque and this constant shear flow is simply derived by considering the torsional equilibrium of the section shown in Fig. 13.16. The torque produced by the

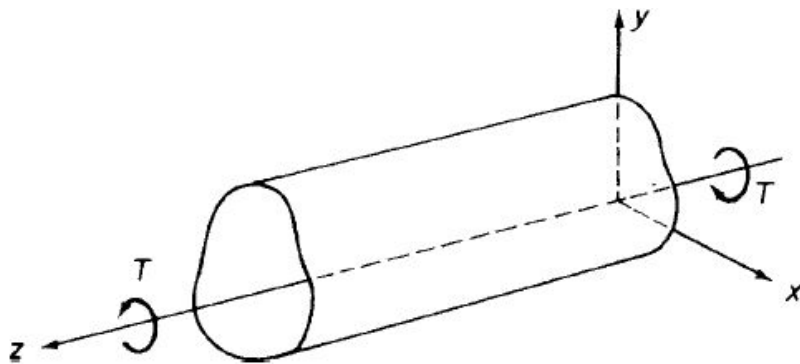


Figure 3.15 Torsion of a closed section beam.

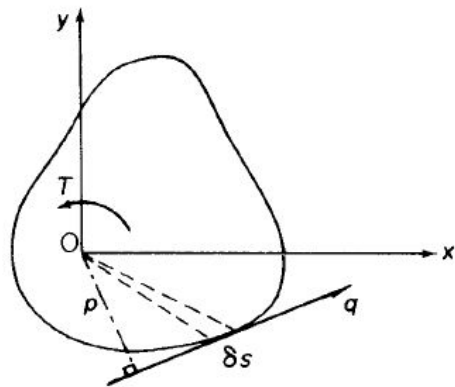


Figure 3.16 Determination of the shear flow distribution in a closed section beam subjected to torsion.

shear flow acting on an element δs of the beam wall is $pq\delta s$. Hence,

$$T = \oint pq \, ds$$

or, since q is constant and $\oint p \, ds = 2A$ (see Section 16.3)

$$T = 2Aq \quad (3.7)$$

Note that the origin O of the axes in Fig. 3.16 may be positioned in or outside the cross section of the beam, since the moment of the internal shear flows (whose resultant is a pure torque) is the same about any point in their plane. For an origin outside the cross section, the term $\oint pds$ will involve the summation of positive and negative areas. The sign of an area is determined by the sign of p , which itself is associated with the sign convention for torque as follows. If the movement of the foot of p along the tangent at any point in the positive direction of s leads to an anticlockwise rotation of p about the origin of axes, p is

positive. The positive direction of s is in the positive direction of q , which is anticlockwise (corresponding to a positive torque). Thus, in Fig. 3.17 a generator OA, rotating about O, will initially sweep out a negative area, since p_A is negative. At B, however, p_B is positive so that the area swept out by the generator has changed sign (at the point where the tangent passes through O and $p=0$). Positive and negative areas cancel each other out as they overlap, so as the generator moves completely around the section, starting and returning to A, say, the resultant area is that enclosed by the profile of the beam.

The theory of the torsion of closed section beams is known as the *Bredt–Batho theory*, and Eq. (3.7) is often referred to as the *Bredt–Batho formula*.

Displacements Associated with the Bredt–Batho Shear Flow

The relationship between q and shear strain γ established, namely,

$$q = Gt \left(\frac{\partial w}{\partial s} + \frac{\partial v_t}{\partial z} \right)$$

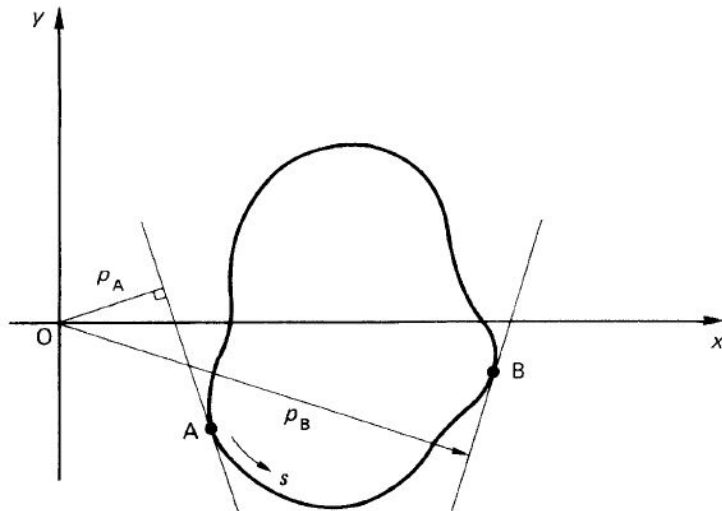


Figure 3.17 Sign convention for swept areas.

is valid for the pure torsion case, where q is constant. Differentiating this expression with respect to z , we have

$$\frac{\partial q}{\partial z} = Gt \left(\frac{\partial^2 w}{\partial z \partial s} + \frac{\partial^2 v_t}{\partial z^2} \right) = 0$$

or

$$\frac{\partial}{\partial s} \left(\frac{\partial w}{\partial z} \right) + \frac{\partial^2 v_t}{\partial z^2} = 0$$

In the absence of direct stresses, the longitudinal strain $\partial w / \partial z (= \varepsilon_z)$ is zero so that

$$\frac{\partial^2 v_t}{\partial z^2} = 0$$

Hence,

$$p \frac{d^2 \theta}{dz^2} + \frac{d^2 u}{dz^2} \cos \psi + \frac{d^2 v}{dz^2} \sin \psi = 0$$

$$\frac{d^2 \theta}{dz^2} = 0, \quad \frac{d^2 u}{dz^2} = 0, \quad \frac{d^2 v}{dz^2} = 0$$

It follows that $\zeta = Az + B$, $u = Cz + D$, $v = Ez + F$, where A , B , C , D , E , and F are unknown constants. Thus, ζ , u , and v are all linear functions of z .

Equation, relating the rate of twist to the variable shear flow q_s developed in a shear loaded closed section beam, is also valid for the case $q_s = q = \text{constant}$. Hence,

$$\frac{d\theta}{dz} = \frac{q}{2A} \oint \frac{ds}{Gt}$$

$$\frac{d\theta}{dz} = \frac{T}{4A^2} \oint \frac{ds}{Gt}$$

$$w_s - w_0 = q \int_0^s \frac{ds}{Gt} - \frac{A_{Os}}{A} q \oint \frac{ds}{Gt}$$

$$w_s - w_0 = \frac{T\delta}{2A} \left(\frac{\delta_{Os}}{\delta} - \frac{A_{Os}}{A} \right)$$

$$\delta = \oint \frac{ds}{Gt} \quad \text{and} \quad \delta_{Os} = \int_0^s \frac{ds}{Gt}$$

TORSION OF OPEN SECTION BEAMS

An approximate solution for the torsion of a thin-walled open section beam may be found by applying the results obtained, for the torsion of a thin rectangular strip. If such a strip is bent to form an open section beam, as shown in Fig. 3.18 (a), and if the distance s measured around the crosssection is large compared with its thickness t , then the contours of the membrane—that is, the linesof shear stress—are still approximately parallel to the inner and outer boundaries. It follows that the shear lines in an element δs of the open section must be nearly the same as those in an element δy of a rectangular strip as demonstrated in Fig. 3.18 (b). Equations) may therefore be applied to the open beam but with reduced accuracy. Referring to Fig. 3.18 (b), we observe that becomes

$$\tau_{zs} = 2Gn \frac{d\theta}{dz}, \quad \tau_{zn} = 0$$

$$\tau_{zs,\max} = \pm Gt \frac{d\theta}{dz}$$

$$J = \sum \frac{st^3}{3} \quad \text{or} \quad J = \frac{1}{3} \int_{\text{sect}} t^3 ds$$

$$T = GJ \frac{d\theta}{dz}$$

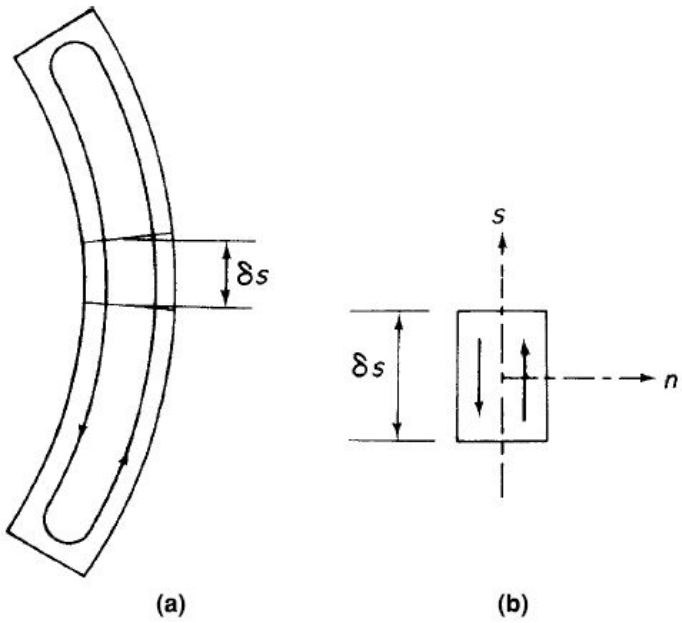


Figure 3.18 (a) Shear lines in a thin-walled open section beam subjected to torsion; (b) approximation of elemental shear lines to those in a thin rectangular strip.

The shear stress distribution and the maximum shear stress are sometimes more conveniently expressed in terms of the applied torque. Therefore, substituting for $d\zeta/dz$ in Eqs.

$$\tau_{zs} = \frac{2n}{J} T, \quad \tau_{zs,\max} = \pm \frac{tT}{J}$$

We assume in open beam torsion analysis that the cross section is maintained by the system of closely spaced diaphragms described in Section 16.1 and that the beam is of uniform section. Clearly, in this problem, the shear stresses vary across the thickness of the beam wall, whereas other stresses, such as axial constraint stresses are assumed constant across the thickness.

Warping of the Cross Section

A thin-walled open section beam suffers warping across its thickness when subjected to torsion. This warping, w_t , may be deduced by comparing Fig. 3.18 (b).

$$w_t = ns \frac{d\theta}{dz}$$

In addition to warping across the thickness, the cross section of the beam will warp in a similar manner to that of a closed section beam.

$$\gamma_{zs} = \frac{\partial w}{\partial s} + \frac{\partial v_t}{\partial z}$$

Referring the tangential displacement v_t to the center of twist R of the cross section, we have

$$\frac{\partial v_t}{\partial z} = p_R \frac{d\theta}{dz}$$

Substituting for $\partial v_t / \partial z$

$$\gamma_{zs} = \frac{\partial w}{\partial s} + p_R \frac{d\theta}{dz}$$

$$\tau_{zs} = G \left(\frac{\partial w}{\partial s} + p_R \frac{d\theta}{dz} \right)$$

On the midline of the section wall $\eta z_s = 0$

$$\frac{\partial w}{\partial s} = -p_R \frac{d\theta}{dz}$$

Integrating this expression with respect to s and taking the lower limit of integration to coincide with the point of zero warping, we obtain

$$w_s = -\frac{d\theta}{dz} \int_0^s p_R ds$$

From Eqs. it can be seen that two types of warping exist in an open section beam. Equation gives the warping of the midline of the beam; this is known as *primary warping* and is assumed to be constant across the wall thickness. Equation gives the warping of the beam across its wall thickness. This is called *secondary warping*, is very much less than primary warping, and is usually ignored in the thin-walled sections common to aircraft structures. Equation may be rewritten in the form

$$w_s = -2A_R \frac{d\theta}{dz}$$

$$w_s = -2A_R \frac{T}{GJ}$$

in which $A_R = \frac{1}{2} \int_0^s p_R ds$ is the area swept out by a generator, rotating about the center of

twist, from the point of zero warping, as shown in figure 3.19. The sign of w_s , for a given direction of torque, depends on the sign of A_R , which in turn depends on the sign of p_R , the perpendicular distance from the center of twist to the tangent at any point. Again, as for closed section beams, the sign of p_R depends on the assumed direction of a positive torque, in this case anticlockwise. Therefore, p_R (and therefore A_R) is positive if movement of the foot of p_R along the tangent in the assumed direction of s leads to an anti-clockwise rotation of p_R about the center of twist. Note that for open section beams the positive direction of s may be chosen arbitrarily, since, for a given torque, the sign of the warping displacement depends only on the sign of the swept area A_R .

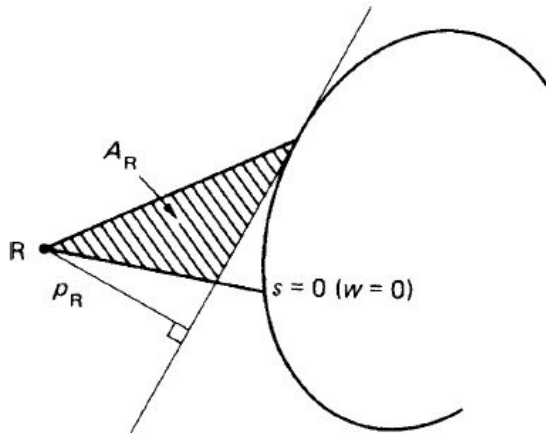


Figure 3.18 Warping of an open section beam.

UNIT-IV

STRUCTURAL IDEALIZATION

STRUCTURAL IDEALIZATION

So far we have been concerned with relatively uncomplicated structural sections which in practice would be formed from thin plate or by the extrusion process. While these sections exist as structural members in their own right, they are frequently used, to stiffen more complex structural shapes such as fuselages, wings, and tail surfaces. Thus, a two-spar wing section could take the form shown in Fig. 4.1, in which Z-section stringers are used to stiffen the thin skin while angle sections form the spar flanges. Clearly, the analysis of a section of this type would be complicated and tedious unless some simplifying assumptions are made. Generally, the number and nature of these simplifying assumptions determine the accuracy and the degree of complexity of the analysis; the more complex the analysis, the greater the accuracy obtained. The degree of simplification introduced is governed by the particular situation surrounding the problem. For a preliminary investigation, speed and simplicity are often of greater importance than extreme accuracy; on the other hand, a final solution must be as exact as circumstances allow.

Complex structural sections may be idealized into simpler —mechanical model forms which behave, under given loading conditions, in the same, or very nearly the same, way as the actual structure. We shall see, however, that different models of the same structure are required to simulate actual behavior under different systems of loading.

PRINCIPLE

In the wing section of Fig. 4.1, the stringers and spar flanges have small cross-sectional dimensions compared with the complete section. Therefore, the variation in stress over the cross section of a stringer

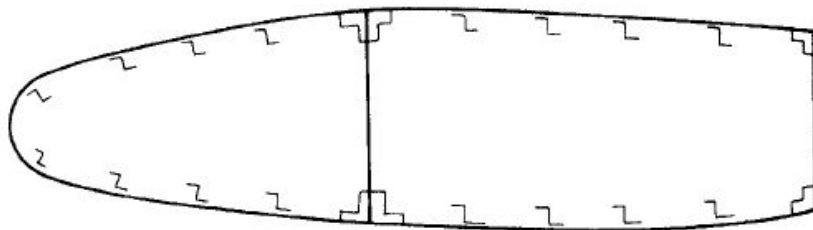


Figure 4.1 Typical wing section.

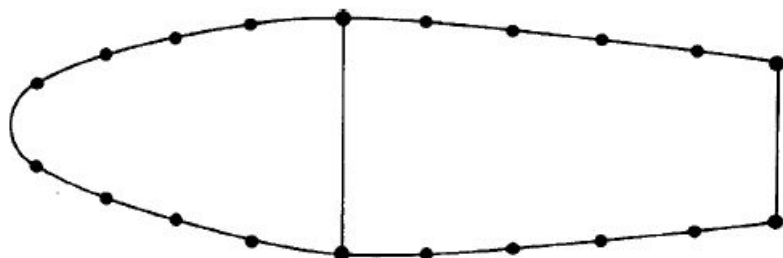


Figure 4.2 Idealization of a wing section.

due to, say, bending of the wing would be small. Furthermore, the difference between the distances of the stringer centroids and the adjacent skin from the wing section axis is small. It would be reasonable to

assume, therefore, that the direct stress is constant over the stringer cross sections. We could therefore replace the stringers and spar flanges by concentrations of area, known as *booms*, over which the direct stress is constant and which are located along the midline of the skin, as shown in Fig. 4.2. In wing and fuselage sections of the type shown in Fig. 4.1, the stringers and spar flanges carry most of the direct stresses, while the skin is mainly effective in resisting shear stresses, although it also carries some of the direct stresses. The idealization shown in Fig. 4.2 may therefore be taken a stage further by assuming that all direct stresses are carried by the booms, while the skin is effective only in shear. The direct stress-carrying capacity of the skin may be allowed for by increasing each boom area by an area equivalent to the direct stress-carrying capacity of the adjacent skin panels. The calculation of these equivalent areas will generally depend on an initial assumption as to the form of the distribution of direct stress in a boom/skin panel.

IDEALIZATION OF A PANEL

Suppose that we wish to idealize the panel of Fig. 4.3(a) into a combination of direct stress-carrying booms and shear-stress-only-carrying skin, as shown in Fig. 4.3 (b). In Fig. 4.3(a), the direct stress-carrying thickness t_D of the skin is equal to its actual thickness t , while in Fig. 4.3(b), $t_D=0$. Suppose also that the direct stress distribution in the actual panel varies linearly from an unknown value ζ_1 to an unknown value ζ_2 . Clearly the analysis should predict the extremes of stress ζ_1 and ζ_2 , although the distribution of direct stress is obviously lost. Since the loading producing the direct stresses in the actual and idealized panels must be the same, we can equate moments to obtain expressions for the boom areas B_1 and B_2 . Thus, taking moments about the right-hand edge of each panel,

$$\sigma_2 t_D \frac{b^2}{2} + \frac{1}{2}(\sigma_1 - \sigma_2)t_D b \frac{2}{3}b = \sigma_1 B_1 b$$

$$B_1 = \frac{t_D b}{6} \left(2 + \frac{\sigma_2}{\sigma_1} \right) \quad (4.1)$$

$$B_2 = \frac{t_D b}{6} \left(2 + \frac{\sigma_1}{\sigma_2} \right) \quad (4.2)$$

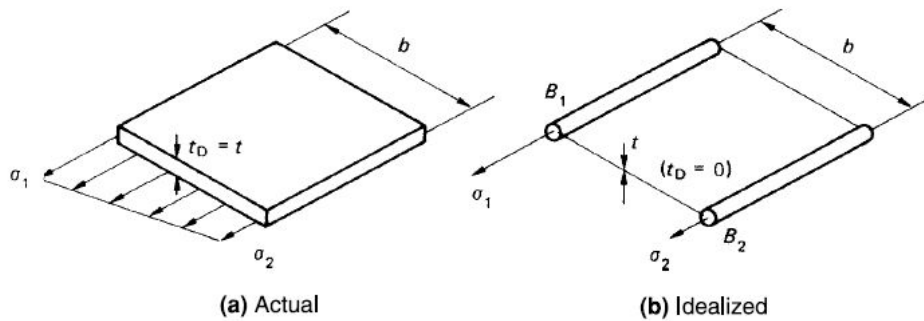


Figure 4.2 Idealization of a panel.

EFFECT OF IDEALIZATION ON THE ANALYSIS OF OPEN AND CLOSED SECTION BEAMS

Suppose that an open or closed section beam is subjected to given bending or shear loads and that the required idealization has been completed. The analysis of such sections usually involves the determination of the neutral axis position and the calculation of sectional properties. The position of the neutral axis is derived from the condition that the resultant load on the beam cross section is zero, that is,

$$\int_A \sigma_z dA = 0$$

The area A in this expression is clearly the direct stress-carrying area. It follows that the centroid of the cross section is the centroid of the direct stress-carrying area of the section, depending on the degree and method of idealization. The sectional properties, I_{xx} , and so on, must also refer to the direct stress-carrying area.

Bending of Open and Closed Section Beams

In direct stress distribution, the coordinates (x, y) of points in the cross section are referred to axes having their origin at the centroid of the direct stress-carrying area. Furthermore, the section properties I_{xx} , I_{yy} , and I_{xy} are calculated for the direct stress-carrying area only. In the case where the beam cross section has been completely idealized into direct stress-carrying booms and shear-stress-only-carrying panels, the direct stress distribution consists of a series of direct stresses concentrated at the centroids of the booms.

Shear of Open Section Beams

The derivation of Eq. (3.6) for the shear flow distribution in the cross section of an open section beam is based on the equilibrium equation. The thickness t in this equation refers to the direct stress-carrying thickness t_D of the skin. Equation (3.6) may therefore be rewritten as

$$q_s = -\left(\frac{S_x I_{xx} - S_y I_{xy}}{I_{xx} I_{yy} - I_{xy}^2} \right) \int_0^s t_D x \, ds - \left(\frac{S_y I_{yy} - S_x I_{xy}}{I_{xx} I_{yy} - I_{xy}^2} \right) \int_0^s t_D y \, ds \quad (4.3)$$

in which $t_D = t$ if the skin is fully effective in carrying direct stress or $t_D = 0$ if the skin is assumed to carry only shear stresses. Again the section properties in Eq. (4.3) refer to the direct stress-carrying area of the section,

Equation (4.3) makes no provision for the effects of booms, which cause discontinuities in the skin and therefore interrupt the shear flow. Consider the equilibrium of the r th boom in the elemental length of beam shown in Fig. 4.3(a) which carries shear loads S_x and S_y acting through its shear center S .

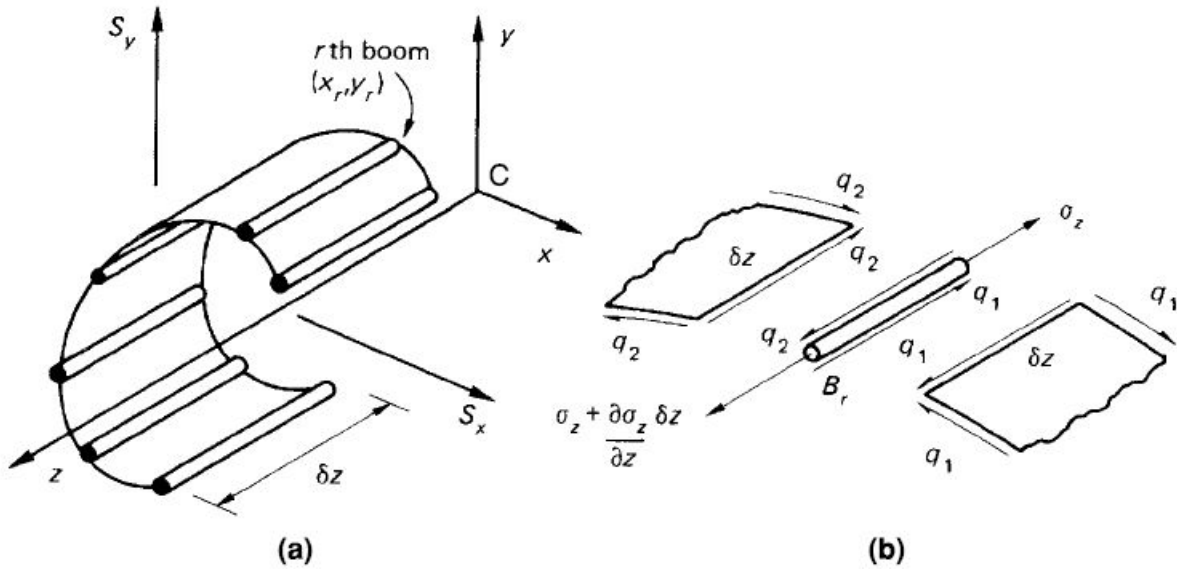


Figure 4.3 (a) Elemental length of shear loaded open section beam with booms; (b) equilibrium of boom element.

These shear loads produce direct stresses due to bending in the booms and skin and shear stresses in the skin. Suppose that the shear flows in the skin adjacent to the r th boom of cross-sectional area B_r are q_1 and q_2 . Then, from Fig. 4.3 (b),

$$\left(\sigma_z + \frac{\partial \sigma_z}{\partial z} \delta z \right) B_r - \sigma_z B_r + q_2 \delta z - q_1 \delta z = 0$$

which simplifies to

$$q_2 - q_1 = -\frac{\partial \sigma_z}{\partial z} B_r \quad (4.4)$$

$$q_2 - q_1 = - \left[\frac{(\partial M_y / \partial z) I_{xx} - (\partial M_x / \partial z) I_{xy}}{I_{xx} I_{yy} - I_{xy}^2} \right] B_r x_r - \left[\frac{(\partial M_x / \partial z) I_{yy} - (\partial M_y / \partial z) I_{xy}}{I_{xx} I_{yy} - I_{xy}^2} \right] B_r y_r$$

$$q_2 - q_1 = - \left(\frac{S_x I_{xx} - S_y I_{xy}}{I_{xx} I_{yy} - I_{xy}^2} \right) B_r x_r - \left(\frac{S_y I_{yy} - S_x I_{xy}}{I_{xx} I_{yy} - I_{xy}^2} \right) B_r y_r \quad (4.5)$$

Equation (4.5) gives the change in shear flow induced by a boom which itself is subjected to a direct load ($\zeta_r B_r$). Each time a boom is encountered, the shear flow is incremented by this amount so that if, at any distance s around the profile of the section, n booms have been passed, the shear flow at the point is given by

$$q_s = - \left(\frac{S_x I_{xx} - S_y I_{xy}}{I_{xx} I_{yy} - I_{xy}^2} \right) \left(\int_0^s t_D dx ds + \sum_{r=1}^n B_r x_r \right) - \left(\frac{S_y I_{yy} - S_x I_{xy}}{I_{xx} I_{yy} - I_{xy}^2} \right) \left(\int_0^s t_D dy ds + \sum_{r=1}^n B_r y_r \right) \quad (4.6)$$

Shear Loading of Closed Section Beams

Arguments identical to those in the shear of open section beams apply in this case. Thus, the shear flow at any point around the cross section of a closed section beam comprising booms and skin of direct stress-carrying thickness t_D is

$$q_s = - \left(\frac{S_x I_{xx} - S_y I_{xy}}{I_{xx} I_{yy} - I_{xy}^2} \right) \left(\int_0^s t_D dx ds + \sum_{r=1}^n B_r x_r \right) - \left(\frac{S_y I_{yy} - S_x I_{xy}}{I_{xx} I_{yy} - I_{xy}^2} \right) \left(\int_0^s t_D dy ds + \sum_{r=1}^n B_r y_r \right) + q_{s,0} \quad (4.7)$$

Note that the zero value of the —basic|| or —open section|| shear flow at the —cut|| in a skin for which $t_D = 0$ extends from the —cut|| to the adjacent booms.

DEFLECTION OF OPEN AND CLOSED SECTION BEAMS

Bending, shear, and torsional deflections of thin-walled beams are readily obtained by application of the unit load method. The displacement in a given direction due to torsion is given directly by,

$$\Delta_T = \int_L \frac{T_0 T_1}{GJ} dz \quad (4.8)$$

where J , the torsion constant, depends on the type of beam under consideration.

Expressions for the bending and shear displacements of unsymmetrical thin-walled beams may also be determined by the unit load method. They are complex for the general case and are most easily derived from first principles by considering the complementary energy of the elastic body in terms of stresses and strains rather than loads and displacements. We observed that the theorem of the principle of the

stationary value of the total complementary energy of an elastic system is equivalent to the application of the principle of virtual work where virtual forces act through real displacements. We may therefore specify that in our expression for total complementary energy, the displacements are the actual displacements produced by the applied loads, while the virtual force system is the unit load. Considering deflections due to bending, the increment in total complementary energy due to the application of a virtual unit load is

$$-\int_L \left(\int_A \sigma_{z,1} \varepsilon_{z,0} dA \right) dz + 1 \Delta_M$$

where $\zeta_{z,1}$ is the direct bending stress at any point in the beam cross section corresponding to the unit load and $\varepsilon_{z,0}$ is the strain at the point produced by the actual loading system. Further, ΔM is the actual displacement due to bending at the point of application and in the direction of the unit load. Since the system is in equilibrium under the action of the unit load, the above expression must equal zero. Hence,

$$\Delta M = \int_L \left(\int_A \sigma_{z,1} \varepsilon_{z,0} dA \right) dz \quad (4.9)$$

$$\begin{aligned} \sigma_{z,1} &= \left(\frac{M_{y,1}I_{xx} - M_{x,1}I_{xy}}{I_{xx}I_{yy} - I_{xy}^2} \right)_x + \left(\frac{M_{x,1}I_{yy} - M_{y,1}I_{xy}}{I_{xx}I_{yy} - I_{xy}^2} \right)_y \\ \varepsilon_{z,0} &= \frac{1}{E} \left[\left(\frac{M_{y,0}I_{xx} - M_{x,0}I_{xy}}{I_{xx}I_{yy} - I_{xy}^2} \right)_x + \left(\frac{M_{x,0}I_{yy} - M_{y,0}I_{xy}}{I_{xx}I_{yy} - I_{xy}^2} \right)_y \right] \end{aligned}$$

where the suffixes 1 and 0 refer to the unit and actual loading systems, and x, y are the coordinates of any point in the cross section referred to a centroidal system of axes. Substituting for $\zeta_{z,1}$ and $\varepsilon_{z,0}$ in Eq. (4.9)

$$\begin{aligned} \Delta M &= \frac{1}{E(I_{xx}I_{yy} - I_{xy}^2)^2} \int_L \left\{ (M_{y,1}I_{xx} - M_{x,1}I_{xy})(M_{y,0}I_{xx} - M_{x,0}I_{xy})I_{yy} \right. \\ &\quad + (M_{x,1}I_{yy} - M_{y,1}I_{xy})(M_{x,0}I_{yy} - M_{y,0}I_{xy})I_{xx} \\ &\quad + [(M_{y,1}I_{xx} - M_{x,1}I_{xy})(M_{x,0}I_{yy} - M_{y,0}I_{xy}) \\ &\quad \left. + (M_{x,1}I_{yy} - M_{y,1}I_{xy})(M_{y,0}I_{xx} - M_{x,0}I_{xy})]I_{xy} \right\} dz \quad (4.10) \end{aligned}$$

For a section having either x or y axis as an axis of symmetry, $I_{xy} = 0$, and Eq. (4.10) reduces to

$$\Delta_M = \frac{1}{E} \int_L \left(\frac{M_{y,1}M_{y,0}}{I_{yy}} + \frac{M_{x,1}M_{x,0}}{I_{xx}} \right) dz \quad (4.11)$$

The derivation of an expression for the shear deflection of thin-walled sections by the unit load method is achieved in a similar manner. By comparing Eq. (4.9), we deduce that the deflection Δ_S , due to shear of a thin-walled open or closed section beam of thickness t , is given by

$$\Delta_S = \int_L \left(\int_{\text{sect}} \tau_1 \gamma_0 t ds \right) dz \quad (4.12)$$

where η_1 is the shear stress at an arbitrary point s around the section produced by a unit load applied at the point and in the direction Δ_S , and γ_0 is the shear strain at the arbitrary point corresponding to the actual loading system. The integral in parentheses is taken over all the walls of the beam. In fact, both the applied and unit shear loads must act through the shear center of the cross section; otherwise additional torsional displacements occur. Where shear loads act at other points, these must be replaced by shear loads at the shear center plus a torque. The thickness t is the actual skin thickness and may vary around the cross section but is assumed to be constant along the length of the beam. Rewriting Eq. (4.12) in terms of shear flows q_1 and q_0 , we obtain

$$\Delta_S = \int_L \left(\int_{\text{sect}} \frac{q_0 q_1}{Gt} ds \right) dz \quad (4.13)$$

where again the suffixes refer to the actual and unit loading systems. In the cases of both open and closed section beams, the general expressions for shear flow are long and are best evaluated before substituting in Eq. (4.13). For an open section beam comprising booms and walls of direct stress-carrying thickness t_D , we have, from Eq. (4.6),

$$q_0 = - \left(\frac{S_{x,0}I_{xx} - S_{y,0}I_{xy}}{I_{xx}I_{yy} - I_{xy}^2} \right) \left(\int_0^s t_D x ds + \sum_{r=1}^n B_r x_r \right) - \left(\frac{S_{y,0}I_{yy} - S_{x,0}I_{xy}}{I_{xx}I_{yy} - I_{xy}^2} \right) \left(\int_0^s t_D y ds + \sum_{r=1}^n B_r y_r \right) \quad (4.14)$$

and

$$\begin{aligned}
q_1 = & - \left(\frac{S_{x,1}I_{xx} - S_{y,1}I_{xy}}{I_{xx}I_{yy} - I_{xy}^2} \right) \left(\int_0^s t_D x \, ds + \sum_{r=1}^n B_r x_r \right) \\
& - \left(\frac{S_{y,1}I_{yy} - S_{x,1}I_{xy}}{I_{xx}I_{yy} - I_{xy}^2} \right) \left(\int_0^s t_D y \, ds + \sum_{r=1}^n B_r y_r \right)
\end{aligned} \tag{4.15}$$

Similar expressions are obtained for a closed section beam from Eq. (4.7).

UNIT-V

ANALYSIS OF FUSELAGE, WING AND LANDING GEAR

Wing Spars and Box Beams

In Unit 3, we established the basic theory for the analysis of open and closed section-in-walled beams subjected to bending, shear, and torsional loads. In addition, in Unit 4, we saw how complex stringer stiffened sections could be idealized into sections more amenable to analysis. We shall now extend this analysis to actual aircraft components, including, in this chapter, wing spars and box beams.

Aircraft structural components are, complex, consisting usually of thin sheets of metal stiffened by arrangements of stringers. These structures are highly redundant and require some degree of simplification or idealization before they can be analyzed. The analysis presented here is therefore approximate, and the degree of accuracy obtained depends on the number of simplifying assumptions made. A further complication arises in that factors such as warping restraint, structural and loading discontinuities, and shear lag significantly affect the analysis. Generally, a high degree of accuracy can only be obtained by using computer-based techniques such as the finite element method. However, the simpler, quicker, and cheaper approximate methods can be used to advantage in the preliminary stages of design when several possible structural alternatives are being investigated; they also provide an insight into the physical behavior of structures which computer-based techniques do not.

Major aircraft structural components such as wings and fuselages are usually tapered along their lengths for greater structural efficiency. Thus, wing sections are reduced both chordwise and in depth along the wing span toward the tip and fuselage sections aft of the passenger cabin taper to provide a more efficient aerodynamic and structural shape.

The analysis of open and closed section beams presented in Unit 3 assumes that the beam sections are uniform. The effect of taper on the prediction of direct stresses produced by bending is minimal if the taper is small and the section properties are calculated at the particular section being considered; Equations may therefore be used with reasonable accuracy. On the other hand, the calculation of shear stresses in beam webs can be significantly affected by taper.

TAPERED WING SPAR

Consider first the simple case of a beam—for example, a wing spar—positioned in the yz plane and comprising two flanges and a web; an elemental length δz of the beam is shown in Fig. 5.1. At the section z , the beam is subjected to a positive bending moment M_x and a positive shear force S_y .

The bending moment resultants $P_{z,1}$ and $P_{z,2}$ are parallel to the z axis of the beam. For a beam in which the flanges are assumed to resist all the direct stresses, $P_{z,1}=Mx/h$ and $P_{z,2}=-Mx/h$. In the case where the web is assumed to be fully effective in resisting direct stress, $P_{z,1}$ and $P_{z,2}$ are determined by multiplying the direct stresses $\zeta_{z,1}$ and $\zeta_{z,2}$ found by the flange areas B_1 and B_2 . $P_{z,1}$ and $P_{z,2}$ are the components in the z direction of the axial loads P_1 and P_2 in the flanges. These have components $P_{y,1}$ and $P_{y,2}$ parallel to the y axis given by

$$P_{y,1} = P_{z,1} \frac{\delta y_1}{\delta z} \quad P_{y,2} = -P_{z,2} \frac{\delta y_2}{\delta z} \quad (5.1)$$

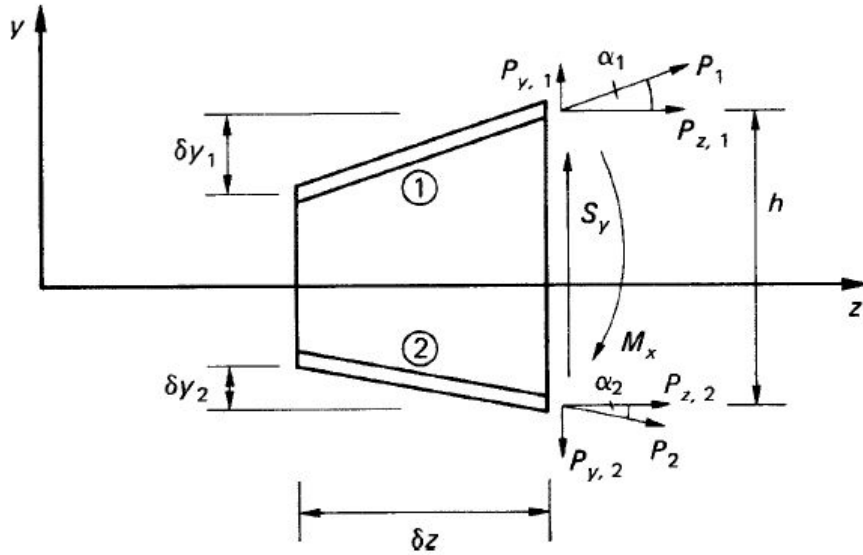


Figure 5.1 Effect of taper on beam analysis.

in which, for the direction of taper shown, δy_2 is negative. The axial load in flange ① is given by

$$P_1 = (P_{z,1}^2 + P_{y,1}^2)^{1/2}$$

Substituting for $P_{y,1}$ from Eq. (5.1), we have

$$P_1 = P_{z,1} \frac{(\delta z^2 + \delta y_1^2)^{1/2}}{\delta z} = \frac{P_{z,1}}{\cos \alpha_1} \quad (5.2)$$

Similarly,

$$P_2 = \frac{P_{z,2}}{\cos \alpha_2} \quad (5.3)$$

The internal shear force S_y comprises the resultant $S_{y,w}$ of the web shear flows together with the vertical components of P_1 and P_2 . Thus,

$$S_y = S_{y,w} + P_{y,1} - P_{y,2}$$

or

$$S_y = S_{y,w} + P_{z,1} \frac{\delta y_1}{\delta z} + P_{z,2} \frac{\delta y_2}{\delta z} \quad (5.4)$$

so that,

$$S_{y,w} = S_y - P_{z,1} \frac{\delta y_1}{\delta z} - P_{z,2} \frac{\delta y_2}{\delta z} \quad (5.5)$$

Again we note that δy_2 in Eqs. (5.4) and (5.5) is negative. Equation (5.5) may be used to determine the shear flow distribution in the web. For a completely idealized beam, the web shear flow is constant through the depth and is given by $S_{y,w}/h$. For a beam in which the web is fully effective in resisting direct stresses, the web shear flow distribution is found, in which S_y is replaced by $S_{y,w}$ and which, for the beam of Fig. 5.1, would simplify to

$$q_s = -\frac{S_{y,w}}{I_{xx}} \left(\int_0^s t_D y \, ds + B_1 y_1 \right) \quad (5.6)$$

or

$$q_s = -\frac{S_{y,w}}{I_{xx}} \left(\int_0^s t_D y \, ds + B_2 y_2 \right) \quad (5.7)$$

OPEN AND CLOSED SECTION BEAMS

We shall now consider the more general case of a beam tapered in two directions along its length and comprising an arrangement of booms and skin. Practical examples of such a beam are complete wings and fuselages. The beam may be of open or closed section; the effects of taper are determined in an identical manner in either case.

Figure 5.2(a) shows a short length δz of a beam carrying shear loads S_x and S_y at the section z ; S_x and S_y are positive when acting in the directions shown. Note that if the beam were of open cross section, the shear loads would be applied through its shear center so that no twisting of the beam occurred.

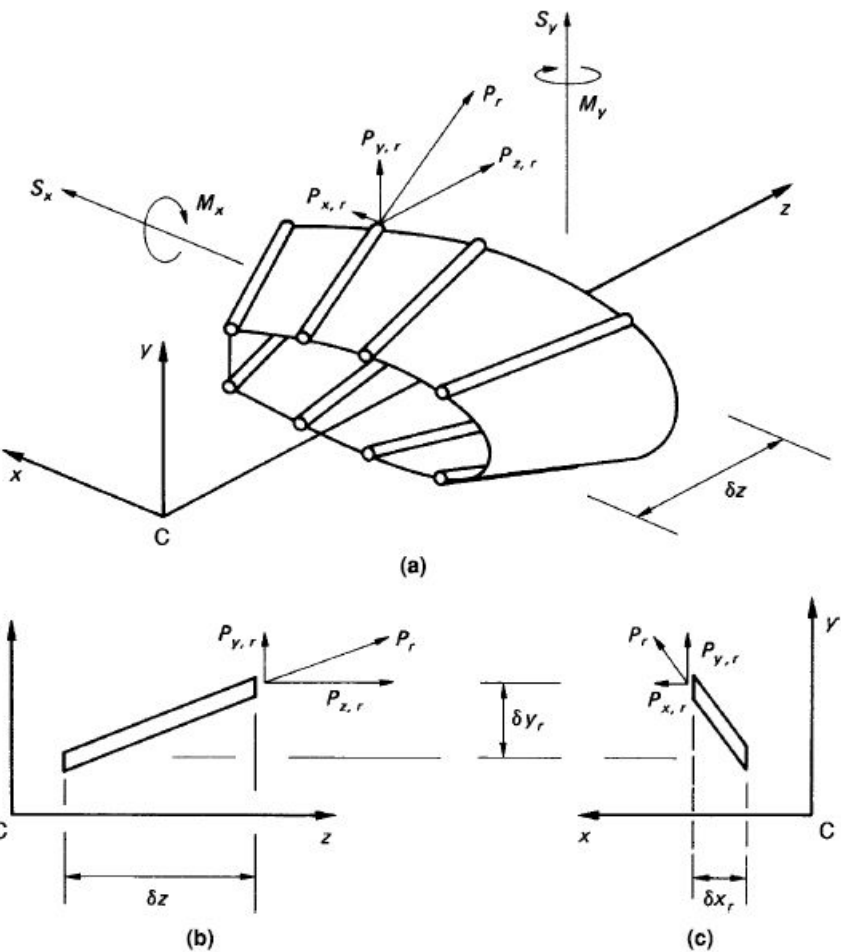


Figure 5.2 Effect of taper on the analysis of open and closed section beams.

In addition to shear loads, the beam is subjected to bending moments M_x and M_y , which produce direct stresses ζ in the booms and skin. Suppose that in the r th boom the direct stress in a direction parallel to the z axis is $\zeta_{z,r}$. The component $P_{z,r}$ of the axial load P_r in the r th boom is then given by

$$P_{z,r} = \sigma_{z,r} B_r \quad (5.8)$$

Where B_r is the cross-sectional area of the r th boom.

From Fig. 5.2 (b),

$$P_{y,r} = P_{z,r} \frac{\delta y_r}{\delta z} \quad (5.9)$$

Further, from Fig. 5.2(c),

$$P_{x,r} = P_{y,r} \frac{\delta x_r}{\delta y_r}$$

or, substituting for $P_{y,r}$ from Eq. (5.9),

$$P_{x,r} = P_{z,r} \frac{\delta x_r}{\delta z} \quad (5.10)$$

The axial load P_r is then given by

$$P_r = (P_{x,r}^2 + P_{y,r}^2 + P_{z,r}^2)^{1/2} \quad (5.11)$$

or

$$P_r = P_{z,r} \frac{(\delta x_r^2 + \delta y_r^2 + \delta z^2)^{1/2}}{\delta z} \quad (5.12)$$

The applied shear loads S_x and S_y are reacted by the resultants of the shear flows in the skin panels and webs, together with the components $P_{x,r}$ and $P_{y,r}$ of the axial loads in the booms. Therefore, if $S_{x,w}$ and $S_{y,w}$ are the resultants of the skin and web shear flows and there is a total of m booms in the section,

$$S_x = S_{x,w} + \sum_{r=1}^m P_{x,r} \quad S_y = S_{y,w} + \sum_{r=1}^m P_{y,r} \quad (5.13)$$

Substituting in Eq. (5.13) for $P_{x,r}$ and $P_{y,r}$ from Eqs. (5.10) and (5.9), we have

$$S_x = S_{x,w} + \sum_{r=1}^m P_{z,r} \frac{\delta x_r}{\delta z} \quad S_y = S_{y,w} + \sum_{r=1}^m P_{z,r} \frac{\delta y_r}{\delta z} \quad (5.14)$$

Hence,

$$S_{x,w} = S_x - \sum_{r=1}^m P_{z,r} \frac{\delta x_r}{\delta z} \quad S_{y,w} = S_y - \sum_{r=1}^m P_{z,r} \frac{\delta y_r}{\delta z} \quad (5.15)$$

The shear flow distribution in an open section beam is now obtained, S_x is replaced by $S_{x,w}$ and S_y by $S_{y,w}$ from Eq. (5.15). Similarly for a closed section beam, S_x and S_y are replaced by $S_{x,w}$ and $S_{y,w}$. In the

latter case, the moment equation requires modification due to the presence of the boom load components $P_{x,r}$ and $P_{y,r}$. Thus, from Fig. 5.3, we

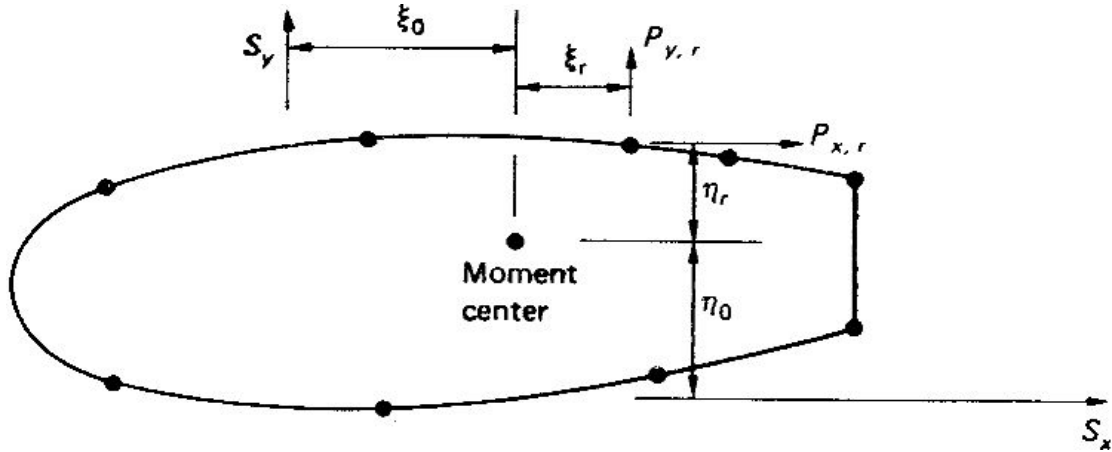


Figure 5.3 Modification of moment equation in shear of closed section beams due to boom load.

$$S_x \eta_0 - S_y \xi_0 = \oint q_b p \, ds + 2Aq_{s,0} - \sum_{r=1}^m P_{x,r} \eta_r + \sum_{r=1}^m P_{y,r} \xi_r \quad (5.16)$$

Equation (5.16) is directly applicable to a tapered beam subjected to forces positioned in relation to the moment center as shown. Care must be taken in a particular problem to ensure that the moments of the forces are given the correct sign.

VARIABLE STRINGER AREAS

In many aircraft, structural beams, such as wings, have stringers whose cross-sectional areas vary in the spanwise direction. The effects of this variation on the determination of shear flow distribution cannot therefore be found by the methods discussed previously which assume constant boom areas. In fact, if the stringer stress is made constant by varying the area of cross section, there is no change in shear flow as the stringer/boom is crossed.

The calculation of shear flow distributions in beams having variable stringer areas is based on the alternative method for the calculation of shear flow distributions. The stringer loads $P_{z,1}$ and $P_{z,2}$ are calculated at two sections z_1 and z_2 of the beam a convenient distance apart. We assume that the stringer load varies linearly along its length so that the change in stringer load per unit length of beam is given by

$$\Delta P = \frac{P_{z,1} - P_{z,2}}{z_1 - z_2}$$

The shear flow distribution follows as previously described.

Wings

Wing sections consist of thin skins stiffened by combinations of stringers, spar webs, and caps and ribs. The resulting structure frequently comprises one, two, or more cells and is highly redundant. However, as in the case of fuselage sections, the large number of closely spaced stringers allows the assumption of a constant shear flow in the skin between adjacent stringers so that a wing section may be analyzed as though it were completely idealized as long as the direct stress-carrying capacity of the skin is allowed for by additions to the existing stringer/boom areas. We shall investigate the analysis of multicellular wing sections subjected to bending, torsional, and shear loads, although, initially, it will be instructive to examine the special case of an idealized three-boom shell.

THREE-BOOM SHELL

The wing section shown in Fig. 5.4 has been idealized into an arrangement of direct stress-carrying booms and shear-stress-only carrying skin panels. The part of the wing section aft of the vertical spar 31 performs an aerodynamic role only and is therefore unstressed.

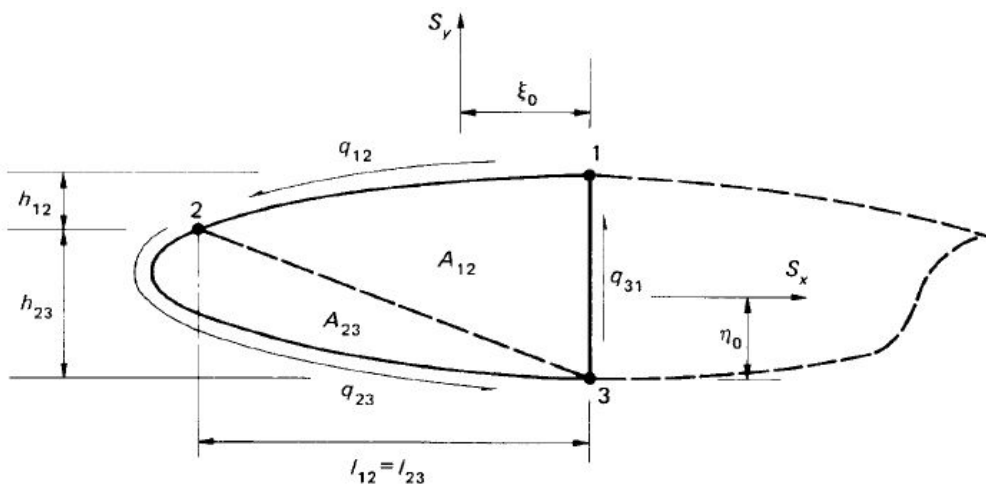


Figure 5.4 Three-boom wing section.

Lift and drag loads, S_y and S_x , induce shear flows in the skin panels, which are constant between adjacent booms, since the section has been completely idealized. Therefore, resolving horizontally and noting that the resultant of the internal shear flows is equivalent to the applied load, we have

$$S_x = -q_{12}l_{12} + q_{23}l_{23} \quad (5.17)$$

Now resolving vertically,

$$S_y = q_{31}(h_{12} + h_{23}) - q_{12}h_{12} - q_{23}h_{23} \quad (5.18)$$

Finally, taking moments about, say, boom 3,

$$S_x\eta_0 + S_y\xi_0 = -2A_{12}q_{12} - 2A_{23}q_{23} \quad (5.19)$$

In the above, there are three unknown values of shear flow, q_{12} , q_{23} , q_{31} , and three equations of statically equilibrium. We conclude therefore that a three-boom idealized shell is statically determinate.

We shall return to the simple case of a three-boom wing section when we examine the distributions of direct load and shear flows in wing ribs. Meanwhile, we shall consider the bending, torsion, and shear of multicellular wing sections.

BENDING

Bending moments at any section of a wing are usually produced by shear loads at other sections of the wing. The direct stress system for such a wing section (Fig. 5.5) is given by either Eq. (3.1) or Eq. (3.2), in which the coordinates (x , y) of any point in the cross section and the sectional properties are referred to axes Cxy in which the origin C coincides with the centroid of the direct stress-carrying area.

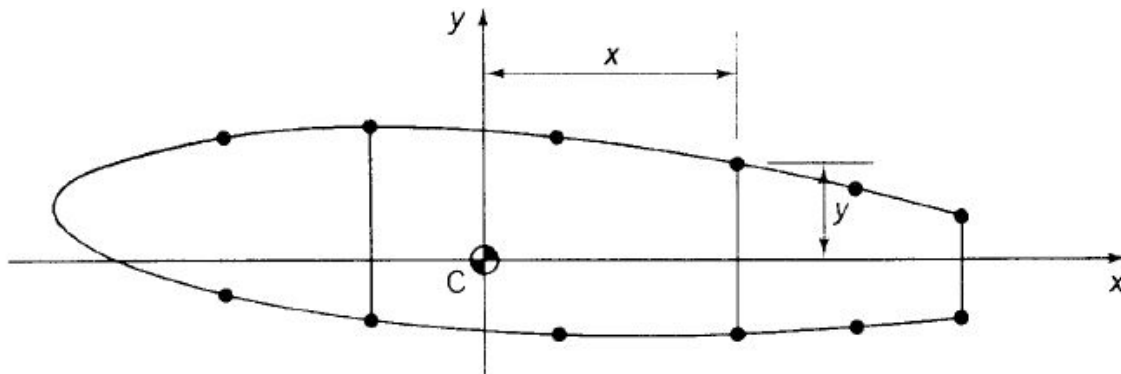


Figure 5.5 Idealized section of a multicell wing.

TORSION

The chord wise pressure distribution on an aerodynamic surface may be represented by shear loads (lift and drag loads) acting through the aerodynamic center together with a pitching moment M_0 . This system of shear loads may be transferred to the shear center of the section in the form of shear loads S_x and S_y , together with a torque T . It is the pure torsion case that is considered here. In the analysis, we assume that no axial constraint effects are present and that the shape of the wing section remains unchanged by the load application. In the absence of axial constraint, there is no development of direct stress in the wing section so that only shear stresses are present. It follows that the presence of booms does not affect the analysis in the pure torsion case.

The wing section shown in Fig. 5.6 comprises N cells and carries a torque T which generates individual but unknown torques in each of the N cells. Each cell therefore develops a constant shearflow $q_1, q_{II}, \dots, q_R, \dots, q_N$.

The total is therefore

$$T = \sum_{R=1}^N 2A_R q_R \quad (5.20)$$

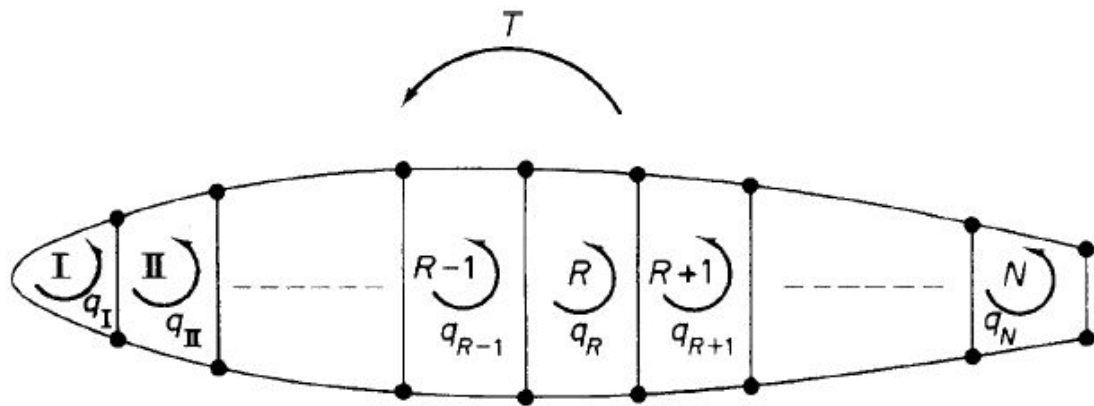


Figure 5.6 Multicell wing section subjected to torsion.

Although Eq. (5.20) is sufficient for the solution of the special case of a single-cell section, which is therefore statically determinate, additional equations are required for an N -cell section. These are obtained by considering the rate of twist in each cell and the compatibility of displacement condition that all N cells possess the same rate of twist $d\zeta/dz$; this arises directly from the assumption of an undistorted cross section.

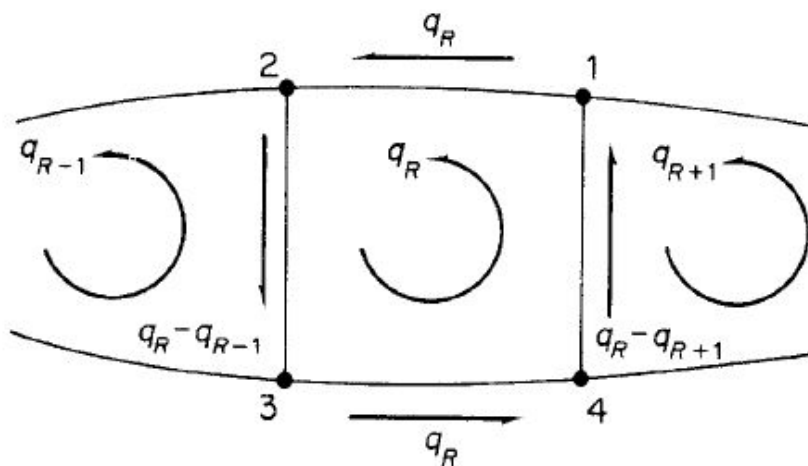


Figure 5.7 Shear flow distribution in the R th cell of an N -cell wing section.

Consider the R th cell of the wing section shown in Fig. 5.7. The rate of twist in the cell is,

$$\frac{d\theta}{dz} = \frac{1}{2A_R G} \oint_R q \frac{ds}{t} \quad (5.21)$$

The shear flow in Eq. (5.21) is constant along each wall of the cell and has the values shown in Fig. 5.7. Writing $\oint ds/t$ for each wall as δ , Eq. (5.21) becomes

$$\frac{d\theta}{dz} = \frac{1}{2A_R G} [q_R \delta_{12} + (q_R - q_{R-1}) \delta_{23} + q_R \delta_{34} + (q_R - q_{R+1}) \delta_{41}]$$

or, rearranging the terms in square brackets,

$$\frac{d\theta}{dz} = \frac{1}{2A_R G} [-q_{R-1} \delta_{23} + q_R (\delta_{12} + \delta_{23} + \delta_{34} + \delta_{41}) - q_{R+1} \delta_{41}]$$

In general terms, this equation may be rewritten in the form

$$\frac{d\theta}{dz} = \frac{1}{2A_R G} (-q_{R-1} \delta_{R-1,R} + q_R \delta_R - q_{R+1} \delta_{R+1,R}) \quad (5.22)$$

in which $\delta_{R-1,R}$ is $\oint ds/t$ for the wall common to the R th and $(R-1)$ th cells, δ_R is $\oint ds/t$ for all the walls enclosing the R th cell, and $\delta_{R+1,R}$ is $\oint ds/t$ for the wall common to the R th and $(R+1)$ th cells.

The general form of Eq. (5.22) is applicable to multicell sections in which the cells are connected consecutively—that is, cell I is connected to cell II, cell II to cells I and III, and so on. In some cases, cell I may be connected to cells II and III, and so on so that Eq. (5.22) cannot be used in its general form. For this type of section, the term $\oint q(ds/t)$ should be computed by considering (ds/t) for each wall of a particular cell in turn.

There are N equations of the type (5.22) which, with Eq. (5.20), comprise the $N+1$ equations required to solve for the N unknown values of shear flow and the one unknown value of $d\zeta/dz$.

Frequently, in practice, the skin panels and spar webs are fabricated from materials possessing different properties such that the shear modulus G is not constant. The analysis of such sections is simplified if the actual thickness t of a wall is converted to a modulus-weighted thickness t^* as follows.

For the R th cell of an N -cell wing section in which G varies from wall to wall, Eq. (5.21) takes the form

$$\frac{d\theta}{dz} = \frac{1}{2A_R} \oint_R q \frac{ds}{Gt}$$

This equation may be rewritten as

$$\frac{d\theta}{dz} = \frac{1}{2A_R G_{\text{REF}}} \oint_R q \frac{ds}{(G/G_{\text{REF}})t} \quad (5.23)$$

in which G_{REF} is a convenient reference value of the shear modulus. Equation (5.23) is now rewritten as

$$\frac{d\theta}{dz} = \frac{1}{2A_R G_{\text{REF}}} \oint_R q \frac{ds}{t^*} \quad (5.24)$$

in which the modulus-weighted thickness t^* is given by

$$t^* = \frac{G}{G_{\text{REF}}} t \quad (5.25)$$

SHEAR

Initially, we shall consider the general case of an N -cell wing section comprising booms and skin panels, the latter being capable of resisting both direct and shear stresses. The wing section is subjected to shear loads S_x and S_y , whose lines of action do not necessarily pass through the shear center S (see Fig. 22.8); the resulting shear flow distribution is therefore due to the combined effects of shear and torsion.

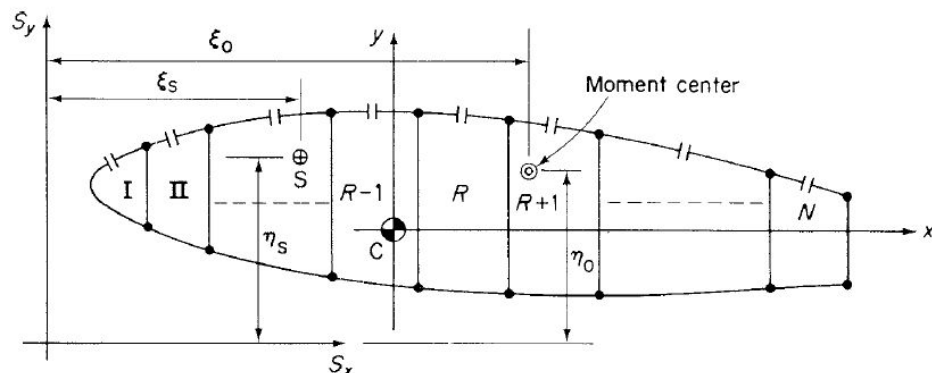


Figure 5.8N-cell wing section subjected to shear loads.

The method for determining the shear flow distribution and the rate of twist is based on a simple extension of the analysis of a single-cell beam subjected to shear loads. Such beam is statically indeterminate, the single redundancy being selected as the value of shear flow at an arbitrarily positioned —cut.|| Thus, the N -cell wing section of Fig. 5.8 may be made statically determinate by —cutting|| a skin panel in each cell as shown. While the actual position of these —cuts|| is theoretically immaterial, there are advantages to be gained from a numerical point of view if the —cuts|| are made near the centre of the top or bottom skin panel in each cell. Generally, at these points, the redundant shear flows ($q_{s,0}$) are small so that the final shear flows differ only slightly from those of the determinate structure. The system of simultaneous equations from which the final shear flows are found will then be —well-conditioned|| and will produce reliable results. The solution of an —ill-conditioned —system of equations would probably involve the subtraction of large numbers of a similar size which would therefore need to be expressed to a large number of significant figures for reasonable accuracy. Although this reasoning does not apply to a completely idealized wing section, since the calculated values of shear flow are constant between the booms, it is again advantageous to —cut|| either top or bottom skin panels for, in the special case of a wing section having a horizontal axis of symmetry, a—cut|| in, say, the top skin panels will result in the —open section|| shear flows (q_b) being zero in the bottom skin panels.

The —open section|| shear flow q_b in the wing section of Fig. 5.8 is given by

$$q_b = - \left(\frac{S_x I_{xx} - S_y I_{xy}}{I_{xx} I_{yy} - I_{xy}^2} \right) \left(\int_0^s t_D x \, ds + \sum_{r=1}^n B_r x_r \right) - \left(\frac{S_y I_{yy} - S_x I_{xy}}{I_{xx} I_{yy} - I_{xy}^2} \right) \left(\int_0^s t_D y \, ds + \sum_{r=1}^n B_r y_r \right)$$

We are left with an unknown value of shear flow at each of the —cuts,|| that is, $q_{s,0,I}, q_{s,0,II}, \dots, q_{s,0,N}$, plus the unknown rate of twist $d\zeta/dz$, which, from the assumption of an undistorted cross section, is the same for each cell. Therefore, as in the torsion case, there are $N + 1$ unknowns requiring $N + 1$ equations for a solution.

Consider the R th cell shown in Fig. 5.9. The complete distribution of shear flow around the cell is given by the summation of the —open section|| shear flow q_b and the value of shear flow at the —cut,|| $q_{s,0,R}$. We may therefore regard $q_{s,0,R}$ as a constant shear flow acting around the cell. The rate of twists again given by,

$$\frac{d\theta}{dz} = \frac{1}{2A_R G} \oint_R q \frac{ds}{t} = \frac{1}{2A_R G} \oint_R (q_b + q_{s,0,R}) \frac{ds}{t}$$

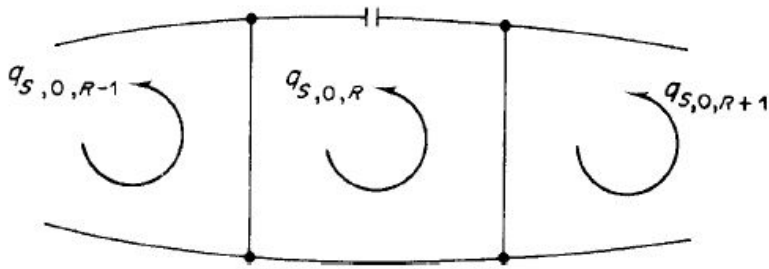


Figure 5.9 Redundant shear flow in the Rth cell of an N-cell wing section subjected to shear.

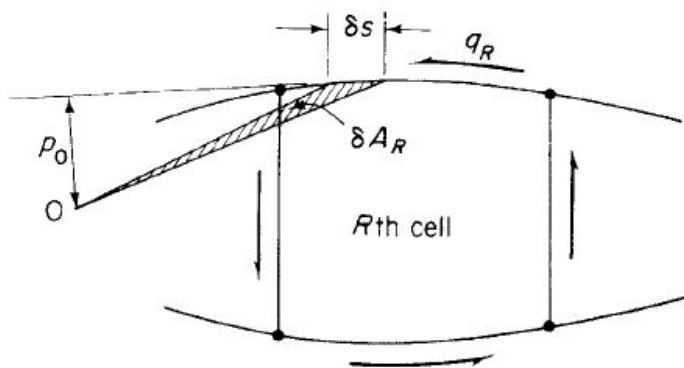


Figure 5.10 Moment equilibrium of Rth cell.

By comparing with the pure torsion case, we deduce that

$$\frac{d\theta}{dz} = \frac{1}{2A_R G} \left(-q_{s,0,R-1}\delta_{R-1,R} + q_{s,0,R}\delta_R - q_{s,0,R+1}\delta_{R+1,R} + \oint_R q_b \frac{ds}{t} \right) \quad (5.26)$$

in which q_b has previously been determined. There are N equations of the type (5.26) so that a further equation is required to solve for the $N+1$ unknowns. This is obtained by considering the moment equilibrium of the Rth cell in Fig. 5.10.

The moment $M_{q,R}$ produced by the total shear flow about any convenient moment center O is given by

$$M_{q,R} = \oint q_R p_0 ds$$

Substituting for q_R in terms of the —open section|| shear flow q_b and the redundant shear flow $q_{s,0,R}$, we have

$$M_{q,R} = \oint_R q_b p_0 ds + q_{s,0,R} \oint_R p_0 ds$$

or

$$M_{q,R} = \oint_R q_b p_0 ds + 2A_R q_{s,0,R}$$

The sum of the moments from the individual cells is equivalent to the moment of the externally applied loads about the same point. Thus, for the wing section of Fig. 5.8,

$$S_x \eta_0 - S_y \xi_0 = \sum_{R=1}^N M_{q,R} = \sum_{R=1}^N \oint_R q_b p_0 ds + \sum_{R=1}^N 2A_R q_{s,0,R} \quad (5.27)$$

If the moment center is chosen to coincide with the point of intersection of the lines of action of S_x and S_y , Eq. (5.27) becomes

$$0 = \sum_{R=1}^N \oint_R q_b p_0 ds + \sum_{R=1}^N 2A_R q_{s,0,R} \quad (5.28)$$

CUTOUTS IN WINGS

Wings, as well as fuselages, have openings in their surfaces to accommodate undercarriages, engine nacelles and weapons installations, and so forth. In addition, inspection panels are required at specific positions so that, as for fuselages, the loads in adjacent portions of the wing structure are modified.

Initially we shall consider the case of a wing subjected to a pure torque in which one bay of the wing has the skin on its undersurface removed.

Fuselage Frames and Wing Ribs

Aircraft are constructed primarily from thin metal skins which are capable of resisting in-plane tension and shear loads but buckle under comparatively low values of in-plane compressive loads. The skins are therefore stiffened by longitudinal stringers which resist the in-plane compressive loads and, at the same

time, resist small distributed loads normal to the plane of the skin. The effective length in compression of the stringers is reduced, in the case of fuselages, by transverse frames or bulkheads or, in the case of wings, by ribs. In addition, the frames and ribs resist concentrated loads in transverse planes and transmit them to the stringers and the plane of the skin. Thus, cantilever wings may be bolted to fuselage frames at the spar caps, while undercarriage loads are transmitted to the wing through spar and rib attachment points.

PRINCIPLES OF STIFFENER/WEB CONSTRUCTION

Generally, frames and ribs are themselves fabricated from thin sheets of metal and therefore require stiffening members to distribute the concentrated loads to the thin webs. If the load is applied in the plane of a web, the stiffeners must be aligned with the direction of the load. Alternatively, if this is not possible, the load should be applied at the intersection of two stiffeners so that each stiffener resists the component of load in its direction.

FUSELAGE FRAMES

We have noted that fuselage frames transfer loads to the fuselage shell and provide column support for the longitudinal stringers. The frames generally take the form of open rings so that the interior of the fuselage is not obstructed. They are connected continuously around their peripheries to the fuselage shell and are not necessarily circular in form but will usually be symmetrical about a vertical axis.

A fuselage frame is in equilibrium under the action of any external loads and the reaction shear flows from the fuselage shell. Suppose that a fuselage frame has a vertical axis of symmetry and carries a vertical external load W , as shown in Fig. 5.11 (a) and (b). The fuselage shell/stringer section has been idealized such that the fuselage skin is effective only in shear. Suppose also that the shear force in the fuselage immediately to the left of the frame is $S_{y,1}$ and that the shear force in the fuselage immediately to the right of the frame is $S_{y,2}$; clearly, $S_{y,2}=S_{y,1}-W$. $S_{y,1}$ and $S_{y,2}$ generate shear flow distributions q_1 and q_2 , respectively, in the fuselage skin, each given by Eq. (21.1), in which $S_{x,1}=S_{x,2}=0$, and $I_{xy}=0$ (C_y is an axis of symmetry). The shear flow q_f transmitted to the periphery of the frame is equal to the algebraic sum of q_1 and q_2 , that is,

$$q_f = q_1 - q_2$$

Thus, substituting for q_1 and q_2 obtained and noting that $S_{y,2} = S_{y,1} - W$, we have

$$q_f = \frac{-W}{I_{xx}} \sum_{r=1}^n B_r y_r + q_{s,0}$$

in which $q_{s,0}$ is calculated, where the shear load is W and

$$q_b = \frac{-W}{I_{xx}} \sum_{r=1}^n B_r y_r$$

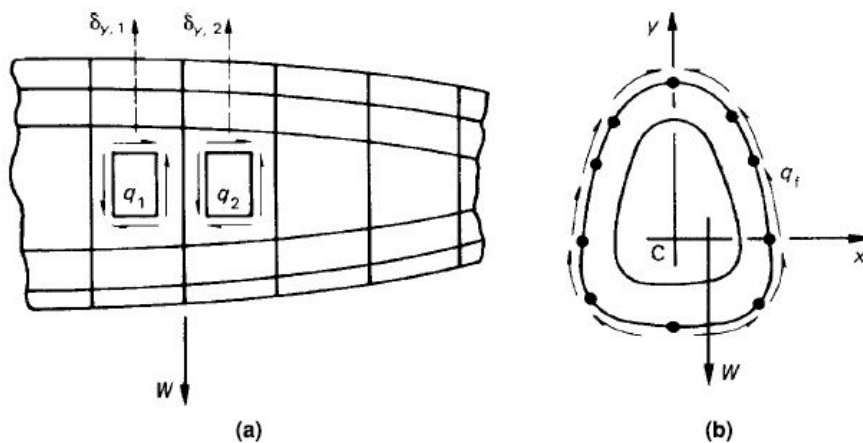


Figure 5.11 Loads on a fuselage frame.

WING RIBS

Wing ribs perform similar functions to those performed by fuselage frames. They maintain the shape of the wing section, assist in transmitting external loads to the wing skin, and reduce the column length of the stringers. Their geometry, however, is usually different in that they are frequently of unsymmetrical shape and possess webs which are continuous except for lightness holes and openings for control runs. Wing ribs are subjected to loading systems which are similar to those applied to fuselage frames. External loads applied in the plane of the rib produce a change in shear force in the wing across the rib; this induces reaction shear flows around its periphery.

Landing Gear and Types

Landing gear is designed to support the load of the aircraft for surface operations

- The landing gear typically consists of three wheels:
 - Two main wheels (one located on each side of the fuselage)
 - A third wheel positioned either at the front or rear of the airplane
- When the third wheel is located on the tail, it is called a tail-wheel, and the design is referred to as conventional gear
- When the third wheel is located on the nose, it is called a nose-wheel, and the design is referred to as a tricycle gear
- Aircraft can also be equipped with floats for water operations or skis for landing on snow

Types of Landing Gear:

There are several types of landing gear which fall into four main categories:

- Conventional (tail-wheel) Gear
- Tricycle Gear
- Pontoon
- Fixed Gear
- Retractable Gear

Conventional Gear:

Landing gear employing a rear-mounted wheel is called conventional landing gear Tail-wheel (Conventional)]

Tail-wheel landing gear aircraft have two main wheels attached to the airframe ahead of its Center of Gravity (CG) that support most of the weight of the structure

Advantages:

- Allows adequate ground clearance for a larger propeller
- More desirable for operations on unimproved fields

Disadvantages:

- With the CG located behind the main gear, directional control of this type aircraft becomes more difficult while on the ground
- If the pilot allows the aircraft to swerve while rolling on the ground at a low speed, he or she may not have sufficient rudder control and the CG will attempt to get ahead of the main gear which may cause the airplane to ground loop
- Lack of good forward visibility when the tail-wheel is on or near the ground
- These inherent problems mean specific training (FAR 61.31) is required in tail-wheel aircraft

Tricycle Gear:

Landing gear employing a front-mounted wheel is called tricycle landing gear

Tricycle landing gear aircraft have two main wheels attached to the airframe behind its CG that support most of the weight of the structure

Additionally, a nose wheel will typically provide some sort of nose wheel steering control

Advantages:

- It allows more forceful application of the brakes during landings at high speeds without causing the aircraft to nose over
- It permits better forward visibility for the pilot during takeoff, landing, and taxiing
- It tends to prevent ground looping (swerving) by providing more directional stability during ground operation since the aircraft's CG is forward of the main wheels
- The forward CG keeps the airplane moving forward in a straight line rather than ground looping

Pontoons:

One or more pontoons, or floats, are mounted under the fuselage to provide buoyancy

By contrast, a flying boat such as the Consolidated PBY Catalina, uses its fuselage for buoyancy

Either type of seaplane may also have landing gear suitable for land, making the vehicle an amphibious aircraft

Landing Gear Design:

Depending on an aircraft's intended operation landing gear may be designed as either:

- Fixed, or
- Retractable

Fixed Gear:

Fixed gear is designed to simplify design and operation

Advantages:

- Always deployed
- Low cost

Disadvantages:

- Creates constant drag, mitigated by the use of a cover called a fairing

Retractable Landing Gear:

A retractable gear is designed to streamline the airplane by allowing the landing gear to be stowed inside the structure during cruising flight

The primary benefits of being able to retract the landing gear are increased climb performance and higher cruise airspeeds due to the resulting decrease in drag

Retractable landing gear systems may be operated either hydraulically or electrically, or may employ a combination of the two systems

Warning indicators are provided in the cockpit to show the pilot when the wheels are down and locked and when they are up and locked or if they are in intermediate positions

Systems for emergency operation are also provided

Disadvantages:

- Increased weight
 - Increased cost
 - Limited to high performance aircraft
-

Text Book

1. —An Introduction to Aircraft Structural Analysis by T. H. G. Megson, Elsevier Ltd., 2010.